

# El Agente Quntur: A research collaborator agent for quantum chemistry

Juan B. Pérez-Sánchez<sup>1,†,✉</sup>, Yunheng Zou<sup>1,6,†,✉</sup>, Jorge A. Campos-Gonzalez-Angulo<sup>1,6,✉</sup>, Marcel Müller<sup>1,6,‡,✉</sup>, Ignacio Gustin<sup>1,‡,✉</sup>, Andrew Wang<sup>1,6,✉</sup>, Han Hao<sup>5,§</sup>, Tsz Wai Ko<sup>1,6,§,✉</sup>, Changhyeok Choi<sup>1,6,§</sup>, Eric S. Isbrandt<sup>5,§</sup>, Mohammad Ghazi Vakili<sup>1,2,6,§,✉</sup>, Hanyong Xu<sup>1,§,✉</sup>, Chris Crebolder<sup>2,5</sup>, Varinia Bernales<sup>\*,2,7,✉</sup>, Alán Aspuru-Guzik<sup>\*,1,2,3,4,5,6,7,8,9,✉</sup>

<sup>1</sup>Department of Chemistry, University of Toronto, 80 St. George St., Toronto, ON M5S 3H6, Canada

<sup>2</sup>Department of Computer Science, University of Toronto, 40 St George St., Toronto, ON M5S 2E4, Canada

<sup>3</sup>Department of Materials Science & Engineering, University of Toronto, 184 College St., Toronto, ON M5S 3E4, Canada

<sup>4</sup>Department of Chemical Engineering & Applied Chemistry, University of Toronto, 200 College St., Toronto, ON M5S 3E5, Canada

<sup>5</sup>Acceleration Consortium, 700 University Ave., Toronto, ON M7A 2S4, Canada

<sup>6</sup>Vector Institute for Artificial Intelligence, W1140-108 College St., Schwartz Reisman Innovation Campus, Toronto, ON M5G 0C6, Canada

<sup>7</sup>Canadian Institute for Advanced Research (CIFAR), 661 University Ave., Toronto, ON M5G 1M1, Canada

<sup>8</sup>NVIDIA, 431 King St. W #6th, Toronto, ON M5V 1K4, Canada

<sup>9</sup>Institute of Medical Science, 1 King's College Circle, Medical Sciences Building, Room 2374, Toronto, ON M5S 1A8, Canada

\*corresponding authors

†,‡,§These authors contributed equally

Quantum chemistry is a foundational enabling tool for the fields of chemistry, materials science, computational biology and others. Despite of its power, the practical application of quantum chemistry simulations remains in the hands of qualified experts due to methodological complexity, software heterogeneity, and the need for informed interpretation of results. To bridge the accessibility gap for these tools and expand their reach to chemists with broader backgrounds, we introduce EL AGENTE QUNTUR, a hierarchical, multi-agent AI system designed to operate not merely as an automation tool but as a research collaborator for computational quantum chemistry. QUNTUR was designed following three main strategies: i) elimination of hard-coded procedural policies in favour of reasoning-driven decisions, ii) construction of general and composable actions that facilitate generalization and efficiency, and iii) implementation of *guided deep research* to integrate abstract quantum-chemical reasoning across subdisciplines and a detailed understanding of the software's internal logic and syntax. Although instantiated in ORCA, these design principles are applicable to research agents more generally and easily expandable to additional quantum chemistry packages and beyond. QUNTUR supports the full range of calculations available in ORCA 6.0 and reasons over software documentation and scientific literature to plan, execute, adapt, and analyze *in silico* chemistry experiments following best practices. We discuss the advances and current bottlenecks in agentic systems operating at the research level in computational chemistry, and outline a roadmap toward a fully autonomous end-to-end computational chemistry research agent.

**Date:** February 5, 2026

**Correspondence:** [varinia@bernales.org](mailto:varinia@bernales.org), and [alan@aspuru.com](mailto:alan@aspuru.com)



Computational chemistry significantly advances the understanding of chemical systems by providing an approximate digital twin of their behaviour. This is achieved by computing the approximate behaviour of electrons and nuclei in molecules and materials. In particular, quantum chemistry calculations have become essential tools in modern drug discovery, offering molecular-level insights that are unattainable through classical computational methods. By solving the Schrödinger equation—albeit approximately due to efficiency and computational complexity constraint—these techniques elucidate molecular electronic structures, energies, and binding affinities critical for understanding drug-target interactions [1–3]. A variety of computational methods, including molecular docking and pharmacophore modeling, are implemented to optimize drug design and enhance the identification of potential drug candidates [4]. Beyond drug discovery, quantum chemistry methods play a vital role in catalyst design and in the exploration of various disciplines, including chemistry, biology, and materials science, fundamentally shaping our understanding of biomolecular functions and material structures. Quantum chemistry approaches illuminate structure-property relationships in organic electronics, enabling rational, systematic design of future high-performance materials [5–7].

The computational implementation of quantum mechanical methods continues to evolve, with developments such as real-space density functional theory on graphical processing units (GPUs) significantly accelerating calculations [8, 9]. These advances in computational efficiency enable the application of quantum chemistry to increasingly complex systems, including enzymatic reaction mechanisms, where quantum-mechanical cluster models can yield highly accurate results that reproduce experimental product distributions and activation free energies [10]. Furthermore, quantum chemistry has provided fundamental insights into biological processes, such as the role of quantum coherence in chromophoric energy transport within photosynthetic protein complexes, including the Fenna-Matthews-Olson complex, where coherent dynamics contribute approximately 10% to energy-transfer efficiency [11]. The continued evolution of quantum chemistry, including the potential integration of quantum computing to accelerate calculations, promises transformative impacts on personalized medicine and the targeting of previously undruggable therapeutic targets [12].

Given the maturity of the field, applying quantum chemistry in practice is far from a simple matter of pressing a button. Each of the numerous electronic structure methods and software packages has its own conventions and limitations; therefore, accurate results require a deep understanding of the theory and the specific code being used [13]. Different programs use different algorithms and very different input and output formats, making it difficult, even for experts, to master more than a few [14]. In practice, many computational setups and parameter choices are guided by human experts' experience rather than by automated rules.

Computational chemists often design workflows to encode efficient and reliable sequences of calculations by pre-selecting methods, parameters, and convergence strategies appropriate for specific classes of problems [15–20]. However, these workflows are severely limited. One limitation is operational complexity: running a calculation often involves scripting multiple steps, selecting computational resources, and actively monitoring progress. Typical failures include convergence issues in geometry or self-consistent field iterations, or exhaustion of allocated wall time on a computing cluster. Handling these failures often requires manual intervention, such as adjusting convergence parameters, restarting jobs with different guesses, or increasing resources. Another limitation is the methodological uncertainty: A user must choose an appropriate level of theory (Hartree-Fock, correlated wavefunction theory, density functional theory, etc.) and a suitable basis set for each problem [21, 22]. No single choice is universally optimal, and different options can give substantially different results. In practice, scientists rely on benchmarking studies or chemical intuition to select appropriate methods, and there is no fully algorithmic way to guarantee reliability in every case. Finally, once a calculation finishes, its raw outputs (energies, optimized geometries, orbital populations, spectral and electrical properties, etc.) must be analyzed to extract chemical meaning. Deciding which results are chemically significant and how they influence one's hypotheses typically requires human insight. For example, when comparing different methods, recognizing that a discrepancy in activation energies is meaningful may depend on knowledge of experimental uncertainties or the chemical context.

These limitations of automation through traditional workflows motivate a fundamentally new approach: the development of agentic AI systems for research [14, 23]. AI agents are currently being designed to autonomously drive scientific inquiry by designing and executing wet-lab and computational experiments, or generating potentially novel materials with applications across various domains. One example in chemistry is COSCIENTIST, in which a team of large language models (LLMs) plans complex synthesis pathways by browsing the literature, parsing hardware documentation, and directly controlling robotic laboratory hardware

[24]. Similarly, CHEMCROW autonomously plans and executes syntheses (e.g., of organocatalysts) and iteratively corrects its procedures [25]. In parallel, some of us developed ORGANA, an LLM-integrated robotic assistant that combines natural-language interaction, perception-driven decision-making, task and motion planning, and parallel execution to autonomously perform diverse chemical procedures in the wet lab [26]. More recently, there has been a surge of agent-based interfaces for computational chemistry, spanning a diverse set of complexity, autonomy, and architectural choices [27–74].

EL AGENTE is an LLM-based multi-agentic system featuring hierarchical task decomposition into different sub-problems and dynamical tool selection, with EL AGENTE Q as its foundational implementation for solving computational quantum chemistry problems [68]. EL AGENTE Q demonstrates the ability to run quantum-chemistry simulations, analyze results, and refine strategies based on feedback from the tools. Moreover, EL AGENTE Q operates at the level of a university student and demonstrated flexibility while performing a restricted set of quantum-chemistry tasks: DFT geometry optimization to equilibrium geometries, vibrational analysis, and single-point excited-state (TD-DFT) calculations. Currently, the architecture of EL AGENTE is being exploited to cover a wide range of fields, including solid-state chemistry [75], drug discovery [76], geometry generation and manipulation [77], Quantum computing and dynamics simulations [78], workflow orchestration for GPU-accelerated molecular and materials simulations [79], and laboratory safety [80], amongst others.

In this work, we introduce EL AGENTE QUNTUR. QUNTUR comprehensively surpasses the capabilities of EL AGENTE Q by reaching an entirely new level in both breadth and depth. In breadth, its design allows it to support a huge range of quantum chemistry calculations, encompassing advanced structure generation, transition-state search and Intrinsic Reaction Coordinate (IRC) calculations, relativistic and dispersion corrections, accurate energy barriers and kinetic isotope effects, spectroscopy calculations (IR/Raman, UV/Vis, NMR, EPR), excited-state kinetics, etc. QUNTUR is a name inspired by the Quechua word *kuntur*, which is the native name for the condor: the bird that is often used as a symbol of south American culture.

We achieve these capabilities by following three improved design strategies: removing certain hard-coded policy choices, designing tools for generalization and efficiency, and conducting guided deep research during execution. These strategies grant QUNTUR complete control over the ORCA 6.0 quantum chemistry package [81, 82]. In-depth, QUNTUR reviews and analyzes software documentation and scientific literature. Therefore, it can plan, justify, execute, and validate diverse multi-stage workflows in accordance with best practices and scientific rigour, while also analyzing the results and comparing them with the literature. These two major advances bring QUNTUR to the category of *research collaborator* as shown in Table 1.

**Table 1** Architectural and functional comparison between EL AGENTE Q and EL AGENTE QUNTUR

System	Agents	Tools	Hierarchical Architecture	Parallel Execution	Image Input	Human in-the-Loop	Domain Breadth	Research Depth
EL AGENTE Q	23	18	Yes	No	No	No	Restricted	Undergraduate
EL AGENTE QUNTUR	58	34	Yes	Yes	Yes	Optional	General	Research collaborator

The denomination of *research collaborator* implies that the agent operates at the level of a graduate student. It can design multi-step computational workflows that go beyond a single prescribed protocol. These workflows include method selection, intermediate analysis, and conditional branching based on results drawn from user input, the scientific literature, or both. Indeed, QUNTUR references published works to motivate methodological choices and during post-analysis. The agent's behaviour is not purely procedural: it exercises judgment when workflows encounter ambiguity, proposes alternative methods, weighs competing convergence strategies, and considers trade-offs between accuracy and cost. It also allows human input for crucial methodological choices or to determine the next steps (human-in-the-loop).

For example, in our own internal group research, EL AGENTE QUNTUR is already being employed to study highly excited electronic states in atoms and to analyze exceptions to Hund's rules at several levels of theory. This task is highly non-trivial, as it requires fine-tuning the self-consistent field settings to preserve spherical symmetry and judiciously designing the model chemistry and the corresponding active space. QUNTUR streamlines workflow production in ORCA, which would otherwise have taken much longer to prepare and debug using traditional methods [83].

## The architecture of EL AGENTE QUNTUR

QUNTUR is built on top of EL AGENTE’s cognitive architecture and graphical user interface (GUI). EL AGENTE’s multi-agent approach serves as a long-term memory module, with procedural memory emerging from a team hierarchy, and agent-specific semantic and episodic memory attached to each agent node [68]. Such a design allows the agentic system to dynamically synthesize and execute reasoning-driven workflows, handle errors flexibly, and form a hierarchical memory that reduces each agent’s cognitive load and supports long-term behaviour.

Although QUNTUR did not change EL AGENTE Q’s core cognitive architecture, it significantly expanded its capabilities thanks to the newly employed three design principles (see [Methods](#) for a detailed explanation):

1. *Removal of hard-coded policies* to enable flexible scientific reasoning across diverse tasks.
2. *Tool design for generalization and efficiency*, allowing tools to be reused and composed across domains.
3. *Guided deep research during execution*, enabling on-demand retrieval of task-relevant context at decision time.

Thanks to these three design principles, we can significantly expand the domain covered with far less design overhead. Compared to EL AGENTE Q, we increase the number of agents from 23 to 58 and the number of tools from 18 to 34. This enables all the agents to reliably reason and execute across different quantum chemistry domains, as well as in the post-analysis stage.

### The procedural memory

Following EL AGENTE’s original template, QUNTUR presents a multi-agent hierarchical architecture that models task decomposition, well-defined job scopes, and coordination mechanisms that characterize human organizations such as companies, governments, and research groups (see Fig. 1). At the top level, we have the **computational chemist** (i.e., a principal investigator), a strategic agent responsible for goal formulation, high-level planning, and result analysis. Instead of interacting with the environment directly, it translates the user’s question into well-defined steps and delegates them to downstream experts. QUNTUR also uses web search and other tools to reason freely over scientific literature, PDFs, and software documentation, rather than relying on human-crafted instructions that limit the agent’s reasoning and the range of problems it can tackle.

In the second layer, we have sub-agents that embody domain expertise—akin to postdocs, engineers, or analysts—each operating under a constrained mandate and with a specific vocabulary and toolset. For QUNTUR, these are agents specialized in geometry generation, quantum chemistry calculations, reading PDF files, and interactions with file management and post-processing. In addition to preventing cognitive overload, this architectural feature enables parallel processing, task decomposition, and the use of optimal models for each task (e.g., the best-performing LLM for geometry generation in visual recognition). Crucially, hierarchy is complemented by feedback loops: lower-level agents report results or failures to higher levels, allowing the system to revise plans or reassign work.

The PDF reader is a specialized agent that reads, summarizes, and answers questions about PDF documents. It uses the MinerU tool to transform PDFs to Markdown files [84]. The geometry generation module showcases tools and other sub-agents for task and tool management. The **interact with OS and files** agent consists of a single LLM with specialized tools, such as an output-section indexer, Python, and Bash, to parse output files. The quantum chemistry expert comprises an input-file service, a guided, in-depth research module, a submission system, and a post-processing system. The **input file service**, the most complex of our agents, has access to our **guided deep research module**, a team of several quantum chemistry domain experts for quantum chemistry reasoning and software adaptation.

# EL Agente Quntur Infrastructure

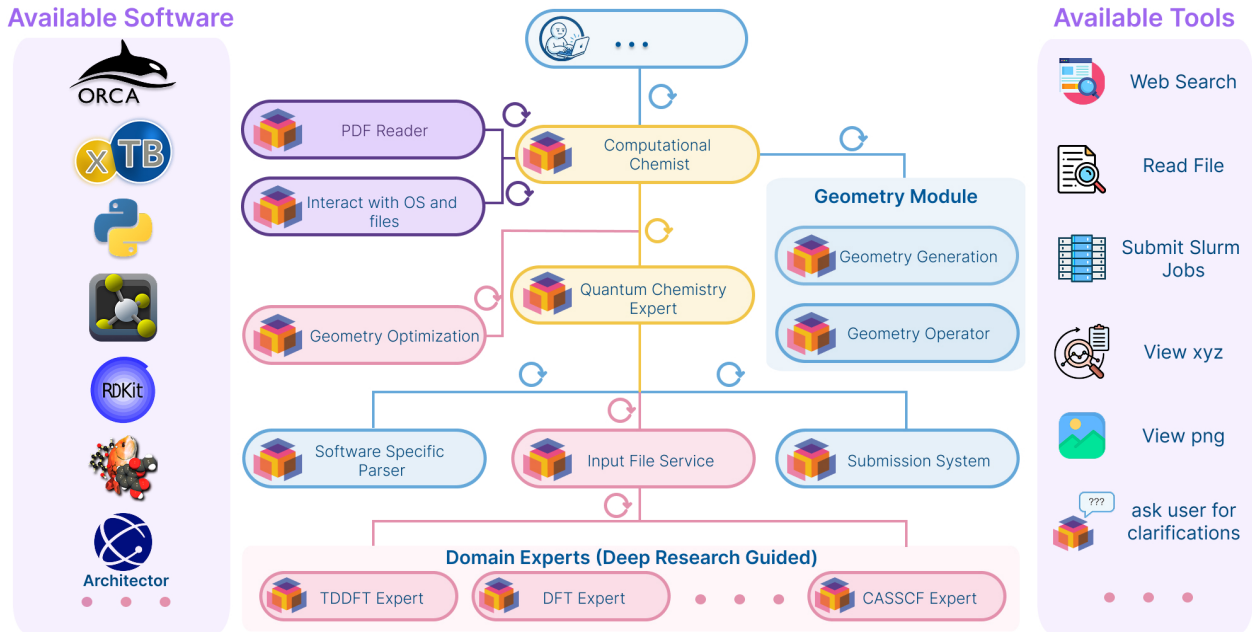


**Figure 1** High-level description of the multi-agentic hierarchical architecture of EL AGENTE QUNTUR. Each module comprises one or more LLMs, each with the tools necessary to fulfill its role.

## Results

### Evaluation of EL AGENTE QUNTUR in computational quantum chemistry tasks

To rigorously evaluate the reliability and breadth of our autonomous quantum chemistry agent, we introduce a benchmark that extends beyond traditional workflows to encompass a broader range of foundational computational chemistry tasks than what we covered in EL AGENTE Q in Table 5. The benchmark spans a broad range of domains, including relativistic and correlated wavefunction properties, thermodynamic cycles, potential-energy-surface (PES) mapping, reaction kinetics, and diverse spectroscopic observables. Furthermore, it covers a range of difficulty levels, spanning from undergraduate exercises to research-level problems, and it systematically probes the agent’s ability to operate across multiple levels of theory.

We asked QUNTUR to *autonomously* execute all questions five times independently to evaluate its robustness and reliability. Evaluating QUNTUR presents a fundamental challenge: many tasks admit multiple valid methodological choices and interpretation pathways, even when the underlying physical question is well-defined. Consequently, the flexibility inherent to each benchmark question cannot be encoded into a deterministic, fully automated grading scheme without penalizing legitimate alternatives. For this reason, we adopt a benchmarking strategy that mirrors how computational chemists are evaluated in practice, emphasizing expert judgment over strict procedural conformity. The rubrics assess QUNTUR’s performance by decomposing each task into planning, geometry generation, input file generation and execution, and post-analysis, thereby allowing expert graders to account for multiple scientifically valid solutions. We provide the general benchmark grading strategy and the rubrics for each particular problem in the [Supporting Information Section C](#). The average score for each question is provided in Fig. 2, while the scores for each skill and repetition can be found in the Supplementary Fig. 5. The files generated by Quntur while answering the questions can be found in our data repository [85].

### EL AGENTE QUNTUR in research-level scenarios

To assess QUNTUR’s performance as a research collaborator, we use a small set of research-oriented case studies that reflect the types of open-ended questions encountered in computational chemistry research.

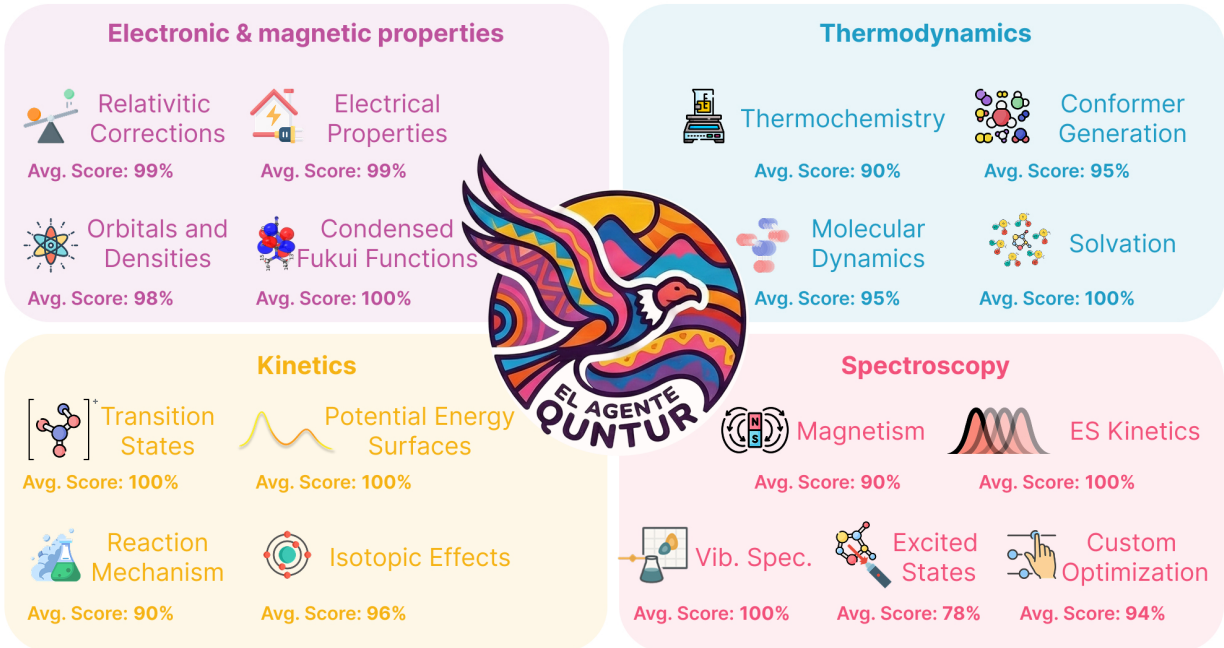


**Figure 2 Capabilities of EL AGENTE QUNTUR and its average score as measured against the benchmark set.** The benchmark is a set of 17 computational quantum chemistry exercises covering several topics from electronic and magnetic properties, thermodynamics, kinetics, and spectroscopy, as well as the various levels of theory and difficulty. The benchmark questions can be found in the [Supporting Information Section B](#). The rubric for each question is in the [Supporting Information Section C](#). Here we show the average score over 5 repetitions per question, but detailed scores for planning, geometry generation, input file generation and execution, and post-analysis are provided in Fig. 5. All benchmarks were conducted using Claude Opus 4.5 as the base language model for all agents.

These case studies also span a broad range of topics (electronic and magnetic properties, thermodynamics, kinetics, and spectroscopy). The prompts for case studies include method selection guided by the literature, comparative analysis across models or levels of theory, options for human-in-the-loop at various levels, and the requirement for post-analysis to obtain chemically meaningful information and interpretations from raw computational data. We present the case studies and the summary of each trajectory in the [Supporting Information Section E](#), while the generated files can be found in a data repository [85]. Yet, to illustrate what QUNTUR can do, we present a simplified sketch of the computational workflow designed to address the *Natural Transition Orbitals visualization and excited states characterization* case study in Fig. 3. We also base our analysis of the capabilities and current bottlenecks of QUNTUR on the case studies.

### Application of Natural Transition Orbitals to excited-state analysis

4-(Dimethylamino)benzonitrile (DMABN) is a prototypical donor–acceptor system that exhibits dual fluorescence arising from the coexistence of locally excited (LE) and twisted intramolecular charge-transfer (TICT) states [86]. We prompt QUNTUR to calculate the lowest two singlet excited states of DMABN and to visualize the associated Natural Transition Orbitals (NTOs), to classify the transitions as either local or charge-transfer-like. From the results, it inferred the nature of each excited state from the final optimized geometries and the qualitative features of the NTOs. QUNTUR also realized that the calculations contradicted the known result that a shift in character between vertical excitation and the relaxed excited-state geometry occurs. A literature search correctly identified that the inconsistency arises because the calculation is performed in the gas phase rather than in solution [87]. QUNTUR solved this case study fully autonomously (without human intervention).



For 4-(dimethylamino)benzonitrile (DMABN), compute the two lowest singlet excited states using TDDFT in ORCA 6.0. Visualize the NTOs for each bright transition and identify states with local  $\pi \rightarrow \pi^*$  versus charge-transfer (CT) or twisted intramolecular charge-transfer (TICT) character. Compare the NTO hole–particle separation between the  $S_1$  state at the ground-state geometry and at the relaxed  $S_1$  geometry.



#### High-Level Plan: DMABN TICT Study (ORCA 6.0, TDDFT).

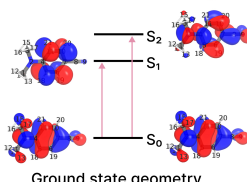
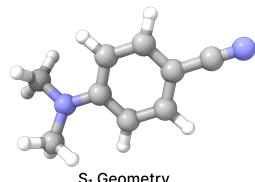
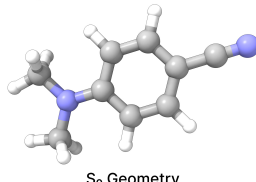
Method: CAM-B3LYP / def2-TZVP

##### Step 1 — $S_0$ Geometry

- Optimize  $S_0$  geometry and compute frequencies.
- Step 2 —  $S_1$  Geometry and vertical excitations at  $S_0$  Geometry**
  - Optimize  $S_1$  geometry and compute frequencies.
  - Compute vertical TDDFT excitations ( $S_1, S_2$ ) at the  $S_0$  geometry and generate NTOs for all bright transitions.
- Step 3 — Geometry-Dependent NTOs**
  - Compute TDDFT at the  $S_1$  geometry and generate NTOs for  $S_0 \rightarrow S_1$ .
- Step 4 — Summary and Report**
  - Assign LE vs CT/TICT character and summarize results.

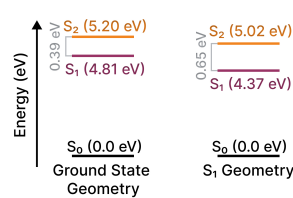
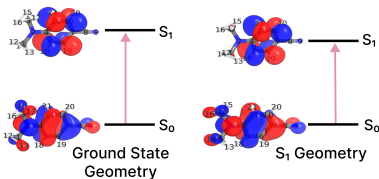


Steps 1 and 2 are complete. Here are the optimized  $S_0$  and  $S_1$  geometries, along with the NTOs for all bright  $S_0 \rightarrow S_1$  and  $S_0 \rightarrow S_2$  transitions.



##### Steps 3 and 4 completed.

Comparison of  $S_0 \rightarrow S_1$  NTOs and excitation energies shows that, at the CAM-B3LYP/def2-TZVP gas-phase level, the  $S_1$  minimum is a planar LE/ICT state rather than a TICT configuration.  $S_2$  is the bright, predominantly  $\pi \rightarrow \pi^*$  state, while  $S_1$  is dark with partial charge-transfer character. No significant increase in hole–particle separation is observed upon  $S_1$  relaxation, indicating that a fully twisted TICT state is not stabilized in the gas phase.



Run Time: ~17.5 h  
ORCA execution



Total Tokens: ~5M



Run Cost: ~25 USD

## Key Agents in This Study

Computational Chemist

Interact with OS and Files

Quantum Chemistry Expert

Geometry Generator

Geometry Optimization

Input File Service

TDDFT Expert

Submission System

Software Specific Parser  
(orca\_plot)

**Figure 3** Simplified sketch of the case study *Natural Transition Orbitals (NTOs) visualization and excited states characterization* as solved by EL AGENTE QUNTUR. Decisions are based on LLMs’ reasoning rather than being hardcoded. Molecular structures were visualized using ChimeraX [88, 89].

## Discussion

### Performance of EL AGENTE QUNTUR in research-level scenarios: strengths and limitations

We summarize the agent’s performance during the case studies in terms of five core *reasoning sub-skills* required to successfully address each case study. These sub-skills are approximately localized within the agent’s modules, as illustrated in Fig. 1. They include *i*) task decomposition, which is partially handled by the computational chemist agent but largely delocalized across the system; *ii*) geometric reasoning, which is primarily performed by the geometry generation module; *iii*) error recovery and adaptability, which are distributed across multiple modules; *iv*) quantum chemistry and software understanding, which are handled by the input file service agent and supported by the guided deep research module; and *v*) post-analysis, which is mainly carried out by the interact with OS and files and computational chemist agents. These sub-skills enable the agent to execute complex tasks end-to-end without excessive human intervention.

### Planning

Planning evaluates the agent’s ability to design a high-level workflow that decomposes the query into a coherent sequence of steps whose execution solves the problem. The plan can be regarded as a hypothesis about the computational experiment that solves the task, and it must be flexible enough to be modified during

execution. The agent must also anticipate challenges, be efficient, and execute jobs in parallel when possible. For example, in the study of *Fluorescence and intersystem crossing rates of anthracene*, QUNTUR correctly identified the need for a multi-stage workflow including ground state optimization, vertical excitation analysis to probe relevant excited states, excited state optimizations, and explicit rate calculations using ORCA’s ESD module [90, 91]. The general workflow for computing these properties is clearly explained in the software’s documentation, but QUNTUR adapts it to handle unforeseen calculation details or the properties of the molecule of interest.

The importance of a good initial plan cannot be overstated. An error at this stage can silently propagate throughout execution, wasting resources and producing incorrect results. A common example occurs when comparing different DFT functionals to calculate some property. As observed in the *<sup>31</sup>P NMR absolute shielding and chemical shift tensor of triphenylphosphine oxide* case study, QUNTUR decides to run NMR calculations with B3LYP [92–94] and  $\omega$ B97X-D3 methods [95], using the same geometry optimized using  $\omega$ B97X-D3. We also observe QUNTUR’s ability to modify its original plan. For studying *Competing mechanisms of Isocyanide isomerization*, QUNTUR mistakenly proposed a reaction mechanism that the calculations revealed to be unfeasible. Subsequently, it removed that mechanism from the workflow and proposed a new triplet carbene pathway, which was explored upon human confirmation. After the newly proposed pathway led to a thermally inaccessible state, it focused solely on the concerted mechanism.

### Geometric reasoning

In addition to generating geometries, QUNTUR must be able to map between natural-language chemical descriptions and three-dimensional molecular representations (e.g., xyz files) and use this mapping to plan, evaluate, and modify geometries as part of a computational workflow. QUNTUR reads a set of coordinates (text-based analysis) or directly views a molecular structure in png format (image-based analysis), either to handle local parameters such as atomic indices, connectivity, and atomic identities, or to recognize global concepts such as symmetry. For example, in the *Global softness and chemoselectivity* case study, ORCA reports atomic charges for each atomic index. QUNTUR must be able to assign atomic indices to each atom correctly to report their reactivity. Similarly, during the *Natural Transition Orbitals visualization and excited states characterization* case study, the `computational_chemist` must realize that the equilibrium geometry of  $S_1$  of DMABN is not twisted but relatively planar.

Although these results are promising, we observe that LLMs struggle with more complex geometry-related tasks. For example, in the *Competing mechanisms of Isocyanide isomerization* case study, QUNTUR mistakenly misrepresented a triplet carbene isomerization pathway due to its inability to recognize that the “CH<sub>3</sub>NC (T<sub>1</sub>)” and “Carbene (T<sub>1</sub>)” optimized structures were actually the same structure (see Fig. 13 in the Supporting Information). Yet, the most significant limitation arises during the geometry-generation stage of transition-state searches. Performing Nudged Elastic Band (NEB) calculations to find transition states and reaction paths [96–98] is a particularly challenging problem for QUNTUR. For simple problems (see benchmark questions), a TS guess can be directly generated, or a relaxed PES scan can be performed through the changing internal coordinate to find a guess for the TS structure. However, many transformations (e.g., those found in catalysis) involve changes in multiple internal coordinates through the TS, and a multidimensional PES scan over several internal coordinates quickly becomes prohibitively expensive (for context, ORCA allows one to vary up to three internal coordinates in a PES scan). QUNTUR was particularly limited in generating geometries when cases required more advanced spatial and geometric understanding and reasoning. We performed two case studies involving NEB: *Migratory insertion of CH<sub>3</sub> into C<sub>2</sub>H<sub>4</sub> on Ni* (based on References [99]), and *Trans effect of ligands on a square planar Pt complex* (based on References [100–102]). Attempts to allow QUNTUR generate the appropriate geometries for the TS search failed. For more complex TS structures, as in the case studies, interpolating from the optimized structures of the endpoints of a reaction path is often a useful way to generate an approximate reaction path with a reasonable TS guess. However, these interpolation methods require the reactant and product to be pre-aligned so that there is a one-to-one mapping between their structures. In other words, not only do the atomic indices of the reactant and product have to match exactly, but the positions of the atoms—except for the ones directly involved in the changing reaction coordinate, have to be at a similar location in three-dimensional space (i.e., the Cartesian coordinates of one molecule cannot be at a completely different location even if the internal coordinates of the two molecules are the same). We were able to complete the case studies only after providing the input geometries for the fixed endpoints of the

interpolation. Based on our observations, we conclude that geometric reasoning is currently a major bottleneck for AI agents in chemistry. This observation is consistent with recent works showing that current LLMs are notoriously limited in their ability to understand and manipulate 3D structure information [77, 103–105]. As discussed in our roadmap (see Fig. 4), we will re-address these types of computational quantum chemistry problems upon the imminent integration of EL AGENTE QUNTUR and EL AGENTE ESTRUCTURAL [77], a specialized agent for geometry generation, manipulation, and reasoning that was released as a preprint the same day this work was reported, in the same repository [77].

### Quantum chemistry and software understanding

A computational quantum chemistry agent must translate each planned step into executable input files. For any quantum chemistry package, this requires a precisely formatted input file specifying the calculation type, molecular structure, chosen level of theory, the properties to be computed, and other settings. In other words, the agent must specify the calculation method in the geometry section and provide additional settings/keywords for special tasks. Indeed, the diversity of input files reflects the field’s vast complexity. In the ORCA 6.0 example, the input file contains a keyword line with dozens of “run types” (e.g., DFT, HF, OPT, FREQ, IRC, etc.). It also comprises dozens of specialized blocks, each with dozens of adjustable settings that govern the calculation of nuanced aspects [82]. Thanks to our guided deep research strategy, described in the Methods Section, El Agente QUNTUR excels at this task, as evidenced by the breadth and sophistication of the benchmark questions and case studies it can address. A particular example is the *Potential energy surface of N<sub>2</sub>* case study, where the challenge lies in assembling input files that correctly combine geometry scans, multiple electronic-structure formalisms, and consistent reference states within a single workflow. Successful assembly of such an input depends on information distributed across different sections of the software manual and distinct conceptual domains of electronic structure theory. QUNTUR’s guided deep research enables efficient setup of these calculations, as the input files are generated in parallel by the corresponding domain experts.

### Error recovery and adaptability

Self-debugging is arguably the most crucial sub-skill for achieving robust autonomy. Like its predecessor, QUNTUR is resilient: when a job fails, produces a warning, or the computed properties (e.g., energies, spin, and vibrational frequencies) indicate that a change in methodology is needed, it does not stop. Instead, it diagnoses the issue and tries a solution. This behaviour is particularly useful during geometry optimizations, where the converged geometry can correspond to a minimum, a first-order saddle point, a second-order saddle point, or other types of extrema. Once again, during the case study *Competing mechanisms of Isocyanide isomerization*, the transition state of the concerted mechanism converges to a second-order saddle point instead of a first-order saddle point (TS), and QUNTUR successfully eliminates the imaginary frequency along the mode orthogonal to the reaction coordinate. In addition, in the same case study, the agent begins with a workflow hypothesis that encompasses two reaction pathways. Upon computational validation that one proposed pathway is unfeasible, the agent autonomously reformulates the workflow to explore an alternative mechanism involving the triplet PES. This instance demonstrates that QUNTUR’s design allows it to revise its high-level plan, indicating that adaptability is not limited to low-level error handling or numerical diagnostics. The same happens for the case study *solvation effects on the keto-enol equilibrium of acetylacetone in water*. The original user prompt specifies the use of both an implicit Conductor-like Continuum Polarization Model (C-PCM) water model [106], and an explicit water-cluster–C-PCM hybrid continuum model to compare solvation free energies. However, both methods fail qualitatively to reproduce the experimentally observed equilibrium. When users subsequently request a comparison with previous computational studies, QUNTUR recommends using the Solvation Model based on Density (SMD) model [107], re-runs the calculations with it, and confirms that it provides the best agreement with experimental results within chemical accuracy (< 1 kcal mol<sup>-1</sup>). These examples demonstrate the agent’s ability to reconsider its initial hypothesis and formulate alternative ones.

### Post-analysis

A research collaborator would not simply run calculations; they must also assess the meaningfulness of the results, verify the success of the computations, and present the findings coherently. This set of tasks is

particularly challenging for LLMs, which tend to be overconfident in their results rather than rigorously checking for methodological errors. To mitigate this effect, QUNTUR analyzes the results by cross-checking the methodology and contextualizing the findings through targeted web searches over relevant literature. Yet we still observe remnants of the problematic behaviour. For example, in the *Trans effect of ligands on a square planar Pt complex* case study, most of the transition-state results are likely incorrect due to limitations in what the agent can achieve with NEB at the time of this manuscript. The trend is clearly different from that reported in the literature; yet the agent rationalized the differences as methodological, even though different methods should still yield the same trends.

On the other hand, the raw outputs often require additional post-processing, as chemically relevant observables are rarely provided directly by the electronic structure code, e.g., thermal populations from energies, reaction rates from energy barriers, reactivity from electronic properties, spectra plots, or reaction pathway diagrams. At present, QUNTUR performs mathematical operations using Python; however, additional safeguards are still required to ensure correct theoretical and mathematical processing, thereby guaranteeing a more reliable transformation of raw outputs into chemically meaningful quantities and visualizations. Finally, we once again showcase QUNTUR’s multimodality across all case studies, as it directly inspects the images it generates during post-analysis. This is central in the case study *Natural Transition Orbitals visualization and excited states characterization*, where QUNTUR correctly assigns qualitative features of the NTOs by inspecting .png images generated with the computed .cube files. Visualization of wavefunctions and densities has the potential to provide not only intuitive interpretations of electronic-state characters, but also autonomous active-space selection for multi-reference methods and autonomous diagnostics for SCF-convergence issues [108].

## Future directions

The alpha version of the EL AGENTE cloud platform will be released alongside the QUNTUR version. The exact release date will be posted on the website [elagente.ca](http://elagente.ca) soon (Stage 1). Following its release, we plan to leverage QUNTUR’s interactive (human-in-the-loop) capabilities to enhance its value as a classroom tool for teaching computational quantum chemistry at the undergraduate and graduate levels (Stage 2). The remainder of the roadmap focuses on transitioning from a research collaborator to a fully autonomous research agent capable of conducting computational chemistry research independently and integrating smoothly into broader end-to-end chemistry research and self-driving laboratory pipelines. The first step in this direction is the increase in breadth: we will enable communication between QUNTUR and other agents within the EL AGENTE network [68, 75, 76, 78, 79, 109] (Stage 3). We will also add support for other quantum chemistry packages [110–115], as well as state-of-the-art machine-learning-based methods (Stages 4 and 5). These capabilities will allow EL AGENTE to address interdisciplinary questions that require computational tools and abilities across all scientific fields. Second, we will work to further advance our agent’s capabilities in depth. We will address current bottlenecks in computational chemistry research, such as structure reasoning, by training our own specialized agents (Stage 6). For example, we will develop an agent to explore potential energy landscapes and identify chemically relevant critical points, such as minima and saddle points. This task is highly hands-on and central to the study of chemical reaction mechanisms [116] (Stage 7). With these developments in hand, we will begin performing autonomous end-to-end chemical research in collaboration with self-driving laboratories [117] (Stages 8-10).

## Methods

### Removing hard-coded policies to facilitate scientific reasoning

As foundation models improve over time, agent design is shifting away from hard-coded policies (e.g., fixed step-by-step instructions) toward higher-level prompts that encourage the model to reason and adaptively select tools. This shift scales better: it reduces the amount of expert-crafted context required and leverages the model’s internal knowledge more effectively, as human-authored policies can, in practice, become a bottleneck.

As an example, consider a hard-coded rule to always run a GFNn-xTB [118–120] semi-empirical relaxation (cheap) before an *ab initio* calculation (e.g., DFT, expensive). This approach is often beneficial because pre-relaxation can accelerate subsequent *ab initio* geometry convergence by providing a reasonable initial



**Figure 4 Development roadmap.** From computational quantum chemistry research collaborator to autonomous research agent.

guess above direct geometry generation. However, such a rigid rule overlooks important edge cases. For instance, when studying transition or excited states, semi-empirical ground state relaxation may distort the geometry and erase features that can only be captured with the *ab initio* method targeting the correct state.

When we remove these hard-coded rules and instead let the agent decide, it can select methods and workflows based on scientific reasoning and the specifics of the input. For example, the agent may consider that a geometry optimization should proceed directly to the *ab initio* stage rather than pre-relaxing the structure with a semi-empirical method. Rigid policies require continuous patching to address exceptions and edge cases, which is time-consuming and still not general. In contrast, reasoning-first approaches tend to generalize better while requiring lower design and maintenance effort.

### Design tools that facilitate generalization and efficiency

Tools are the core interface between an agent’s reasoning and its environment. An agent decides which actions to take using its tools, observes the results, and iterates until the goal is achieved. Designing tools that are both general and efficient is therefore fundamental. If the action space is too narrow, the agent may reason correctly about what to do, yet still be unable to complete the task. Worse, overly specialized tools can mislead the agent by hiding relevant out-of-domain context. In other words, general tools enable the agent to tackle a far broader problem space by allowing it to read, discover, execute, and process, and by facilitating the flexible handling of constraints such as a limited LLM context window.

A concrete example of the points discussed above is the task of parsing ORCA outputs. Some quantum chemistry calculations can produce files exceeding 10,000 lines, far beyond what most LLMs can read within a context window. These outputs contain many properties, and their structures vary by calculation type in ways that are neither consistent nor thoroughly documented. Traditional solutions rely on case-specific parsers (often regex-based), which are not scalable: it is impractical to manually implement robust, manageable parsers for every property and output variant. In EL AGENTE Q, we initially addressed this challenge by predefining a set of output sections and allowing the model to read only the relevant ones [68]. While this strategy has achieved strong results, it remained brittle: new calculation modes introduce additional sections, and even a single section can remain extremely long, particularly those containing tables or charts. Early scaling revealed frequent parsing errors driven by these limitations.

QUNTR’s solution is expanding the action space with two tools: (1) a dynamic section indexer that discovers section names and their line ranges directly from the output, and (2) a bash terminal interface that enables targeted inspection (e.g., reading specific line ranges or searching keywords) without loading entire sections into the LLM context. For large tables and chart-like blocks, the agent can sample the header and a few rows to infer the format, then programmatically extract the table and convert it to CSV for downstream analysis in Python. This pattern allows the agent to generalize during parsing, as tools do not prevent it from accessing

any context in long documents, and the Bash shell interface is flexible enough for the agent to handle context smartly rather than forcing it to read a long context.

### Guided Deep Research for ORCA input file synthesis

Deep research on public sources or custom documentation expands the agent’s capabilities by enabling it to retrieve task-relevant context on demand through iterative reasoning. A *guided* deep research variant further constrains this process by steering retrieval toward specific sources, scopes, or investigative directions, improving efficiency and reducing spurious exploration. In QUNTUR, this skill is instantiated during *input file synthesis*. Instead of encoding quantum chemistry and software-syntactic knowledge for every task in advance, we rely on execution-time reasoning and retrieval.

The focus on input file synthesis is deliberate. Synthesizing computational quantum chemistry input files couples three forms of expertise. Firstly, the agent must perform *quantum-chemistry reasoning*: selecting physically meaningful electronic-structure methods, approximations, and observables that are consistent with the research question and the molecular system. Secondly, *physical chemistry reasoning*: In some computational chemistry packages like ORCA, a substantial portion of what is often treated as post-processing is specified directly in the main input file. Population analysis, excited-state analysis, calculation of vibrational and electronic spectra, thermochemistry, kinetics, and wavefunction transformations are encoded as input directives rather than post-run scripts [81, 82]. Finally, it must perform *software realization*: mapping those conceptual decisions onto software-specific keywords, blocks, dependencies, and execution pathways. These two aspects are inseparable in practice: a scientifically sensible choice that is incorrectly encoded yields an invalid calculation, while a syntactically correct input that encodes the wrong conceptual assumptions produces meaningless results. As a result, generating the correct ORCA input files is a particularly demanding process in which LLMs are known to perform poorly [121].

To support this level of complexity, QUNTUR organizes input file generation around a central *orchestrator* agent (*input file service*) and a set of *domain specialists* agents (guided deep research module). The orchestrator operates at a high level. It determines *i*) whether additional research is required at a given decision point, *ii*) which sources are admissible for that research (e.g., ORCA documentation, scientific literature), and *iii*) which domain specialists should be consulted. Its primary role is not to generate detailed input sections directly, but to reason about the overall structure of the calculation: which conceptual components are relevant, how they interact, and how they should be assembled into a coherent whole. Domain specialists are also agents. Each is biased toward a particular class of scientific subproblems (e.g., multi-reference methods, geometry handling, NEB and scanning parameters, excited-state analysis blocks, etc.). They conduct in-depth research across relevant sections of the software manual and related literature, removing hallucinations and enabling appropriate method selection in line with best practices. Because we transformed the block experts of EL AGENTE Q into general quantum chemistry domain experts (about 20 domains), QUNTUR also facilitates future integration of other quantum chemistry packages such as Q-CHEM [110], GAUSSIAN [111], OPENMOLCAS [112], PYSCF [113], GAMESS [114], and PSI4 [115].

The hierarchical organization of the input file generation emerged from practical experience rather than theoretical arguments. In particular, we observed that single-agent systems exhibited a recurring failure mode: over-confidence driven by shallow retrieval. A monolithic agent would often read a single relevant documentation page, conclude that it had sufficient context, and proceed to plan and execute based solely on that limited view. For example, we observe that LLMs usually do not adapt parallelization or memory settings to the molecule of interest during geometry optimization. By contrast, the hierarchical system first reasons at a higher level about the structure of the calculation, identifying that a `%pal` section may be required. Thus, guided deep research at the orchestrator level expands the search space conceptually (“*what sections might be relevant?*”), while deeper investigation by domain specialists refines the details (“*how many cores should I use for this molecule and in this cluster?*”). We do not claim that hierarchy is strictly necessary in all cases, nor that a sufficiently capable single agent could not be instructed on similar behaviours. Rather, this architecture provides evidence that combining hierarchical planning with guided deep research during execution mitigates common failure modes of monolithic agents, enabling more reliable and higher-quality input synthesis.

Guided deep research allows the system to scale across any software’s feature space without relying on human-crafted surrogate documentation or static semantic memories. Instead of encoding procedural knowledge for

each calculation type, the system design focuses on providing correct sources, role biases, and orchestration logic to guide agents' search and reasoning. Overall, this system demonstrates that execution-time guided deep research, combined with hierarchical orchestration and domain-focused investigation, can support complex scientific workflows through direct input-file synthesis.

## Data and code availability

All the data required to evaluate the presented conclusions are available via <https://doi.org/10.5683/SP3/RDSOEA>.

## References

- [1] Gómez-Bombarelli, R. *et al.* Design of efficient molecular organic light-emitting diodes by a high-throughput virtual screening and experimental approach. *Nat. Mater.* **15**, 1120–1127 (2016).
- [2] Lin, X., Li, X. & Lin, X. A review on applications of computational methods in drug screening and design. *Molecules* **25**, 1375 (2020).
- [3] Breijeh, Z. & Karaman, R. Enzyme models—from catalysis to prodrugs. *Molecules* **26**, 3248 (2021).
- [4] Cova, T. F. G. G. & Pais, A. A. C. C. Deep learning for deep chemistry: Optimizing the prediction of chemical patterns. *Fchem* **7** (2019).
- [5] Hachmann, J. *et al.* The harvard clean energy project: Large-scale computational screening and design of organic photovoltaics on the world community grid. *J. Phys. Chem. Lett.* **2**, 2241–2251 (2011).
- [6] Hachmann, J. *et al.* Lead candidates for high-performance organic photovoltaics from high-throughput quantum chemistry – the harvard clean energy project. *Energy Environ. Sci.* **7**, 698–704 (2014).
- [7] Huggins, D. J. *et al.* Biomolecular simulations: From dynamics and mechanisms to computational assays of biological activity. *WIREs Comput. Mol. Sci.* **9**, e1393 (2019).
- [8] Andrade, X. & Aspuru-Guzik, A. Real-space Density Functional Theory on graphical processing units: Computational approach and comparison to gaussian basis set methods. *J. Chem. Theory Comput.* **9**, 4360–4373 (2013).
- [9] Olivares-Amaya, R. *et al.* Accelerating correlated quantum chemistry calculations using graphical processing units and a mixed precision matrix multiplication library. *J. Chem. Theory Comput.* **6**, 135–144 (2010).
- [10] de Visser, S. P., Wong, H. P. H., Zhang, Y., Yadav, R. & Sastri, C. V. Tutorial review on the set-up and running of quantum mechanical cluster models for enzymatic reaction mechanisms. *Chem. Eur. J.* **30**, e202402468 (2024).
- [11] Rebentrost, P., Mohseni, M. & Aspuru-Guzik, A. Role of quantum coherence and environmental fluctuations in chromophoric energy transport. *J. Phys. Chem. B* **113**, 9942–9947 (2009).
- [12] Niazi, S. K. Quantum mechanics in drug discovery: A comprehensive review of methods, applications, and future directions. *Int. J. Mol. Sci.* **26**, 6325 (2025).
- [13] Huber, S. P. *et al.* Common workflows for computing material properties using different quantum engines. *npj Comput. Mater.* **7**, 136 (2021).
- [14] Aspuru-Guzik, A. & Bernales, V. The rise of agents: Computational chemistry is ready for (r)evolution. *Polyhedron* **281**, 117707 (2025).
- [15] Wu, T., Sun, M. & Huang, B. A review of automated workflow pipelines for computational chemists. *Small Methods* **9**, 2500308 (2025).
- [16] Curtarolo, S. *et al.* Aflow: An automatic framework for high-throughput materials discovery. *Comput. Mater. Sci.* **58**, 218–226 (2012).
- [17] Pizzi, G., Cepellotti, A., Sabatini, R., Marzari, N. & Kozinsky, B. AiiDA: automated interactive infrastructure and database for computational science. *Comput. Mater. Sci.* **111**, 218–230 (2016).
- [18] Hjorth Larsen, A. *et al.* The atomic simulation environment—a python library for working with atoms. *J. Phys. Condens. Matter* **29**, 273002 (2017).

[19] Alegre-Requena, J. V., Sowndarya S. V., S., Pérez-Soto, R., Alturaifi, T. M. & Paton, R. S. Aqme: Automated quantum mechanical environments for researchers and educators. *WIREs Comput. Mol. Sci.* **13**, e1663 (2023).

[20] Hicks, C. B. & Martinez, T. J. Massively scalable workflows for quantum chemistry: BigChem and ChemCloud. *J. Chem. Phys.* **160**, 142501 (2024).

[21] Cohen, A. J., Mori-Sánchez, P. & Yang, W. Challenges for Density Functional Theory. *Chem. Rev.* **112**, 289–320 (2012).

[22] Bursch, M., Mewes, J.-M., Hansen, A. & Grimme, S. Best-practice DFT protocols for basic molecular computational chemistry. *Angew. Chem. Int. Ed.* **61**, e202205735 (2022).

[23] Wei, J. *et al.* From AI for science to agentic science: A survey on autonomous scientific discovery. Preprint at <https://arxiv.org/abs/2508.14111> (2025).

[24] Boiko, D. A., MacKnight, R., Kline, B. & Gomes, G. Autonomous chemical research with large language models. *Nature* **624**, 570–578 (2023).

[25] M. Bran, A. *et al.* Augmenting large language models with chemistry tools. *Nat. Mach. Intell.* **6**, 525–535 (2024).

[26] Darvish, K. *et al.* Organa: A robotic assistant for automated chemistry experimentation and characterization. *Matter* **8**, 101897 (2025).

[27] Ansari, M. & Moosavi, S. M. Agent-based learning of materials datasets from the scientific literature. *Digit. Discov.* **3**, 2607–2617 (2024).

[28] McNaughton, A. D. *et al.* Cactus: Chemistry agent connecting tool usage to science. *ACS Omega* **9**, 46563–46573 (2024).

[29] Ruan, Y. *et al.* An automatic end-to-end chemical synthesis development platform powered by large language models. *Nat. commun.* **15**, 10160 (2024).

[30] Dai, T. *et al.* Autonomous mobile robots for exploratory synthetic chemistry. *Nature* **635**, 890–897 (2024).

[31] Sprueill, H. W. *et al.* Chemreasoner: Heuristic search over a large language model’s knowledge space using quantum-chemical feedback. Preprint at <https://arxiv.org/abs/2402.10980> (2024).

[32] Song, T. *et al.* A multiagent-driven robotic AI chemist enabling autonomous chemical research on demand. *J. Am. Chem. Soc.* **147**, 12534–12545 (2025).

[33] Chen, K. *et al.* ChemMiner: A large language model agent system for chemical literature data mining. Preprint at <https://arxiv.org/abs/2402.12993> (2025).

[34] Tang, X. *et al.* ChemAgent: Self-updating library in large language models improves chemical reasoning. Preprint at <https://arxiv.org/abs/2501.06590> (2025).

[35] Yang, Z. *et al.* MOOSE-Chem: Large language models for rediscovering unseen chemistry scientific hypotheses. Preprint at <https://arxiv.org/abs/2410.07076> (2025).

[36] Yamada, Y. *et al.* The AI scientist-v2: Workshop-level automated scientific discovery via agentic tree search. Preprint at <https://arxiv.org/abs/2504.08066> (2025).

[37] Mitchener, L. *et al.* Kosmos: An AI scientist for autonomous discovery Preprint at <https://arxiv.org/abs/2511.02824> (2025).

[38] Liu, W. *et al.* MOOSE-Chem3: Toward experiment-guided hypothesis ranking via simulated experimental feedback. Preprint at <https://arxiv.org/abs/2505.17873> (2025).

[39] Li, Z. *et al.* ChemHAS: Hierarchical agent stacking for enhancing chemistry tools. Preprint at <https://arxiv.org/abs/2505.21569> (2025).

[40] Yu, B. *et al.* ChemToolAgent: The impact of tools on language agents for chemistry problem solving. Preprint at <https://arxiv.org/abs/2411.07228> (2025).

[41] Li, R. *et al.* LabUtopia: High-fidelity simulation and hierarchical benchmark for scientific embodied agents. Preprint at <https://arxiv.org/abs/2505.22634> (2025).

[42] Ma, K. AI agents in chemical research: GVIM – an intelligent research assistant system. *Digit. Discov.* **4**, 355–375 (2025).

[43] Kim, H., Jang, Y. & Ahn, S. MT-Mol: Multi agent system with tool-based reasoning for molecular optimization. Preprint at <https://arxiv.org/abs/2505.20820> (2025).

[44] Che, X. *et al.* Csstep: Step-by-step exploration of the chemical space of drug molecules via multi-agent and multi-stage reinforcement learning. *Chemical Engineering Science* **317**, 122048 (2025).

[45] Callahan, T. J., Park, N. H. & Capponi, S. Agentic mixture-of-workflows for multi-modal chemical search. Preprint at <https://arxiv.org/abs/2502.19629> (2025).

[46] Chen, K. *et al.* Chemist-X: Large language model-empowered agent for reaction condition recommendation in chemical synthesis. Preprint at <https://arxiv.org/abs/2311.10776> (2025).

[47] Inizan, T. J. *et al.* System of agentic AI for the discovery of metal-organic frameworks. Preprint at <https://arxiv.org/abs/2504.14110> (2025).

[48] Ghafarollahi, A. & Buehler, M. J. Automating alloy design and discovery with physics-aware multimodal multiagent AI. *Proc. Natl. Acad. Sci. U. S. A.* **122**, e2414074122 (2025).

[49] Pu, Y., Lin, T. & Chen, H. Piflow: Principle-aware scientific discovery with multi-agent collaboration. Preprint at <https://arxiv.org/abs/2505.15047> (2025).

[50] Ghafarollahi, A. & Buehler, M. J. Autonomous inorganic materials discovery via multi-agent physics-aware scientific reasoning. Preprint at <https://arxiv.org/abs/2508.02956> (2025).

[51] Wang, X. *et al.* S1-MatAgent: A planner driven multi-agent system for material discovery. Preprint at <https://arxiv.org/abs/2509.14542> (2025).

[52] Jia, S., Zhang, C. & Fung, V. Llmatdesign: Autonomous materials discovery with large language models. Preprint at <https://arxiv.org/abs/2406.13163> (2024).

[53] Ding, K. *et al.* SciToolAgent: a knowledge-graph-driven scientific agent for multitool integration. *Nature Computational Science* **5**, 962–972 (2025).

[54] Chiang, Y., Hsieh, E., Chou, C.-H. & Riebesell, J. LLaMP: Large language model made powerful for high-fidelity materials knowledge retrieval and distillation. Preprint at <https://arxiv.org/abs/2401.17244> (2024).

[55] Zhang, B. *et al.* TopoMAS: Large language model driven topological materials multiagent system. Preprint at <https://arxiv.org/abs/2507.04053> (2025).

[56] Petković, M., Menkovski, V. & Calero, S. Towards fully automated molecular simulations: Multi-agent framework for simulation setup and force field extraction. Preprint at <https://arxiv.org/abs/2509.10210> (2025).

[57] Zhou, L. *et al.* Toward greater autonomy in materials discovery agents: Unifying planning, physics, and scientists. Preprint at <https://arxiv.org/abs/2506.05616> (2025).

[58] Xia, Z. *et al.* An agentic framework for autonomous materials computation. Preprint at <https://arxiv.org/abs/2512.19458> (2025).

[59] Liu, J. *et al.* VASPilot: MCP-facilitated multi-agent intelligence for autonomous VASP simulations. *Chinese Physics B* **34**, 117106 (2025).

[60] Wang, Z. *et al.* DREAMS: Density Functional Theory based research engine for agentic materials simulation. Preprint at <https://arxiv.org/abs/2507.14267> (2025).

[61] Pham, T. D., Tanikanti, A. & Keçeli, M. ChemGraph: An agentic framework for computational chemistry workflows. Preprint at <https://arxiv.org/abs/2506.06363> (2025).

[62] Polat, C., Tuncel, M., Kurban, M., Serpedin, E. & Kurban, H. xChemAgents: Agentic AI for explainable quantum chemistry. Preprint at <https://arxiv.org/abs/2505.20574> (2025).

[63] Gadde, R. S. K. *et al.* Chatbot-assisted quantum chemistry for explicitly solvated molecules. *Chem. Sci.* **16**, 3852–3864 (2025).

[64] Chandrasekhar, A. & Farimani, A. B. Automating MD simulations for proteins using large language models: NAMD-agent. Preprint at <https://arxiv.org/abs/2507.07887> (2025).

[65] Campbell, Q., Cox, S., Medina, J., Watterson, B. & White, A. D. MDCrow: Automating molecular dynamics workflows with large language models. Preprint at <https://arxiv.org/abs/2502.09565> (2025).

[66] Shi, Z. *et al.* A fine-tuned large language model based molecular dynamics agent for code generation to obtain material thermodynamic parameters. *Sci. Rep.* **15**, 10295 (2025).

[67] Masters, C., Grześkiewicz, M. & Albrecht, S. V. Arcane: A multi-agent framework for interpretable and configurable alignment. Preprint at <https://arxiv.org/abs/2512.06196> (2025).

[68] Zou, Y. *et al.* El Agente: An autonomous agent for quantum chemistry. *Matter* **8**, 102263 (2025).

[69] Guilbert, S., Masschelein, C., Goumaz, J., Naida, B. & Schwaller, P. Dynamate: An autonomous agent for protein-ligand molecular dynamics simulations. Preprint at <https://arxiv.org/abs/2512.10034> (2025).

[70] Soleymanibrojeni, M. *et al.* Genius: An agentic AI framework for autonomous design and execution of simulation protocols. Preprint at <https://arxiv.org/abs/2512.06404> (2025).

[71] Lahouari, A., Rogal, J. & Tuckerman, M. E. Automated machine learning pipeline: Large language models-assisted automated data set generation for training machine-learned interatomic potentials. *J. Chem. Theory Comput.* **22**, 305–317 (2026).

[72] Li, W., Ren, J., Cheng, L. & Gong, C. Autonomous quantum simulation through large language model agents. Preprint at <https://arxiv.org/abs/2601.10194> (2026).

[73] Vriza, A., Kornu, U., Koneru, A., Chan, H. & Sankaranarayanan, S. K. R. S. Multi-agentic AI framework for end-to-end atomistic simulations. *Digit. Discov.* **5**, 440–452 (2026).

[74] Kim, S. *et al.* Materealize: a multi-agent deliberation system for end-to-end material design and synthesis. Preprint at <https://arxiv.org/abs/2601.15743> (2026).

[75] Hari Kumar, S. G. *et al.* El Agente Sólido: A new agent for solid state simulations (2026). Manuscript in preparation.

[76] Müller, M. *et al.* El Agente Fármaco: Agentic AI for autonomous in-silico drug discovery (2026). Manuscript in preparation.

[77] Choi, C. *et al.* El Agente Estructural: An agent for structural manipulation of molecular systems (2026). Manuscript in preparation.

[78] Gustin, I. *et al.* El Agente Cuántico: Automating quantum simulations. Preprint at <https://arxiv.org/abs/2512.18847> (2026).

[79] Bai, J. *et al.* El Agente Gráfico: Structured Execution Graph for Scientific Agents (2026). Manuscript in preparation.

[80] Kang, Y. *et al.* El Agente Seguro. (2026). Manuscript in preparation.

[81] Neese, F. The ORCA program system. *WIREs Comput. Mol. Sci.* **2**, 73–78 (2012).

[82] Neese, F. Software update: The ORCA program system—version 6.0. *WIREs Comput. Mol. Sci.* **15**, e70019 (2025).

[83] Campos-Gonzalez-Angulo, J. A., Linazzi Peracchi, M. L., Aldossari, A. & Aspuru-Guzik, A. Hund’s rule: reloaded - a modern take on the alternating rule and unnatural parity in atoms (2026). Manuscript in preparation.

[84] Wang, B. *et al.* Mineru: An open-source solution for precise document content extraction. Preprint at <https://arxiv.org/abs/2409.18839> (2024).

[85] The Matter Lab. Replication data for: El Agente Quntur: A research collaborator agent for computational quantum chemistry. Available at <https://borealisdata.ca/dataset.xhtml?persistentid=doi:10.5683/sp3/rdsoea> (2026).

[86] Lippert, E., Lüder, W. & Boß, H. Über die duale fluoreszenz aromatischer aminverbindungen. In Mangini, A. (ed.) *Advances in Molecular Spectroscopy*, 443–461 (Pergamon Press, Oxford, 1962). Proceedings of the International Meeting on Molecular Spectroscopy.

[87] Georgieva, I. *et al.* Intramolecular charge-transfer excited-state processes in 4-(n,n-dimethylamino)benzonitrile: The role of twisting and the  $\pi\sigma^*$  state. *J. Phys. Chem. A* **119**, 6232–6243 (2015).

[88] Pettersen, E. F. *et al.* Ucsf chimeraX: Structure visualization for researchers, educators, and developers. *Protein Sci.* **30**, 70–82 (2021).

[89] Meng, E. C. *et al.* UCSF ChimeraX: Tools for structure building and analysis. *Protein Sci.* **32**, e4792 (2023).

[90] de Souza, B., Neese, F. & Izsák, R. On the theoretical prediction of fluorescence rates from first principles using the path integral approach. *J. Chem. Phys.* **148**, 034104 (2018).

[91] de Souza, B., Farias, G., Neese, F. & Izsák, R. Predicting phosphorescence rates of light organic molecules using time-dependent Density Functional Theory and the path integral approach to dynamics. *J. Chem. Theory Comput.* **15**, 1896–1904 (2019).

[92] Becke, A. D. Density-functional thermochemistry. III. The role of exact exchange. *J. Chem. Phys.* **98**, 5648–5652 (1993).

[93] Lee, C., Yang, W. & Parr, R. G. Development of the Colle-Salvetti correlation-energy formula into a functional of the electron density. *Phys. Rev. B* **37**, 785–789 (1988).

[94] Stephens, P. J., Devlin, F. J., Chabalowski, C. F. & Frisch, M. J. Ab Initio Calculation of Vibrational Absorption and Circular Dichroism Spectra Using Density Functional Force Fields. *J. Phys. Chem.* **98**, 11623–11627 (1994).

[95] Lin, Y. S., Li, G. D., Mao, S. P. & Chai, J. D. Long-range corrected hybrid density functionals with improved dispersion corrections. *J. Chem. Theory Comput.* **9**, 263–272 (2013).

[96] Mills, G., Jónsson, H. & Schenter, G. K. Reversible work transition state theory: application to dissociative adsorption of hydrogen. *Surf. Sci.* **324**, 305–337 (1995).

[97] Berne, B. J., Ciccotti, G. & Coker, D. F. *Classical and Quantum Dynamics in Condensed Phase Simulations* (WORLD SCIENTIFIC, 1998).

[98] Henkelman, G. & Jónsson, H. Improved tangent estimate in the nudged elastic band method for finding minimum energy paths and saddle points. *J. Chem. Phys.* **113**, 9978–9985 (2000).

[99] Musaev, D. G., Froese, R. D. J., Svensson, M. & Morokuma, K. A density functional study of the mechanism of the diimine-nickel-catalyzed ethylene polymerization reaction. *J. Am. Chem. Soc.* **119**, 367–374 (1997).

[100] Maiti, S. R., Buttar, D. & Duarte, F. Benchmark of double-ended transition state search methods for metal-catalysed reactions. Preprint at <https://chemrxiv.org/doi/abs/10.26434/chemrxiv-2025-hssg2> (2025).

[101] Pinter, B., Van Speybroeck, V., Waroquier, M., Geerlings, P. & De Proft, F. trans effect and trans influence: importance of metal mediated ligand–ligand repulsion. *Phys. Chem. Chem. Phys.* **15**, 17354–17365 (2013).

[102] Zumdahl, S. S. & Drago, R. S. A molecular orbital study of the trans influence and kinetic trans effect in square-planar platinum(II) complexes. *J. Am. Chem. Soc.* **90**, 6669–6675 (1968).

[103] Lv, T. *et al.* Atomworld: A benchmark for evaluating spatial reasoning in large language models on crystalline materials. Preprint at <https://arxiv.org/abs/2510.04704> (2025).

[104] Yamada, Y., Bao, Y., Lampinen, A. K., Kasai, J. & Yildirim, I. Evaluating spatial understanding of large language models. Preprint at <https://arxiv.org/abs/2310.14540> (2024).

[105] Jang, Y., Kim, J. & Ahn, S. Structural reasoning improves molecular understanding of LLM. Preprint at <https://arxiv.org/abs/2410.05610> (2025).

[106] Barone, V. & Cossi, M. Quantum calculation of molecular energies and energy gradients in solution by a conductor solvent model. *J. Phys. Chem. A* **102**, 1995–2001 (1998).

[107] Marenich, A. V., Cramer, C. J. & Truhlar, D. G. Universal solvation model based on solute electron density and on a continuum model of the solvent defined by the bulk dielectric constant and atomic surface tensions. *J. Phys. Chem. B* **113**, 6378–6396 (2009).

[108] Hughes, W., Popescu, M. & Paton, R. Fundamental study of Density Functional Theory applied to triplet state reactivity: Introduction of the trip50 dataset. Preprint at <https://chemrxiv.org/doi/abs/10.26434/chemrxiv-2025-zfrhn> (2025).

[109] Zhang, Z. *et al.* El Agente Forjador: Task-driven agent generation for quantum simulation (2026). Manuscript in preparation.

[110] Epifanovsky, E. *et al.* Software for the frontiers of quantum chemistry: An overview of developments in the Q-Chem 5 package. *J. Chem. Phys.* **155**, 084801 (2021).

[111] Frisch, M. J. *et al.* Gaussian™16 Revision C.01 (2016). Gaussian Inc. Wallingford CT.

[112] Fdez. Galván, I. *et al.* OpenMolcas: From source code to insight. *J. Chem. Theory Comput.* **15**, 5925–5964 (2019).

[113] Sun, Q. *et al.* PySCF: the python-based simulations of chemistry framework. *WIREs Comput. Mol. Sci.* **8**, e1340 (2018).

[114] Alexeev, Y., P. Mazanetz, M., Ichihara, O. & G. Fedorov, D. GAMESS as a free quantum-mechanical platform for drug research. *Curr. Top. Med. Chem.* **12**, 2013–2033 (2012).

[115] Turney, J. M. *et al.* Psi4: an open-source ab initio electronic structure program. *WIREs Comput. Mol. Sci.* **2**, 556–565 (2012).

[116] Ser, C. T. *et al.* Bulky Phosphine ligands promote Palladium-catalyzed protodeboronation. *J. Am. Chem. Soc.* **147**, 43884–43901 (2025).

[117] Tom, G. *et al.* Self-driving laboratories for chemistry and materials science. *Chem. Rev.* **124**, 9633–9732 (2024).

[118] Grimme, S., Bannwarth, C. & Shushkov, P. A Robust and Accurate Tight-Binding Quantum Chemical Method for Structures, Vibrational Frequencies, and Noncovalent Interactions of Large Molecular Systems Parametrized for All spd-Block Elements (Z = 1–86). *J. Chem. Theory Comput.* **13**, 1989–2009 (2017).

[119] Bannwarth, C., Ehlert, S. & Grimme, S. GFN2-xTB - An Accurate and Broadly Parametrized Self-Consistent Tight-Binding Quantum Chemical Method with Multipole Electrostatics and Density-Dependent Dispersion Contributions. *J. Chem. Theory Comput.* **15**, 1652–1671 (2019).

[120] Bannwarth, C. *et al.* Extended tight-binding quantum chemistry methods. *WIREs Comput. Mol. Sci.* **11**, 1–49 (2021).

[121] Jacobs, P. F. & Pollice, R. Developing large language models for quantum chemistry simulation input generation. *Digit. Discov.* **4**, 762–775 (2025).

[122] Weigend, F. & Ahlrichs, R. Balanced basis sets of split valence, triple zeta valence and quadruple zeta valence quality for H to Rn: Design and assessment of accuracy. *Phys. Chem. Chem. Phys.* **7**, 3297–3305 (2005).

[123] van Lenthe, E., Baerends, E. J. & Snijders, J. G. Relativistic regular two-component Hamiltonians. *J. Chem. Phys.* **99**, 4597–4610 (1993).

[124] Dunning, T. H. Gaussian basis sets for use in correlated molecular calculations. i. the atoms boron through neon and hydrogen. *J. Chem. Phys.* **90**, 1007–1023 (1989).

[125] Kendall, R. A., Dunning, T. H. & Harrison, R. J. Electron affinities of the first-row atoms revisited. systematic basis sets and wave functions. *J. Chem. Phys.* **96**, 6796–6806 (1992).

[126] Guo, Y. *et al.* Communication: An improved linear scaling perturbative triples correction for the domain based local pair-natural orbital based singles and doubles coupled cluster method [DLPNO-CCSD(T)]. *J. Chem. Phys.* **148**, 011101 (2018).

[127] de Souza, B. GOAT: A Global Optimization Algorithm for Molecules and Atomic Clusters. *Angew. Chem. Int. Ed.* **64**, e202500393 (2025).

[128] Grimme, S., Hansen, A., Ehlert, S. & Mewes, J. M. R2SCAN-3c: A "Swiss army knife" composite electronic-structure method. *J. Chem. Phys.* **154**, 64103 (2021).

[129] Grimme, S., Antony, J., Ehrlich, S. & Krieg, H. A consistent and accurate ab initio parametrization of density functional dispersion correction (DFT-D) for the 94 elements H–Pu. *J. Chem. Phys.* **132**, 154104 (2010).

[130] Grimme, S., Ehrlich, S. & Goerigk, L. Effect of the damping function in dispersion corrected density functional theory. *J. Comp. Chem.* **32**, 1456–1465 (2011).

[131] Adamo, C. & Barone, V. Toward reliable density functional methods without adjustable parameters: The PBE0 model. *J. Chem. Phys.* **110**, 6158–6170 (1999).

[132] Hehre, W. J., Ditchfield, R. & Pople, J. A. Self-consistent molecular orbital methods. xii. further extensions of gaussian-type basis sets for use in molecular orbital studies of organic molecules. *J. Chem. Phys.* **56**, 2257–2261 (1972).

[133] Chai, J.-D. & Head-Gordon, M. Long-range corrected hybrid density functionals with damped atom–atom dispersion corrections. *Phys. Chem. Chem. Phys.* **10**, 6615–6620 (2008).

[134] Yanai, T., Tew, D. P. & Handy, N. C. A new hybrid exchange–correlation functional using the Coulomb-attenuating method (CAM-B3LYP). *Chem. Phys. Lett.* **393**, 51–57 (2004).

[135] Geerlings, P., De Proft, F. & Langenaeker, W. Conceptual Density Functional Theory. *Chem. Rev.* **103**, 1793–1874 (2003).

[136] Gorenstein, D. G. Non-biological aspects of phosphorus-31 NMR spectroscopy. *Prog. Nucl. Magn. Reson. Spectrosc.* **16**, 1–98 (1984).

[137] Hersh, W. H. & Chan, T.-Y. Improving the accuracy of 31P NMR chemical shift calculations by use of scaling methods. *Beilstein J. Org. Chem.* **19**, 36–56 (2023).

[138] Huszár, B., Mucsi, Z. & Keglevich, G. Microwave-assisted P–C coupling of the less reactive chlorobenzene and  $>\text{P}(\text{O})\text{H}$  reagents in the absence of the usual mono- and bidental P-ligands. *Molecules* **30**, 1045 (2025).

[139] Spange, S., Weiß, N., Schmidt, C. H. & Schreiter, K. Reappraisal of empirical solvent polarity scales for organic solvents. *Chem. Methods* **1**, 42–60 (2020).

[140] Kennedy, J. D. & McFarlane, W. Phosphorus-31 chemical shift anisotropies in organophosphorus compounds. *J. Chem. Soc., Chem. Commun.* 666 (1976).

[141] Rzepiela, K., Kaminský, J., Buczek, A., Broda, M. A. & Kupka, T. Electron correlation or basis set quality: How to obtain converged and accurate NMR shieldings for the third-row elements? *Molecules* **27**, 8230 (2022).

[142] Fukal, J., Páv, O., Buděšínský, M., Šebera, J. & Sychrovský, V. The benchmark of 31P NMR parameters in phosphate: a case study on structurally constrained and flexible phosphate. *Phys. Chem. Chem. Phys.* **19**, 31830–31841 (2017).

[143] Rusakov, Y. Y. & Rusakova, I. L. New efficient pecS-n ( $n = 1, 2$ ) basis sets for quantum chemical calculations of 31P NMR chemical shifts. *Phys. Chem. Chem. Phys.* **25**, 18728–18741 (2023).

[144] Lagier, C. M. *et al.* Solution and solid state proton transfer from phenols to triphenylphosphine oxide studied by 1H, 13C and 31P NMR spectroscopy. *J. Chem. Soc., Perkin Trans. 2* 1325 (1996).

[145] Pascual-Borràs, M., López, X. & Poblet, J. M. Accurate calculation of 31P NMR chemical shifts in polyoxometalates. *Phys. Chem. Chem. Phys.* **17**, 8723–8731 (2015).

[146] Rusakova, I. L. Quantum chemical approaches to the calculation of NMR parameters: From fundamentals to recent advances. *Magnetochemistry* **8**, 50 (2022).

[147] Shenderovich, I. G. 1,3,5-triaza-7-phosphaadamantane (pta) as a 31P NMR probe for organometallic transition metal complexes in solution. *Molecules* **26**, 1390 (2021).

[148] Kondrashova, S. A., Polyancev, F. M. & Latypov, S. K. DFT calculations of 31P NMR chemical shifts in palladium complexes. *Molecules* **27**, 2668 (2022).

[149] Klose, G., Trahms, L. & Möps, A. Chemical shift anisotropy of 31P in phosphonic acids and their esters. *Chem. Phys. Lett.* **122**, 545–549 (1985).

[150] Larina, L. Organophosphorus azoles incorporating a tetra-, penta-, and hexacoordinated phosphorus atom: NMR spectroscopy and quantum chemistry. *Molecules* **28**, 669 (2023).

[151] Ostras, A. S., Ivanov, D. M., Novikov, A. S. & Tolstoy, P. M. Phosphine oxides as spectroscopic halogen bond descriptors: IR and NMR correlations with interatomic distances and complexation energy. *Molecules* **25**, 1406 (2020).

[152] Badillo-Camacho, J., Gutiérrez-Ortega, J. A., Shenderovich, I. G., Velázquez-Galván, Y. G. & Manríquez-González, R. Monitoring lead–phosphorus interactions through 31P-NMR used as a sensor in phosphine functionalized silica gel adsorbent. *Gels* **11**, 580 (2025).

[153] Iglesias, E. Determination of keto–enol equilibrium constants and the kinetic study of the nitrosation reaction of  $\beta$ -dicarbonyl compounds. *J. Chem. Soc., Perkin Trans. 2* 431–440 (1997).

[154] Mehrani, S., Tayyari, S., Heravi, M. & Morsali, A. Theoretical investigation of solvent effect on the keto–enol tautomerization of pentane-2, 4-dione and a comparison between experimental data and theoretical calculations. *Can. J. Chem.* **99**, 411–424 (2021).

[155] Ser, C. T. *et al.* Bulky phosphine ligands promote palladium-catalyzed protodeboronation. *J. Am. Chem. Soc.* **147** (2025).

[156] Scholes, G. D., Fleming, G. R., Olaya-Castro, A. & van Grondelle, R. Lessons from nature about solar light harvesting. *Nat. Chem.* **3**, 763–774 (2011).

[157] Forrest, S. R. The path to ubiquitous and low-cost organic electronic appliances on plastic. *Nature* **428**, 911–918 (2004).

[158] Grabowski, Z. R., Rotkiewicz, K. & Rettig, W. Structural changes accompanying intramolecular electron transfer: Focus on twisted intramolecular charge-transfer states and structures. *Chem. Rev.* **103**, 3899–4032 (2003).

[159] Tozer, D. J. & Handy, N. C. On the determination of excitation energies using Density Functional Theory. *Phys. Chem. Chem. Phys.* **2**, 2117–2121 (2000).

[160] Dreuw, A. & Head-Gordon, M. Failure of Time-Dependent Density Functional Theory for long-range charge-transfer excited states: The Zincbacteriochlorin-bacteriochlorin and Bacteriochlorophyll-spheroidene complexes. *J. Am. Chem. Soc.* **126**, 4007–4016 (2004).

[161] Adachi, C. Third-generation organic electroluminescence materials. *Jpn. J. Appl. Phys.* **53**, 060101 (2014).

[162] de Silva, P., Kim, C. A., Zhu, T. & Van Voorhis, T. Extracting design principles for efficient thermally activated delayed fluorescence (TADF) from a simple four-state model. *Chem. Mater.* **31**, 6995–7006 (2019).

[163] Faulstich, F. M. *et al.* Numerical and theoretical aspects of the dmrg-tcc method exemplified by the Nitrogen dimer. *J. Chem. Theory Comput.* **15**, 2206–2220 (2019).

[164] Boyn, J.-N. & Mazziotti, D. A. Elucidating the molecular orbital dependence of the total electronic energy in multireference problems. *J. Chem. Phys.* **156** (2022).

[165] Chattopadhyay, S. Investigation of multiple-bond dissociation using brillouin–wigner perturbation with improved virtual orbitals. *J. Phys. Chem. A* **124**, 1444–1463 (2020).

[166] Aroeira, G. J., Davis, M. M., Turney, J. M. & Schaefer III, H. F. Coupled cluster externally corrected by adaptive configuration interaction. *J. Chem. Theory Comput.* **17**, 182–190 (2020).

[167] Ashida, Y. *et al.* Catalytic Nitrogen fixation using visible light energy. *Nat. commun.* **13**, 7263 (2022).

[168] Chen, Z., Liu, C., Sun, L. & Wang, T. Progress of experimental and computational catalyst design for electrochemical Nitrogen fixation. *ACS Catalysis* **12**, 8936–8975 (2022).

[169] Weaving, T., Ralli, A., Love, P. J., Succi, S. & Coveney, P. V. Contextual subspace variational quantum eigensolver calculation of the dissociation curve of molecular Nitrogen on a superconducting quantum computer. *Npj Quantum Inf.* **11**, 25 (2025).

[170] Choi, S., Loaiza, I., Lang, R. A., Martínez-Martínez, L. A. & Izmaylov, A. F. Probing quantum efficiency: Exploring system hardness in electronic ground state energy estimation. *J. Chem. Theory Comput.* **20**, 5982–5993 (2024).

[171] Musaev, D. G., Froese, R. D. J., Svensson, M. & Morokuma, K. A density functional study of the mechanism of the Diimine-Nickel-catalyzed Ethylene polymerization reaction. *J. Am. Chem. Soc.* **119**, 367–374 (1997).

## Acknowledgments

We gratefully acknowledge the longstanding contributions of the Matter Lab's current and past group members ([matter.toronto.edu](http://matter.toronto.edu)), and in particular from El Agente's team. I.G., J.A.C.G.A, and J.B.P.S. acknowledge funding of this project by the National Sciences and Engineering Research Council of Canada (NSERC) Alliance Grant #ALLRP587593-23 (Quantamole). T. W. K. acknowledges the support of the Vector Distinguished Postdoctoral Fellowship. J.A.C.G.A acknowledges support from the Council for Science, Technology and Innovation (CSTI), Cross-ministerial Strategic Innovation Promotion Program (SIP), "Promoting the application of advanced quantum technology platforms to social issues" (Funding agency: QST). A. W. acknowledges support from NSERC through their Canada Graduate Scholarships - Doctoral (CGS-D) program as well as support from the Lawson Climate Institute. C.C. acknowledges support from the DOE grant with the University of Minnesota award #A006801504 and the Basic Science Research Program through the National Research Foundation of Korea (NRF) funded by the Ministry of Education (RS-2025-02634334). A.A.-G. thanks Anders G. Frøseth for his generous support. A.A.-G. and V.B. acknowledge the generous support of Natural Resources Canada and the Canada 150 Research Chairs program and the University of Toronto's Acceleration Consortium, which receives funding from the CFREF-2022-00042 Canada First Research Excellence Fund. This work was supported by the AI2050 program of Schmidt Sciences.

## Supporting Information

### A List of Agents

In this section, we summarize the agents that constitute EL AGENTE QUNTUR.

**Table 2** Agent roster

Label	Description
autoci_expert	Configures internally contracted multi-reference (FIC-MR) methods using canonical orbitals
basis_expert	Defines the primary orbital basis and auxiliary fitting bases, segmented vs general contraction, decontracting, adding polarization/diffuse functions, element-specific basis overrides, and other basis-related settings
casresp_expert	Provides keywords or blocks that configure CASSCF response property calculations
casscf_expert	Provides casscf settings for multiconfigurational SCF calculations
cim_expert	Configures Cluster-in-Molecule (CIM) settings
cis_tddft_expert	Provides computational settings for excited-state calculations using Configuration Interaction Singles (CIS), Time-Dependent Density Functional Theory (TDDFT), and Spin-Flip TDA (SF-TDA)
compound_expert	Expert on ORCA's embedded scripting/driver language compound
computational_chemist	Designs high-level plans, delegates all engine-specific details to specialist agents, and perform post-analysis
configuration_recommender	Recommend a suitable wavefunction method, DFT functional, semi-empirical method, as well as suggests when dispersion corrections are needed, that fits the user request
conical_expert	Controls how ORCA searches conical intersections (CIs) between two electronic states
cosmors_expert	cosmors configures the OpenCOSMO-RS solvation interface in ORCA
cpcm_expert	Controls settings for implicit solvation modeling using the Conductor-like Polarizable Continuum Model or other solvation models
docker_expert	Performs automated docking of one or more GUEST structures onto a HOST
el_prop_expert	The elprop expert provides settings for calculating electrical properties: dipole, quadrupole, static/dynamic polarizabilities, mixed dipole-quadrupole and quadrupole-quadrupole polarizabilities
eprnmr_expert	The eprnmr expert configures EPR and NMR property calculations
esd_expert	The esd expert configures excited-state kinetics and spectroscopic calculations including vibronic effects
freq_expert	Controls frequency analysis, sets numerical differentiation controls, applies frequency scaling, controls projection/invariance, thermochemistry (T, P), and other related tasks
geom_expert	Set up geometry constraints, relaxed (not rigid) scans (1D or simultaneous), TS search, non-default step/trust/tolerances, Hessian control, fragment connectivity/constraints, external optimizer hooks, or wall potentials
geometry_generation	Handles the initial geometry creation process with diverse toolkits
geometry_operator	Perform arbitrary geometry editing
geometry_optimization	Expert that optimizes molecular geometries at different levels of theory
geometry_section	Generates the ORCA geometry section, referencing external xyz files, inline coordinates, or internal coordinates
goat_expert	Configures ORCA's GOAT global optimizer, controlling workers, iterations, conformer filtering, entropy-based stopping, and optional free-topology/reactive settings
ice_expert	Configures Iterative Configuration Expansion CI
imaginary_frequency_expert	Handles imaginary-frequency analysis and correction, including selective mode removal and verification

**Table 3** Agent roster (continuation)

Label	Description
input_file_service	Creates and debugs ORCA 6.0 input files using the ORCA manual and scientific literature
input_keywords_expert	Controls ORCA input keywords and legacy ORCA blocks (e.g., base, maxcore, moinp, pointcharges)
interact_with_os_and_files	Performs file-system operations such as reading, parsing, moving, copying, and deleting files
irc_expert	Configures Intrinsic Reaction Coordinate (IRC) calculations from transition states
loc_expert	loc expert provides loc settings to control post-SCF molecular orbital localization (e.g., Pipek-Mezey or Foster-Boys)
mcrpa_expert	Provides settings to computes excitation energies and transition properties from the linear response of a converged CASSCF reference
md_expert	Configures and runs ORCA's ab initio molecular dynamics (AIMD) and related MD tools
mdci_expert	Configures Matrix Driven Configuration Interaction engine for correlated wavefunction methods and excited-state solvers
mecp_expert	Configures Minimum Energy Crossing Point (MECP) optimizations to find the lowest-energy geometry where two potential energy surfaces (PES1 and PES2) intersect
metal_complex_geometry_generation	Generates metal complex geometry files
method_expert	Configures global, method-level options shared across ORCA modules
mp2_expert	Configures second-order Møller-Plesset correlation
mrcc_expert	Links ORCA to Mihael Kállay's MRCC program. It selects high-level coupled-cluster methods (e.g., CCSDT, CC3, CCSD(T) variants) to run on an SCF reference produced by ORCA
mrci_expert	Configures ORCA's traditional uncontracted multi-reference correlation module (orca_mrci)
mtr_expert	Performs mode tracking scans along selected vibrational normal modes using a precomputed Hessian
nbo_expert	Forwards literal NBO keylists (\$NBO, \$DEL, etc.) from ORCA to an external NBO6/7 executable
ndoparas_expert	Customizes semiempirical NDO model parameters (CNDO/INDO/NDDO) by setting element- and index-specific constants, INDO/S interaction factors, and the INDO/S Coulomb-integral parameter
neb_expert	Configures the Nudged Elastic Band (NEB) method to locate a minimum energy path (MEP) between given reactant and product structures
numgrad_expert	Configures numerical differentiation for energy gradients
orca_plotting_agent	Generating visualizations using orca utility programs and other tools
output_expert	Controls properties to be printed in the output
pal_expert	Controls settings for parallel execution across multiple processors or nodes
paras_expert	Defines named numeric parameters (scalars, ranges, or explicit lists) for later substitution elsewhere in the input
plots_expert	Defines settings for the input file to generate 2D contour plots and 3D surface plots for atomic/molecular/natural/corresponding orbitals and (spin) densities
quantum_chemistry_calculation_expert	Expert in performing wavefunction-based quantum chemistry calculations, semi-empirical calculations, DFT calculations, conformer search, molecular dynamics calculations, DOCKER for posing pairs of molecules, explicit solvation, and all other calculations supported by ORCA 6.0
rel_expert	Controls relativistic Hamiltonians and spin-orbit coupling (SOC) operators. Provides settings for scalar-relativistic methods (DKH/ZORA/IO-RA/X2C), picture-change effects for properties, finite nucleus models, and detailed construction of spin orbit couplings

**Table 4** Agent roster (continuation)

Label	Description
rocis_expert	Configures calculations of excited states via ROCIS (CIS on ROHF/UHF/RHF references) and spectra
rr_expert	The rr expert configures resonance Raman-related tasks that rely on a precomputed nuclear Hessian
run_orca	Slurm Job Submitter. Submit Slurm job/jobs to HPC to run ORCA calculations
runtypes_keyword_expert	This expert provides runtype keywords for basic calculation settings (SP, EnergyGrad, Opt, FREQ, PrintThermoChem, PropertiesOnly, EDA, HF, DFT, FREQ, etc)
scf_expert	Controls the target precision of the energy and the wavefunction
solvator_expert	Configures automatic explicit solvation of molecules
symmetry_expert	The symmetry expert controls symmetry handling for a calculation

## B The benchmark set

**Table 5 The benchmark.** A set of 17 computational quantum chemistry exercises covering several topics from electronic and magnetic properties, thermodynamics, kinetics, and spectroscopy, as well as various levels of theory.

Field	Topic	Level of theory	Question
Electronic and magnetic properties	Relativistic Corrections	DFT/ZORA ZORA-def2-TZVP [122, 123]	Calculate the $^{195}\text{Pt}$ NMR shielding constant of the square-planar Pt(II) complex $[\text{PtCl}_4]^{2-}$ using ORCA. Compare two methods: a non-relativistic DFT/PBE0-D4 NMR calculation with a def2-TZVP basis, and a scalar-relativistic DFT/PBE0-D4/ZORA calculation using the ZORA-def2-TZVP basis. Generate a final Markdown report.
	Electrical Properties	MP2/aug-cc-pVDZ [124, 125]	Compute the permanent dipole moment and the static polarizability tensor of nitrobenzene. Then compare these values to those of benzene and explain how the $-\text{NO}_2$ substituent alters the molecular charge distribution and the anisotropy of the polarizability. Use MP2/aug-cc-pVDZ for all calculations. Generate a final markdown report.
	Orbitals and Densities	UHF/cc-pVDZ [124]	Visualize and analyze the SOMO and spin density of the Piperidine N-oxide radical and the pyridinium N-oxide cation radical; compare their radical stabilities. Use UHF/cc-pVDZ. Generate a final markdown report.
	Condensed Fukui Functions	ROHF/cc-pVTZ [124]	Using ROHF/cc-pVTZ, compute condensed Fukui functions $f^+$ (for nucleophilic attack) and $f^-$ (for electrophilic attack) for the carbon atoms in toluene using ORCA by finite-difference of electron number (N, N+1, N-1). Compare the condensed Fukui indices for different population schemes (Mulliken, Hirshfeld, and Loewdin). Generate a final markdown report.
Thermodynamics	Thermochemistry	DLPNO-CCSD(T)/def2-TZVPP [122, 126]	Using DLPNO-CCSD(T)/def2-TZVPP, use a thermodynamic cycle to compute $\Delta G_{\text{deprot}}$ for acetic acid in the gas phase and in water (implicit solvent). Compute the predicted pKa. Generate a final markdown report.
	Conformer Generation	GFN2-xTB and B3LYP/def2-SVP [92–94, 119]	Using ORCA GOAT [127], generate a diverse set of conformers for serine at the GFN2-xTB level. Re-optimize at a B3LYP/def2-SVP level and identify the lowest-energy structure. Compute Boltzmann populations at 298 K in the gas phase. Generate a final markdown report.
	Molecular Dynamics	GFN2-xTB [119, 128]	Simulate a hydrated chloride ion cluster, $\text{Cl}^-(\text{H}_2\text{O})_n$ ( $n \geq 12$ ) at 300 K using AIMD. From the trajectory, compute the Cl-O radial distribution function $g(\text{Cl}-\text{O})$ and coordination number. Use GFN2-xTB. Simulate 0.1 ps with a 1 fs timestep after equilibration. Generate a final markdown report.
	Explicit solvation	$r^2\text{SCAN-3c}$ [128]	Build explicit microsolvated clusters of acetic acid with 3, 5, and 7 water molecules [ $\text{AcOH} \cdot (\text{H}_2\text{O})_n$ ] and optimize with $r^2\text{SCAN-3c}$ in the gas phase and with CPCM water. Compute deprotonation free energies for each cluster size and compare the convergence of the predicted pKa toward experiment as $n$ increases. Generate a final markdown report.
Kinetics	Potential Energy Surfaces	CASSCF(4,4)/cc-pVDZ [124]	Using CASSCF(4,4)/cc-pVDZ, calculate the potential energy surface for rotation between s-cis and s-trans butadiene conformers. Identify all stationary points along the dihedral: both minima and the maximum energy structure. Compute the energy barrier and generate a final markdown report.
	Transition State Methods	PBE0-D3(BJ)/def2-TZVP [122, 129–131]	Set up a nudged elastic band (NEB) calculation in ORCA for the double proton transfer in the formic acid dimer. Use the optimized symmetric dimer as the reactant and the fully transferred dimer as the product, generate a reasonable band of images, and refine the NEB path to obtain an approximate transition structure. Then perform an OPTTS calculation starting from the highest-energy NEB image and follow it by an IRC to obtain $\Delta G^\ddagger$ , $\Delta H^\ddagger$ , and $\Delta S^\ddagger$ for the process. Use PBE0-D3(BJ)/def2-TZVP in all calculations. Generate a final markdown report.
	Reaction Mechanisms	MP2/cc-pVTZ [124]	Using MP2/cc-pVTZ, locate and verify the transition state for the chloride attack on methyl chloride. Validate connectivity using IRC. Extract $\Delta G^\ddagger$ , $\Delta H^\ddagger$ , and $\Delta S^\ddagger$ . Generate a final markdown report.
	Isotopic Effects	HF/6-31G(d) [132]	Consider the solvolysis of para-substituted benzyl chlorides as a model $\text{S}_{\text{N}}1$ reaction in implicit water. Use ORCA to compute secondary kinetic isotope effects by substituting ring hydrogen atoms with deuterium and evaluating $\Delta G^\ddagger$ for H and D cases. Analyze how changes in hybridization and resonance stabilization between the ground state and carbocation intermediate influence the magnitude and sign of the secondary KIE. Use HF/6-31G(d) for all calculations. Generate a final markdown report.

**Table 6 The benchmark (continuation).** A set of 17 computational quantum chemistry exercises covering several topics from electronic and magnetic properties, thermodynamics, kinetics, and spectroscopy, as well as various levels of theory.

Field	Topic	Level of theory	Question
Spectroscopy	Excited States	TD-DFT (PBE0 / $\omega$ B97X-D)/def2-TZVP [122, 131, 133]	Compare TD-DFT excitation energies of <i>p</i> -nitroaniline using PBE0 and $\omega$ B97X-D, both using the def2-TZVP basis set. Generate a final markdown report.
	Excited-State Kinetics	TD-DFT CAM-B3LYP/def2-TZVP [122, 134]	Compute the fluorescence rate of formaldehyde from the S <sub>1</sub> state using TDDFT CAM-B3LYP def2-TZVP. Assume gas phase. Generate a final markdown report.
	NMR and Magnetic Properties	HF/aug-cc-pVTZ [124, 125]	Using HF/aug-cc-pVTZ, compute <sup>19</sup> F and <sup>1</sup> H chemical shifts for fluorobenzene and pentafluorobenzene. Compare shielding changes with respect to substituent effects, ring current anisotropy, and substituent inductive/mesomeric effects. Generate a final markdown report.
	Vibrational Spectroscopy	CCSD/cc-pVDZ [124]	Using CCSD/cc-pVDZ, compute vibrational spectra for H <sub>2</sub> O and D <sub>2</sub> O and compare theoretical isotopic shifts against $\sqrt{\mu_D/\mu_H}$ scaling predictions. Generate a final markdown report.
	Custom Optimizations	TD-DFT CAM-B3LYP/6-31G [132, 134]	Locate (i) the S <sub>0</sub> /T <sub>1</sub> MECP and (ii) the S <sub>0</sub> /S <sub>1</sub> CI for twisted ethylene (C <sub>2</sub> H <sub>4</sub> ). Use TDDFT/TDA with CAM-B3LYP/6-31G; employ spin-flip TDDFT where necessary to ensure a stable description in the biradical region near the CI or MECP. Start from a 90° twisted geometry. Report optimized geometries and final residual gaps at convergence. Produce a Markdown report.

## C Evaluation of EL AGENTE QUNTUR on the benchmark set

### C.1 General evaluation rubric for benchmark questions

The following is a general rubric to evaluate the performance of EL AGENTE QUNTUR on the benchmark set (see Table 2 in the manuscript). The percentages shown are default and are subsequently adjusted to adapt to each problem (e.g., geometry-generation percentages are increased for geometry-heavy tasks).

#### C.1.1 Planning (~15%)

- **Efficiency:** Calculations that are independent of each other are executed in parallel, while calculations that require outputs from previous steps are executed sequentially.
- **Flexibility:** The computational plan is modified by the agent when needed (e.g., upon failure, convergence issues, or new information). These methodological deviations must be properly justified.
- **Scientific validity:** The final computational plan answers the prompt.

#### C.1.2 Geometry Generation (~20%)

- **Geometries generated correctly:** All required geometries for the task are generated.
- **Additional geometry-related tasks:** Correct handling of geometry-related operations such as distortions, trajectory files, in-line geometry sections, use of internal coordinates, or inclusion of isotopic effects, etc.

#### C.1.3 Input File Generation and Execution (~35%)

Multiple computational strategies are acceptable as long as the input is internally consistent, executable, and appropriate for the task. The input file is validated during execution. Therefore, if there is nothing obviously incorrect, the calculation completes successfully, and the final numbers are correct, the input file is considered correct.

#### Keyword Line

- Correct run type for the task (e.g., OPT, FREQ, SP, IRC).
- Correct method choice for the problem.

- Correct basis set.

*Extra keywords are acceptable if optional and non-conflicting.*

### Blocks

- All necessary blocks for the task are present.
- Commands inside blocks are syntactically correct and consistent with the keyword line.
- Blocks ensure that the requested outputs are produced.

*Extra blocks or options are acceptable if optional and non-conflicting.*

### Geometry Section

- Correct charge and multiplicity.
- Valid ORCA geometry syntax.

### C.1.4 Postprocessing and reporting (~30%)

- **Extraction of data from output files:** Relevant quantities are correctly extracted from ORCA output files.
- **Postprocessing into chemical information:** Extracted data are correctly transformed into chemically meaningful results (e.g., energies, spectra, thermodynamic quantities).
- **Final report:** Generation of report, comparison with literature, inclusion of references.

## C.2 Rubric and evaluation of each benchmark question:

### C.2.1 Evaluation of the benchmark question representative of the topic “Relativistic Corrections”.

**Table 7 Evaluation Rubric.** The rubric used to grade the benchmark question representative of the topic “Relativistic Corrections”.

Topic	Criterion	Weight	Task
Relativistic Corrections	Planning	15%	Single geometry used for all calculations. Parallel execution of independent NMR jobs. Same XC functional in both calculations. Correct handling of relativistic vs non-relativistic workflow.
	Geometry generation	15%	Square-planar $[\text{PtCl}_4]^{2-}$ structure. Correct connectivity and symmetry. Charge = -2, multiplicity = 1. Geometry reused consistently.
	Input file generation	40%	<b>Non-relativistic NMR:</b> DFT + def2-TZVP (ECP on Pt). NMR shielding enabled. <b>Scalar-relativistic NMR:</b> ZORA Hamiltonian. ZORA-def2-TZVP / SARC-ZORA-TZVP. Correct auxiliary bases.
	Postprocessing and reporting	30%	Valid ORCA syntax and block structure. Extraction of $^{195}\text{Pt}$ isotropic shielding. Side-by-side comparison of methods. Identification of relativistic effect. Quality of final report.

**Table 8** Per-iteration evaluation score for the benchmark question representative of the topic “Relativistic Corrections”. Scores assigned to each independent execution of the benchmark task, using the rubric defined above.

Iteration	Planning (%)	Geometry (%)	Input (%)	Postproc. (%)	Total (%)
Run 1	15	15	40	30	100
Run 2	12	15	40	30	97
Run 3	15	15	40	30	100
Run 4	15	15	40	30	100
Run 5	15	15	40	30	100
<b>Average</b>	14.4	15	40	30	99.4

- Run 1: The agent explicitly decomposed the NMR shielding (diamagnetic vs paramagnetic contributions) and correctly attributed discrepancies to core-electron treatment in the ECP-based calculation. The agent also contextualizes the results against known limitations of non-relativistic Pt NMR.
- Run 2: The agent showed robust parallelization and execution hygiene, but included unnecessary exploratory steps and tool consultations that do not materially contribute to task completion.
- Run 3: The agent reported that large relativistic corrections to the diamagnetic and paramagnetic terms nearly cancel, yielding a very small net change in isotropic shielding between the “non-relativistic” and ZORA setups, while still showing large changes in the components. Independently, it showed deliberate project tidying (foldering initial geometries and final report artifacts, removing temp files).
- Run 4: The agent recognized that a def2-TZVP/ECP calculation on Pt is not strictly non-relativistic and avoided an over-literal interpretation of the benchmark labels. Postprocessing prioritized inspecting tensor components and ensuring symmetry consistency before narrative reporting, reflecting an interpretation-driven analysis style.
- Run 5: The agent explicitly identified the methodological ceiling of scalar-relativistic GIAO NMR for 5d elements and flagged spin-orbit coupling as the missing ingredient for quantitative accuracy. The agent clearly delineated what conclusions are and are not supported by the chosen level of theory.

### C.2.2 Evaluation of the benchmark question representative of the topic “Electrical Properties”.

**Table 9 Evaluation Rubric.** The rubric used to grade the benchmark question representative of the topic “Electrical Properties”.

Topic	Criterion	Weight	Task
Electrical Properties	Planning	10%	Generation of the initial nitrobenzene and benzene structures. Optimization of the structure with a reasonable level (same level of theory, semiempirical quantum mechanical or efficient DFT method). Electronic structure calculation at the MP2/aug-cc-pVDZ level of theory of all compounds to obtain the static dipole moments and polarizability tensors. Successful generation of the benzene and nitrobenzene structures.
	Geometry generation	10%	
	Input file generation	40%	Optimization at a consistent and appropriate level of theory (same level of theory as property calculation, semiempirical quantum mechanical or efficient DFT method). keyword line (property calculation): ! RI-MP2 aug-cc-pVDZ blocks: %elprop Dipole true Polar true end . Dipole is set by default, thus leaving it out is acceptable.
	Postprocessing and reporting	40%	Read out the dipole moment (single value as the Euclidean norm) and the dipole polarizability tensor (six values) from the outputs for both structures. <i>Optional:</i> Read the isotropic polarizability. Comparison of the absolute dipole moments of benzene and nitrobenzene and analogously, comparison of anisotropy of the static polarizability tensor. Quality of final report, particularly regarding the analysis of how and why the electron-withdrawing nitro group changes both properties.

**Table 10 Per-iteration evaluation score for the benchmark question representative of the topic “Electrical Properties”.** Scores assigned to each independent execution of the benchmark task, using the rubric defined above.

Iteration	Planning (%)	Geometry (%)	Input (%)	Postproc. (%)	Total (%)
Run 1	10	10	40	40	100
Run 2	10	10	40	40	100
Run 3	10	10	35	40	100
Run 4	10	10	40	40	100
Run 5	10	10	39	40	99
<b>Average</b>	10	10	38.8	40	98.8

- Run 1: Extensive analysis on changes in the distinct polarizability tensor components (good).
- Run 2: No specific observations identified.
- Run 3: Quntur tries to set up a compound script, which leads to a postprocessing (CSV-related) error in ORCA. The geometry optimizations, the calculations of the electrical properties, and the related level of theories were unaffected, however.
- Run 4: No specific observations identified.
- Run 5: No specific observations identified.

### C.2.3 Evaluation of the benchmark question representative of the topic “Orbitals and densities”.

**Table 11 Evaluation Rubric.** The rubric used to grade the benchmark question representative of the topic “Orbitals and densities”.

Topic	Criterion	Weight	Task
Orbitals and densities	Planning	10%	Generation of both structures. Geometry optimizations and plots for molecular orbitals and densities for both structures. Repeat the previous step with a different method to correct for spin contamination (optional).
	Geometry generation	20%	Generation of cube files from .gbw files using orca_plot (optional). Successful generation of piperidine N-oxide radical geometry and pyridinium N-oxide cation radical.
	Input file generation	20%	<b>1. Piperidine N-oxide radical optimization:</b> keyword line: ! HF cc-pVDZ Opt UNO UCO, UHF, and convergence or grid settings allowed. blocks (optional): %plots Format Gaussian_Cube dim1 80 dim2 80 dim3 80 min1 0 max1 0 min2 0 max2 0 min3 0 max3 0 SpinDens("piperidine_noxide_spindens.cube"); MO("piperidine_noxide_somo.cube", 27, 0); end. geometry section: * xyzfile 0 2 piperidine_noxide_radical_initial.xyz. <b>2. pyridinium N-oxide radical cation optimization:</b> keyword line: ! HF cc-pVDZ Opt UNO UCO, UHF, and convergence or grid settings allowed. Repeating optimizations with a new method to correct for spin contamination is optional. blocks (optional): %plots Format Gaussian_Cube dim1 80 dim2 80 dim3 80 min1 0 max1 0 min2 0 max2 0 min3 0 max3 0 SpinDens("pyridinium_noxide_spindens.cube"); MO("pyridinium_noxide_somo.cube", 24, 0); end. geometry section: * xyzfile 1 2 pyridinium_noxide_radical_initial.xyz.
	Postprocessing and reporting	50%	Tracking spin contamination after optimization of both structures. Suggesting or performing a change of method. Orbitals cube files generation. Densities cube files generation. plots visualization and interpretation: spin density in N-O fragment vs delocalized over the ring. Quality of final report. No quantitative results should be claimed for the pyridinium due to significant spin contamination.

**Table 12 Per-iteration evaluation score for the benchmark question representative of the topic “Orbitals and densities”.** Scores assigned to each independent execution of the benchmark task, using the rubric defined above.

Iteration	Planning (%)	Geometry (%)	Input (%)	Postproc. (%)	Total (%)
Run 1	10	20	20	50	100
Run 2	10	20	20	50	100
Run 3	10	20	20	50	100
Run 4	10	10	20	50	80
Run 5	10	20	20	50	100
<b>Average</b>	10	18	20	50	98

- Run 1: No issues identified.
- Run 2: No issues identified.

- Run 3: No issues identified.
- Run 4: The initial geometry for the pyridinium N-oxide cation radical was incorrect. The nitrogen was swapped with the carbon at the ortho position. The agent did not check the structure after it was generated. Everything else was correct and similar to what would be obtained with the correct structured.
- Run 5: No issues identified.

#### C.2.4 Evaluation of the benchmark question representative of the topic “Condensed Fukui functions”.

**Table 13 Evaluation Rubric.** The rubric used to grade the benchmark question representative of the topic “Condensed Fukui functions”.

Topic	Criterion	Weight	Task
Condensed Fukui functions	Planning Geometry generation Input file generation Postprocessing and reporting	10% 10% 40% 40%	Optimization only for neutral species. Single point calculations for neutral, anion, and cation, at the optimized geometry of neutral toluene. Generate reference geometry. <b>1. Neutral toluene optimization:</b> keyword line: ! HF cc-pVTZ Opt Freq, other convergence or grid settings allowed. blocks: none required. geometry section: * xyzfile 0 1 toluene_initial.xyz. <b>2. Neutral toluene single point calculation</b> keyword line: ! HF cc-pVTZ Hirshfeld, other convergence or grid settings allowed. blocks: %output Print[ P_Mulliken ] 1 Print[ P_Loewdin ] 1 Print[ P_Hirshfeld ] 1 end. ROHF can also be specified in the main keyword line. geometry section: * xyzfile 0 1 neutral_toluene_opt.xyz. <b>3. Anion toluene single point calculation</b> keyword line: ! HF cc-pVTZ Hirshfeld, other convergence or grid settings allowed. blocks: %scf HFTyp ROHF end. %output Print[ P_Mulliken ] 1 Print[ P_Loewdin ] 1 Print[ P_Hirshfeld ] 1 end. ROHF can also be specified in the main keyword line. geometry section: * xyzfile -1 2 neutral_toluene_opt.xyz <b>4. Cation toluene single point calculation</b> keyword line: ! HF cc-pVTZ Hirshfeld, other convergence or grid settings allowed. blocks: %scf HFTyp ROHF end. %output Print[ P_Mulliken ] 1 Print[ P_Loewdin ] 1 Print[ P_Hirshfeld ] 1 end. ROHF can also be specified in the main keyword line. geometry section: * xyzfile 1 2 neutral_toluene_opt.xyz Angles and energies for minima and transition state. Extraction of thermodynamic properties ( $\Delta G$ , $\Delta H$ , $\Delta S$ ). Quality of final report.

**Table 14 Per-iteration evaluation score for the benchmark question representative of the topic “Fukui functions”.** Scores assigned to each independent execution of the benchmark task, using the rubric defined above.

Iteration	Planning (%)	Geometry (%)	Input (%)	Postproc. (%)	Total (%)
Run 1	10	10	40	40	100
Run 2	10	10	40	40	100
Run 3	10	10	40	40	100
Run 4	10	10	40	40	100
Run 5	10	10	40	40	100
<b>Average</b>	10	10	40	40	100

- Run 1: It attempted to run ROHF for the neutral species, but correctly switched to HF (RHF) after ORCA error.
- Run 2: No issues observed.

- Run 3: No issues observed.
- Run 4: No issues observed.
- Run 5: No issues observed.

### C.2.5 Evaluation of the benchmark question representative of the topic “Thermochemistry”.

**Table 15 Evaluation Rubric.** The rubric used to grade the benchmark question representative of the topic “Thermochemistry”.

Topic	Criterion	Weight	Task
Thermochemistry	Planning	30%	<p>Literature search of thermal chemistry cycle and thermal dynamic data of AcOH and proton</p> <p>Geometry generation of all species.</p> <p>Parallel optimization and frequency calculation + Single point calculations with implicit solvation.</p>
	Geometry generation	10%	Generate geometries of AcOH and $\text{AcO}^-$
	Input file generation	30%	<p><b>1. AcOH and <math>\text{AcO}^-</math> optimization and frequency in gas phase:</b> keyword line: B3LYP Def2-SVP OptFreq TightOpt, other reasonable functionals, equal or higher levels of basis set, other convergence or grid settings allowed.</p> <p>geometry section: * xyzfile 0 1 acetic_acid_xtb.xyz for AcOH, * xyzfile -1 1 acetate_xtb.xyz for <math>\text{AcO}^-</math></p> <p><b>2. AcOH and <math>\text{AcO}^-</math> single point in gas phase:</b></p> <p>keyword line: DLPNO-CCSD(T) def2-TZVPP TightSCF.</p> <p>geometry section: * xyzfile 0 1 acetic_acid_opt.xyz for AcOH, * xyzfile -1 1 acetate_opt.xyz for <math>\text{AcO}^-</math></p> <p><b>3. AcOH and <math>\text{AcO}^-</math> single point in gas phase:</b></p> <p>keyword line: DLPNO-CCSD(T) def2-TZVPP TightSCF</p> <p>blocks: %cpcm smd true SMDsolvent “water” end</p> <p>geometry section: * xyzfile 0 1 acetic_acid_opt.xyz for AcOH, * xyzfile -1 1 acetate_opt.xyz for <math>\text{AcO}^-</math></p>
	Postprocessing and reporting	30%	<p>Thermodynamic cycle equation for pKa calculation.</p> <p>Calculated pKa of AcOH in gas phase and in implicit water.</p> <p>Comparison of calculated pKa with literature value and rationalization of potential errors.</p> <p>Quality of final report.</p>

**Table 16 Per-iteration evaluation score for the benchmark question representative of the topic “Thermochemistry”.** Scores assigned to each independent execution of the benchmark task, using the rubric defined above.

Iteration	Planning (%)	Geometry (%)	Input (%)	Postproc. (%)	Total (%)
Run 1	25	10	30	25	90
Run 2	25	10	20	25	80
Run 3	25	10	30	25	90
Run 4	30	10	20	25	90
Run 5	30	10	30	25	95
<b>Average</b>	27	10	26	25	88

- Run 1: Used  $\text{H}_2\text{O}/\text{OH}^-$  with fragile anion in thermal cycle. For AcOH and  $\text{H}_2\text{O}$ , should use  $\text{H}_3\text{O}^+/\text{H}_2\text{O}$  pairs. Did not try to reason to correct the thermal calc equation after finding the final value is off.
- Run 2: Used  $\text{H}_2\text{O}/\text{OH}^-$  with fragile anion in thermal cycle. For AcOH and  $\text{H}_2\text{O}$ , should use  $\text{H}_3\text{O}^+/\text{H}_2\text{O}$  pairs. Wrong calculation level for single point (should be DLPNO-CCSD(T), get B3LYP D4 def2-TZVP). Did not try to reason to correct the thermal calc equation after finding the final value is off.
- Run 3: Used  $\text{H}_2\text{O}/\text{OH}^-$  with fragile anion in thermal cycle. For AcOH and  $\text{H}_2\text{O}$ , should use  $\text{H}_3\text{O}^+/\text{H}_2\text{O}$  pairs. Did not try to reason to correct the thermal calc equation after finding the final value is off.

- Run 4: Wrong calculation level for single point (should be DLPNO-CCSD(T), get B3LYP D4 def2-TZVP). Did not try to reason to correct the thermal calc equation after finding the final value is off.
- Run 5: Result is off.

### C.2.6 Evaluation of the benchmark question representative of the topic “Conformer Generation”.

**Table 17 Evaluation Rubric.** The rubric used to grade the benchmark question representative of the topic “Conformer Generation”.

Topic	Criterion	Weight	Task
Conformer Generation	Planning	20%	<p>Generation of the initial Serine structure.  Conformer search using an appropriate tool such as CREST or GOAT.  Parsing of the conformers as single three-dimensional structures.  DFT reoptimization of each of the structures.  <i>Optional:</i> Check for conformers that fell into the same local minimum (similar total energy and virtually zero structural RMSD).</p>
	Geometry generation	20%	<p>Re-calculate the Boltzmann weights for the conformer ensemble and report the lowest-energy structure together with the total ensemble.  Successful generation of the serine geometry. L-serine should be chosen, as it's the biologically active form and is usually used. The protonation state can be either, but in the gas phase, it's the neutral form.</p>
	Input file generation	30%	<p><b>1. Serine conformer generation:</b>  keyword line: ! XTB GOAT  blocks (optional): Specifications about GOAT, which might be reasonable. Not critical for the run.</p> <p><b>2. Re-optimization of the structures on the DFT level:</b>  keyword line: ! B3LYP D4 (or D3(BJ)), other convergence or grid settings allowed. QUINTUR shall either include the dispersion correction as suggested or inform the user that it's missing. The basis set can be explicitly stated or not, since it is the default anyway.</p>
	Postprocessing and reporting	30%	<p><i>Between step 1 and 2:</i> Parsing of the conformers as single three-dimensional structures and preparing distinct calculations for them. <i>Optional:</i> Set an upper threshold for high-energy conformers.  <i>After step 2:</i> Reading out DFT energies from ORCA.  <i>Optional:</i> Check for conformers that fell into the same local minimum (similar total energy and virtually zero structural RMSD).  Re-calculate Boltzmann weights for the conformer ensemble.  Quality of the final report, particularly regarding the Boltzmann ensemble and the lowest-energy structure.</p>

**Table 18 Per-iteration evaluation score for the benchmark question representative of the topic “Conformer Generation”.** Scores assigned to each independent execution of the benchmark task, using the rubric defined above.

Iteration	Planning (%)	Geometry (%)	Input (%)	Postproc. (%)	Total (%)
Run 1	20	20	25	25	90
Run 2	20	20	30	26	96
Run 3	20	20	30	27.5	97.5
Run 4	20	20	30	25	95
Run 5	20	20	25	25	90
<b>Average</b>	20	20	28	25.7	93.7

- Run 1: No comment on the flawed theory level (missing dispersion correction). No check for conformers falling into the same local minimum (even though it seems likely from the output). Used GOAT-ENTROPY instead of simple GOAT, which makes sense since a “*diverse set of conformers*”, i.e. a complete ensemble was requested.
- Run 2: Usage of B3LYP-D3(BJ) (good). It is implicitly mentioned that conformers might have been falling into the same local minimum.

- Run 3: Usage of B3LYP-D3(BJ) (good). It is explicitly mentioned that the two lowest conformers are degenerate.
- Run 4: Usage of B3LYP-D3(BJ) (good). No check for conformers falling into the same local minimum (even though it seems likely from the output).
- Run 5: No comment on the flawed theory level (missing dispersion correction). A cutoff of 3 kcal/mol is applied for the DFT optimizations (neutral). No check for conformers falling into the same local minimum (even though it seems likely from the output).  $\text{kcal mol}^{-1}$  is used for the DFT optimizations.

### C.2.7 Evaluation of the benchmark question representative of the topic: “Molecular Dynamics”.

**Table 19 Evaluation Rubric.** The rubric used to grade the benchmark question representative of the topic “Molecular Dynamics”.

Topic	Criterion	Weight	Task
Molecular Dynamics	Planning Geometry generation Input file generation	10%	<p>Generating an initial structure for the Chloride ion, along with 12 water molecules</p> <p>Performing the geometry optimization using GFN2-xTB</p> <p>Performing AIMD simulations with short equilibration and then production</p> <p>Extracting the AIMD trajectory and then analysing the radial distribution function of Cl and O</p> <p>Generate physically reasonable initial geometry for hydrated chloride ion cluster, with correct charge, and spin multiplicity.</p> <p><b>1. Geometry relaxation <math>\text{Cl}^- (\text{H}_2\text{O})_{12}</math>:</b> Check if the agent used the xTB tool to perform geometry relaxation. geometry section: *xyz file -1 1 cl_12water_initial.xyz</p> <p><b>2. AIMD <math>\text{Cl}^- (\text{H}_2\text{O})_{12}</math>:</b> keyword line: ! XTB2 MD block: % md Timestep = 0.5 for step size Initvel 300_K for velocity initialization Thermostat settings for equilibration Run the equilibration command with the specified number of steps. Thermostat settings for production Dump settings for storing production trajectory "prod_traj.xyz" Run command for 0.1 ps production. geometry section: * xyz file -1 1 cl_12water_optimized.xyz</p> <p>Correct extraction of the production MD trajectories. Computing the radial distribution function of Cl and O.</p>
		20%	
		30%	
	Postprocessing and reporting	40%	<p>Results should be presented in a final markdown report that is comprehensive and easy to interpret with primary literature sources.</p>

**Table 20 Per-iteration evaluation score for the benchmark question representative of the topic “Molecular Dynamics”.** Scores assigned to each independent execution of the benchmark task, using the rubric defined above.

Iteration	Planning (%)	Geometry (%)	Input (%)	Postproc. (%)	Total (%)
Run 1	10	20	30	40	100
Run 2	10	20	20	40	90
Run 3	10	20	30	40	100
Run 4	10	20	15	40	85
Run 5	10	20	25	40	95
<b>Average</b>	10	20	24	40	94

- Run 1:  
The agent first performed a geometry optimization using GFN2-xTB, followed by an AIMD simulation consisting of a 1.0 ps equilibration phase under the Berendsen thermostat and a 0.1 ps production phase under the Canonical Sampling through Velocity Rescaling (CSVR) thermostat. Two trajectories were saved, and a radial distribution function (RDF) analysis was carried out on the production trajectory.
- Run 2:  
The agent did not perform a geometry optimization and instead directly carried out an AIMD simulation, consisting of a 0.5 ps equilibration phase followed by a 0.1 ps production phase under a CSVR thermostat. Only the production trajectory was saved for RDF analysis. Notably, the agent successfully troubleshooted and resolved an error caused by the invalid syntax in the Dump Position Off command.
- Run 3:

The agent performed a geometry optimization using GFN2-xTB, followed by an AIMD simulation consisting of a 0.5 ps equilibration phase under a Berendsen thermostat and a 0.1 ps production phase under a Nose–Hoover chain (NHC) thermostat. Two trajectories were saved, and a radial distribution function (RDF) analysis was subsequently performed on the production trajectory.

- Run 4:

The agent first performed geometry optimization using GFN2-xTB, followed by redundant frequency calculations. Molecular dynamics simulations were then conducted with a time step of 1 fs, using a very short equilibration phase of 0.1 ps under a Berendsen thermostat, followed by a 0.1 ps production run under a Nosé–Hoover chain (NHC) thermostat. Due to the brevity of the equilibration stage, only the production trajectory was saved for subsequent radial distribution function (RDF) analysis.

- Run 5:

The agent performed a geometry optimization using GFN2-xTB, followed by an AIMD simulation consisting of a 0.25 ps equilibration phase under a Berendsen thermostat and a 0.1 ps production phase under a Nose–Hoover chain (NHC) thermostat. Two trajectories were saved, and a radial distribution function (RDF) analysis was subsequently performed on the production trajectory. An irrelevant keyword, "Manage\_Covar", was included in the MD input file.

### C.2.8 Evaluation of the benchmark question representative of the topic “Explicit solvation”.

**Table 21 Evaluation Rubric.** The rubric used to grade the benchmark question representative of the topic “Explicit solvation”.

Topic	Criterion	Weight	Task
Explicit solvation	Planning	10%	<p>Generating an initial structure for <math>\text{AcOH}(\text{H}_2\text{O})_3</math>, <math>\text{AcOH}(\text{H}_2\text{O})_5</math>, <math>\text{AcOH}(\text{H}_2\text{O})_7</math>, <math>\text{AcO}^-(\text{H}_2\text{O})_3</math>, <math>\text{AcO}^-(\text{H}_2\text{O})_5</math>, <math>\text{AcO}^-(\text{H}_2\text{O})_7</math></p> <p>Perform geometry optimizations using r2SCAN-3c, with and without an implicit CPCM solvent model.</p> <p>Extract Gibbs free energies from all calculations and compute pKa values for each cluster size in both gas-phase and CPCM environments, analyzing convergence toward experimental pKa values.</p> <p>Generate a summary report that includes pKa convergence plots across different cluster sizes, with direct comparisons between gas-phase and CPCM results as well as against literature values.</p>
	Geometry generation	30%	<p>Generate physically reasonable initial geometry for the solvation of Acetic Acid by Water Molecules and implicit solvent, with correct charge, and spin multiplicity.</p> <p><b>1. Geometry relaxation <math>\text{AcOH}/\text{AcO}^-(\text{H}_2\text{O})_n</math>:</b>          keyword line: ! r2SCAN-3c TightOpt FREQ          geometry section: *xyz file -1 1 AcO_3water_initial.xyz, *xyz file -1 1 AcO_5water_initial.xyz, *xyz file -1 1 AcO_7water_initial.xyz, *xyz file 0 1 AcOH_3water_initial.xyz *xyz file 0 1 AcOH_5water_initial.xyz *xyz file 0 1 AcOH_7water_initial.xyz</p>
	Input file generation	30%	<p>Generate physically reasonable initial geometry for the solvation of Acetic Acid by Water Molecules and implicit solvent, with correct charge, and spin multiplicity.</p> <p><b>1. Geometry relaxation <math>\text{AcOH}/\text{AcO}^-(\text{H}_2\text{O})_n</math>:</b>          keyword line: ! r2SCAN-3c TightOpt FREQ          geometry section: *xyz file -1 1 AcO_3water_initial.xyz, *xyz file -1 1 AcO_5water_initial.xyz, *xyz file -1 1 AcO_7water_initial.xyz, *xyz file 0 1 AcOH_3water_initial.xyz *xyz file 0 1 AcOH_5water_initial.xyz *xyz file 0 1 AcOH_7water_initial.xyz</p>
	Postprocessing and reporting	30%	<p>Electronic energies and thermal corrections obtained from frequency calculations were combined to yield Gibbs free energies, which were then used to compute deprotonation free energies and pKa values.</p> <p>Results should be presented in a final markdown report that is comprehensive and easy to interpret with primary literature sources.</p>

**Table 22 Per-iteration evaluation score for the benchmark question representative of the topic “Explicit solvation”.** Scores assigned to each independent execution of the benchmark task, using the rubric defined above.

Iteration	Planning (%)	Geometry (%)	Input (%)	Postproc. (%)	Total (%)
Run 1	10	20	30	30	90
Run 2	10	15	30	30	85
Run 3	10	20	30	30	90
Run 4	10	15	30	30	85
Run 5	10	15	30	30	85
<b>Average</b>	10	17	30	30	87

- Run 1:  
 The agent first performed a geometry optimization using GFN2-xTB, followed by refinement with r2SCAN-3c. When the r2SCAN-3c optimization reached the maximum number of iterations, the agent successfully restarted the calculation. Gibbs free energies were extracted from the output files and used to compute deprotonation free energies and the corresponding pKa values. However, for the initial configuration, the agent usually failed to generate the lowest-energy structure of AcOH, which negatively affected the accuracy of the free energy calculations.
- Run 2:  
 The agent first performed a geometry optimization using GFN2-xTB, followed by refinement with r2SCAN-3c. When the r2SCAN-3c optimization reached the maximum number of iterations, the agent successfully restarted the calculation. Gibbs free energies were extracted from the output files and used to compute deprotonation free energies and the corresponding pKa values. However, for the initial

configuration, the agent always failed to generate the lowest-energy structure of AcOH, which negatively affected the accuracy of the free energy calculations.

- Run 3:

The agent first performed a geometry optimization using GFN2-xTB, followed by refinement with r2SCAN-3c. When the r2SCAN-3c optimization reached the maximum number of iterations, the agent successfully restarted the calculation. Gibbs free energies were extracted from the output files and used to compute deprotonation free energies and the corresponding pKa values. However, for the initial configuration, the agent usually failed to generate the lowest-energy structure of AcOH, which negatively affected the accuracy of the free energy calculations.

- Run 4:

The agent first performed a geometry optimization using GFN2-xTB, followed by refinement with r2SCAN-3c. When the r2SCAN-3c optimization reached the maximum number of iterations, the agent successfully restarted the calculation. Gibbs free energies were extracted from the output files and used to compute deprotonation free energies and the corresponding pKa values. However, for the initial configuration, the agent always failed to generate the lowest-energy structure of AcOH, which negatively affected the accuracy of the free energy calculations.

- Run 5:

The agent first performed a geometry optimization using GFN2-xTB, followed by refinement with r2SCAN-3c. When the r2SCAN-3c optimization reached the maximum number of iterations, the agent successfully restarted the calculation. Gibbs free energies were extracted from the output files and used to compute deprotonation free energies and the corresponding pKa values. However, for the initial configuration, the agent always failed to generate the lowest-energy structure of AcOH, which negatively affected the accuracy of the free energy calculations.

### C.2.9 Evaluation of the benchmark question representative of the topic “Potential Energy Surfaces”.

**Table 23 Evaluation Rubric.** The rubric used to grade the benchmark question representative of the topic “Potential Energy Surfaces”.

Topic	Criterion	Weight	Task
Potential Energy Surfaces	Planning Geometry generation Input file generation Postprocessing and reporting	10% 20% 40% 30%	Complete dihedral relaxed scan between 0 and $180^0$ , no optimization needed. Optimizations for each stationary point are optional. Rigid scan instead of a relaxed scan (half credit, no credit if no optimization was run before rigid scan). Generate reference geometry (trans or cis) Correct choice of minima and top-of-barrier geometries. <b>1. Butadiene trans optimization (optional):</b> keyword line: CASSCF cc-pVDZ TightOpt NumFreq, other convergence or grid settings allowed. blocks: %casscf nel 4 norb 4 mult 1 nroots 1 end. geometry section: * xyzfile 0 1 butadiene_initial.xyz (it can use trans or cis initial geometry; it can also use inline or internal coordinates). This step is not necessary when geom scan is used. <b>2. Butadiene PES scan:</b> keyword line: ! CASSCF cc-pVDZ Opt, other convergence or grid settings allowed. blocks: %casscf nel 4 norb 4 mult 1 nroots 1 end. %geom Scan D 0 1 2 3 = 180.0, 0.0, 19 end end. The number of grid points must be reasonable. Scan directionality must be consistent with the initial geometry. geometry section: * xyzfile 0 1 butadiene_initial.xyz (again, cis or trans). <b>3. Butadiene single-point calculations (optional):</b> keyword line: ! CASSCF cc-pVDZ, other convergence or grid settings allowed. blocks: %casscf nel 4 norb 4 mult 1 nroots 1 end. geometry section: * xyzfile 0 1 some_geometry.xyz (to replace scan). Angles and energies for minima (cis is not planar but gauche). Energy barrier along dihedral. Quality of final report.

**Table 24 Per-iteration evaluation score for the benchmark question representative of the topic “Potential Energy surfaces”.**  
 Scores assigned to each independent execution of the benchmark task, using the rubric defined above.

Iteration	Planning (%)	Geometry (%)	Input (%)	Postproc. (%)	Total (%)
Run 1	10	20	40	30	100
Run 2	10	20	40	30	100
Run 3	10	20	40	30	100
Run 4	10	20	40	30	100
Run 5	10	20	40	30	100
<b>Average</b>	10	20	40	30	100

- Run 1: The scan failed initially because the agent started from an s-trans ( $180^0$ ) geometry, but tried to scan from  $0^0$  to  $180^0$  (instead of from  $180^0$  to  $0^0$ ). The agent found the error and fixed it, so no points were deducted.
- Run 2: The scan was set up properly. The agent also performed optimizations for each stationary point, finding the cis, trans, and main transition states. These calculations are optional and are not graded.
- Run 3: Same as Run 1.

- Run 4: Same as Run 1
- Run 5: Same issue as Run 1 with scan directionality. During debugging, the agent avoided including the trans configuration, but obtained it later via geometry optimization.

### C.2.10 Evaluation of the benchmark question representative of the topic “Transition State Methods”.

**Table 25 Evaluation Rubric.** The rubric used to grade the benchmark question representative of the topic “Transition State Methods”.

Topic	Criterion	Weight	Task
Transition State Methods	Planning Geometry generation Input file generation Postprocessing and reporting	20% 10% 40% 30%	Optimization of reaction substrate and product. Transition state search using NEB. Transition state localization using OptTS. Transition state verification using IRC. Generate reference geometry with correct atom order and symmetry. <b>1. Substrate and product geometry optimization:</b> keyword line: ! PBE0 D3BJ Def2-TZVP Opt Freq, other convergence or grid settings allowed. blocks: none required. geometry section: * xyzfile 0 1 formic_acid_dimer_reactant.xyz for reactant, * xyzfile 0 1 formic_acid_dimer_product.xyz for product. <b>2. NEB calculation for transition state localization</b> keyword line: ! PBE0 D3BJ Def2-TZVP NEB, other convergence or grid settings allowed. Must be consistent with the previous step. NEB-CI is valid. blocks: %neb Product "product.xyz" NImages 8 Interpolation IDPP MaxIter 500 ConvType all Tol_Scale 10.0 PrintLevel 1 end. Other settings on NImages, tolerances, and MaxIter are valid if reasonable. If NEB-CI is chosen, it's better to set Tol_Turn_On_CI. geometry section: * xyzfile 0 1 reactant.xyz <b>3. Transition state geometry optimization calculation</b> keyword line: ! PBE0 D3BJ Def2-TZVP OptTS, other convergence or grid settings allowed. Must be consistent with the previous step. blocks: %geom Calc_Hess true end geometry section: * xyzfile 0 1 TS_guess.xyz <b>4. Transition state verification via IRC</b> keyword line: ! PBE0 D3BJ Def2-TZVP IRC, other convergence or grid settings allowed. Must be consistent with the previous step. blocks: %irc Direction both InitHess read Hess_Filename "TS.hess" MaxIter 50 end. Other settings, such as Init_Displ, DE_Init_Displ, TolMaxG, TolRMSG, etc., are allowed if reasonable. Calc_Hess True, valid, but lower marks. geometry section: * xyzfile 0 1 TS.xyz NEB-CI calculation converged. Imaginary freq verified. Backward and forward IRC paths verified. Extraction of thermodynamic properties ( $\Delta G$ , $\Delta H$ , $\Delta S$ ). Quality of final report.

**Table 26 Per-iteration evaluation score for the benchmark question representative of the topic “Transition State Methods”.**  
 Scores assigned to each independent execution of the benchmark task, using the rubric defined above.

Iteration	Planning (%)	Geometry (%)	Input (%)	Postproc. (%)	Total (%)
Run 1	20	10	40	30	100
Run 2	20	10	40	30	100
Run 3	20	10	38	30	98
Run 4	20	10	40	30	100
Run 5	20	10	40	30	100
<b>Average</b>	20	10	39.6	30	99.6

- Run 1: No issues observed.
- Run 2: No issues observed.
- Run 3: Used NEB-CI but did not specify a threshold.
- Run 4: No issues observed.
- Run 5: No issues observed.

**C.2.11 Evaluation of the benchmark question representative of the topic “Reaction Mechanisms”.**

**Table 27 Evaluation Rubric.** The rubric used to grade the benchmark question representative of the topic “Reaction Mechanisms”.

Topic	Criterion	Weight	Task
Reaction Mechanisms	Planning	20%	Optimizes encounter complex and TS followed by IRC on TS structure
	Geometry generation	20%	Generates correct encounter complex and TS guess
	Input file generation	20%	Key input file settings across all calculations (i.e. functional/basis set, syntax) and for each type of calculation (i.e. “opt” and “freq” for encounter complex, “optts” and “freq” for transition state, “irc” for IRC)
	Postprocessing and reporting	40%	Confirms presence of 1 imaginary frequency that is sufficiently large (10%) Report generated and contains $\Delta G^\ddagger$ , $\Delta H^\ddagger$ , $\Delta H^\ddagger$ (10 %) Overall quality of report (interpretation of results, comparison with literature, formatting, etc., 10%) Accuracy of results (values of G, H, S from the output files for encounter complex and TS, reported $\Delta G^\ddagger$ , $\Delta H^\ddagger$ , $\Delta H^\ddagger$ ; each compared to a set of manual calculations and weighed equally to form a total of 10%)

**Table 28 Per-iteration evaluation score for the benchmark question representative of the topic “Reaction Mechanisms”.** Scores assigned to each independent execution of the benchmark task, using the rubric defined above.

Iteration	Planning (%)	Geometry (%)	Input (%)	Postproc. (%)	Total (%)
Run 1	20	20	20	36.7	96.7
Run 2	20	20	20	36.7	96.7
Run 3	20	20	20	36.7	96.7
Run 4	10	20	10	33.3	73.3
Run 5	10	20	20	35.6	85.6
<b>Average</b>	16	20	18	35.8	89.8

- Run 1: Everything looks correct and reasonable
- Run 2: In input file, used RI-MP2 instead of MP2 and added cc-pVTZ/C in addition to cc-PVTZ in input
- Run 3: Did compound scripts for optimization of encounter complex and TS, mainly involving printing thermochemical data that already appeared earlier in the output file (no compound script for IRC)
- Run 4: Did not encounter the complex, but rather  $\text{CH}_3\text{Cl}$  and  $\text{Cl}^-$  separately in input file, used RI-MP2 instead of MP2 and added cc-pVTZ/C in addition to cc-PVTZ in input; also had additional freq block; for  $\text{Cl}^-$ , didn't have freq but in the end managed to estimate enthalpy from the statistical mechanics of a monoatomic ideal gas and entropy from the Sackur-Tetrode equation (no evidence that it actually used the data from the single point calculation to calculate, might be extracted from online sources)

- Run 5: Also did not do encounter complex; input file had some additional had geom block with "inhess" and "xtb2" which was not necessary; also RI-MP2 and cc-PVTZ/C as observed in Runs 2 and 4; Compound scripts also used, similarly (but not the exact same) as in Run 4; IRC had quite a bit more parameters that were unnecessary

### C.2.12 Evaluation of the benchmark question representative of the topic “Isotopic Effects”.

**Table 29 Evaluation Rubric.** The rubric used to grade the benchmark question representative of the topic “Isotopic Effects”.

Topic	Criterion	Weight	Task
Isotopic Effects	Planning	10%	geometry generation of benzyl chlorides and carbocations. TS optimizations are allowed, but they are significantly more complex. Optimizations only for non-deuterated species.
	Geometry generation	30%	recalculation of thermodynamic quantities for deuterated species from non-deuterated Hessians.
	Input file generation	30%	Geometry generation of benzyl chlorides. Geometry generation of carbocations. <b>1. geometry optimizations:</b> keyword line: ! HF 6-31G(d) OPT FREQ CPCM(Water), other convergence or grid settings allowed. Other solvent models, such as SMD, are allowed. blocks: No blocks are required. geometry section: * xyzfile 0 1 benzyl_chloride_initial.xyz. * xyzfile 1 1 benzyl_cation_initial.xyz.
	Postprocessing and reporting	30%	<b>2. Thermochemistry of deuterated species:</b> keyword line: ! PRINTTHERMOCHEM. blocks: %geom INHESSNAME "benzyl_cation_opt.hess" end. geometry section: * xyzfile 0 1 benzyl_chloride_initial.xyz. * xyzfile 1 1 benzyl_cation_initial.xyz. Atomic mass change for deuterated species via "M 2.00141". <b>3. Transition state optimization (optional):</b> keyword line: ! HF 6-31G(d) OptTS Freq CPCM(water). blocks: %geom Calc_Hess true TS_Active_Atoms 0 1 end modify_internal B 0 1 A end. geometry section: * xyzfile 0 1 benzyl_chloride_initial.xyz. Extraction of Final Gibbs free energy. Calculation of Final Gibbs free energies for deuterated species using thermal correction from the PRINTTHERMOCHEM calculation. Calculation of KIE. Quality of final report.

**Table 30 Per-iteration evaluation score for the benchmark question representative of the topic “Isotopic Effects”.** Scores assigned to each independent execution of the benchmark task, using the rubric defined above.

Iteration	Planning (%)	Geometry (%)	Input (%)	Postproc. (%)	Total (%)
Run 1	10	30	30	30	100
Run 2	10	30	30	30	100
Run 3	10	30	30	30	80
Run 4	10	30	10	30	100
Run 5	8	30	30	30	100
<b>Average</b>	9.6	30	26	30	96

- Run 1: No issues observed.
- Run 2: No issues observed.
- Run 3: No issues observed.
- Run 4: The agent tried to compute the KIE accurately by obtaining transition states for 3 substituted

benzyl chlorides. Only one of the three transition-state optimizations converged. Correct analysis continued with the converged species (-OCH<sub>3</sub> substituted).

- Run 5: El Agente runs a frequency calculation to obtain the Gibbs free energies for deuterated species, which is unnecessary. No other issues observed.

### C.2.13 Evaluation of the benchmark question representative of the topic “Excited States”.

**Table 31 Example of Evaluation Rubric.** The rubric used to grade the benchmark question representative of the topic “Excited States”.

Topic	Criterion	Weight	Task
Excited States	Planning	20%	Identify the required workflow: ground-state geometry optimization followed by TDDFT excited-state calculations. Correct selection of the two functionals (PBE0 and $\omega$ B97X-D) with the def2-TZVP basis set. Clear definition of the quantities to be compared, namely, vertical excitation energies.
	Geometry generation	10%	Generate a physically reasonable equilibrium geometry for p-nitroaniline in its ground electronic state, with correct molecular structure, charge, and spin multiplicity. Ground-state optimization at the DFT level is expected and should be reused consistently for TDDFT calculations.
	Input file generation	30%	<b>1. Ground-state optimization:</b> keyword line using either PBE0 or $\omega$ B97X-D with the def2-TZVP basis set, including correct charge and spin multiplicity. <b>2. TDDFT excitation energies:</b> TDDFT calculations performed on the optimized ground-state geometry of the appropriate functional, with the same basis set and a consistent number of requested excited states.
	Postprocessing	40%	Correct extraction of excitation energies from both TDDFT calculations. Clear tabulation and comparison of the results, and discussion of trends between the two functionals. Results should be presented in a final markdown report with brief physical interpretation and comments on methodological limitations.

**Table 32 Per-iteration evaluation score for the benchmark question representative of the topic “Excited States”.** Scores assigned to each independent execution of the benchmark task, using the rubric defined above.

Iteration	Planning (20)	Geometry (10)	Input (30)	Postproc. (40)	Total (100)
Run 1	10	10	30	40	90
Run 2	10	10	30	40	90
Run 3	10	10	30	40	90
Run 4	10	10	30	40	90
Run 5	10	10	30	40	90
<b>Average</b>	10	10	30	40	90

In all cases, the proposed plan optimized the ground-state geometry exclusively at the PBE0 level and applied alternative functionals only in the TDDFT step, thereby comparing excitation energies on a common PBE0-optimized structure. While this approach is sometimes adopted in computational chemistry, particularly when benchmarking against experiment, and is unlikely to introduce large structural differences for a small organic molecule such as *p*-nitroaniline, it is nonetheless not fully methodologically sound. In particular, this strategy is inappropriate for the  $\omega$ B97X-D functional, whose excited-state predictions should ideally be assessed on geometries optimized consistently with the same functional. While all calculations were internally consistent with the original plan, the protocol itself remains suboptimal for a fully fair and meaningful comparison between the two functionals.

Notably, when we prompt GPT-5.2 and Gemini to generate an overall plan for this task, we observed systematic differences in methodological reasoning. Specifically, GPT-5.2 reproduced the flawed strategy described above by proposing a single PBE0 ground-state optimization. By contrast, Gemini 3.0 correctly identified the

need for fully consistent ground- and excited-state treatments at each functional level for fair comparison. This observation highlights that current LLMs can differ substantially in their implicit assumptions about electronic-structure workflows, even when responding to identical queries. Therefore, a systematic evaluation of foundation models on such chemically sensitive planning tasks is a crucial direction for future work, both to assess their reliability in methodological decision-making and to identify failure modes not evident from numerical output alone.

**C.2.14 Evaluation of the benchmark question representative of the topic “Excited-State Kinetics”.**

**Table 33 Example of Evaluation Rubric.** The rubric used to grade the benchmark question representative of the topic “Excited-State Kinetics”.

Topic	Criterion	Weight	Task
Excited-State Kinetics	Planning	10%	Identify the required workflow: ground-state geometry optimization and an excited-state ( $S_1$ ) calculation using TDDFT. Evaluation of the fluorescence rate using the Hessians. Accurate selection of CAM-B3LYP/def2-TZVP and gas-phase conditions.
	Geometry generation	20%	Generate a physically reasonable equilibrium geometry for formaldehyde in its ground electronic state, with correct molecular structure, charge, and spin multiplicity. Ground-state optimization at the DFT level is expected.
	Input file generation	40%	<p><b>1. Ground-state optimization and frequencies:</b> keyword line: ! CAM-B3LYP def2-TZVP Opt NumFreq (or equivalent). Correct charge and multiplicity.</p> <p><b>2. Excited-state optimization and frequencies:</b> keyword line: ! CAM-B3LYP def2-TZVP TDDFT Opt NumFreq TightSCF (or equivalent), requesting an appropriate number of excited states and correctly identifying and following the <math>S_1</math> state.</p> <p><b>3. Fluorescence rate evaluation:</b> inclusion of the appropriate ESD(Fluor) settings such that the fluorescence rate is obtained directly from the excited-state Hessian and printed in the output.</p>
	Postprocessing	30%	<p>Correct extraction of the fluorescence rate as reported by ESD(Fluor)</p> <p>Verification of its physical plausibility</p> <p>Clear presentation in a final markdown report.</p> <p>Discussion of assumptions and interpretation of the result.</p>

**Table 34 Per-iteration evaluation score for the benchmark question representative of the topic “Excited-State Kinetics”.** Scores assigned to each independent execution of the benchmark task, using the rubric defined above.

Iteration	Planning (10)	Geometry (20)	Input (40)	Postproc. (30)	Total (100)
Run 1	10	20	40	30	100
Run 2	10	20	40	30	100
Run 3	10	20	40	30	100
Run 4	10	20	40	30	100
Run 5	10	20	40	30	100
<b>Average</b>	10	20	40	30	100

Across repeated runs, the fluorescence rate varied between  $\sim 2.45 \times 10^5 \text{ s}^{-1}$  and  $3.5 \times 10^5 \text{ s}^{-1}$ . This variability arises from differences in post-processing choices, including the use of zero versus room temperature (298 K) and different spectral broadening models (Voigt or Lorentzian with varying weights). The number of TDDFT roots used for the excited-state calculations ranged from two to five, which is acceptable for this system. Overall, the observed variability reflects insufficiently constrained prompt instructions rather than a lack of consistency in the underlying calculation.

**C.2.15 Evaluation of the benchmark question representative of the topic “NMR and Magnetic Properties”.**

**Table 35 Evaluation Rubric.** The rubric used to grade the benchmark question representative of the topic “NMR and Magnetic Properties”.

Topic	Criterion	Weight	Task
NMR and Magnetic Properties	Planning	20%	<p>Geometry generation of fluorobenzene, pentafluorobenzene, along with tetramethylsilane (TMS) and trichlorofluoromethane ( CFCl<sub>3</sub>): standard <sup>1</sup>H and <sup>19</sup>F NMR references</p> <p>Geometry optimizations were performed for all four molecules at the HF/aug-cc-pVTZ level of theory or an appropriate alternative DFT method or basis set.</p> <p>Absolute NMR shielding constants were calculated for all molecules for the relevant nuclei (<sup>1</sup>H and/or <sup>19</sup>F), using the GIAO method at the HF/aug-cc-pVTZ level of theory.</p> <p>Convert shielding values (<math>\sigma_{iso}</math>) to chemical shifts in ppm (<math>\delta</math>). Analyze trends and discuss anisotropy effects.</p>
	Geometry generation	20%	<p>Generate physically reasonable equilibrium geometries for fluorobenzene, pentafluorobenzene, TMS, CFCl<sub>3</sub> in their ground electronic state, with correct molecular structure, charge, and spin multiplicity.</p>
	Input file generation	30%	<p><b>1. Geometry optimization CFCl<sub>3</sub>, fluorobenzene, pentafluorobenzene, TMS:</b>          keyword line: ! RHF aug-cc-pVTZ OPT FREQ TightSCF.          geometry section: * xyzfile 0 1 CFCl3_initial.xyz, * xyzfile 0 1 fluorobenzene_initial.xyz, * xyzfile 0 1 pentafluorobenzene_initial.xyz, * xyzfile 0 1 TMS_initial.xyz</p> <p><b>2. NMR shielding CFCl<sub>3</sub>, fluorobenzene, pentafluorobenzene, TMS:</b>          keyword line: ! RHF aug-cc-pVTZ TIGHTSCF          geometry section: * xyzfile 0 1 CFCl3_opt.xyz, * xyzfile 0 1 pentafluorobenzene_opt.xyz, * xyzfile 0 1 fluorobenzene_opt.xyz, * xyzfile 0 1 TMS_opt.xyz          block: %eprnmr Ori = GIAO Nuclei = all H shift Nuclei = all F shift end.          Note: NMR keyword can also be used to call %eprnmr block.</p>
	Postprocessing and reporting	30%	<p><sup>1</sup>H and <sup>19</sup>F NMR properties of fluorobenzene and pentafluorobenzene calculated.</p> <p>Chemical shielding values (<math>\sigma_{iso}</math>) and chemical shifts (<math>\delta</math>) are reported to determine the shielding effect of fluorination on an aromatic ring.</p> <p>Results should be presented in a final markdown report that is comprehensive and easy to interpret with primary literature sources.</p>

**Table 36 Per-iteration evaluation score for the benchmark question representative of the topic “NMR and Magnetic Properties”.**  
 Scores assigned to each independent execution of the benchmark task, using the rubric defined above.

Iteration	Planning (%)	Geometry (%)	Input (%)	Postproc. (%)	Total (%)
Run 1	20	20	30	30	100
Run 2	20	20	30	30	100
Run 3	20	20	30	25	95
Run 4	0	10	20	15	45
Run 5	20	20	30	25	95
<b>Average</b>	16	18	28	25	87

- Run 1:  
 Parallel workflows were run where possible. Agent ran geometry optimization with B3LYP def2-TZVP RIJCOSX. Optionally, RIJCOSX with aug-cc-pVTZ was explicitly assigned aug-cc-pVTZ/JK to AuxJ in %basis block.
- Run 2:  
 Parallel workflows were run where possible. Agent ran geometry optimization with HF/aug-cc-pVTZ.

The agent was able to troubleshoot and seamlessly rename directories to resolve a naming issue.

- Run 3:

Parallel workflows were run where possible. Agent ran geometry optimization with HF/def2-TZVP. Error in the markdown report for literature chemical shift values of fluorobenzene  $\delta_{\text{exp}}$  (ppm) - the protons meta to fluorine should be the most deshielded. The theoretical justification of the  $^1\text{H}$  chemical shifts of fluorobenzene was absent in most other iterations.

- Run 4:

Parallel workflows were run where possible. In contrast to other runs, the agent did not consider referencing NMR results to TMS (for  $^1\text{H}$ ) or  $\text{CFCl}_3$  (for  $^{19}\text{F}$ ). No alternative references were considered. Agent ran geometry optimization with B3LYP def2-TZVP RIJCOSX. The agent identified a pathing issue in the input files and corrected it. The Markdown report contains incorrectly drawn chemical structures of fluorobenzene and pentafluorobenzene - this was not requested, and other runs did not attempt to draw chemical structures. Additionally,  $^{13}\text{C}$  chemical shielding values were computed, something which was not requested. As a result of not referencing the chemical shifts, the calculated chemical shift values ( $\delta$ ) were not discussed in the final report. One point to flag from this run is that the agent initially asked whether the user wanted to proceed using common NMR references and to compare the results against literature values. Because this study was executed in full-auto mode, the user provided no additional details or guidance, and the agent decided to proceed without incorporating these aspects.

- Run 5: Parallel workflows were run where possible. Agent ran geometry optimization with HF/cc-pVTZ. The agent recognized that coordinates must be placed before the %eprnmr block in ORCA input files and fixed this error. Theoretical justification of the  $^1\text{H}$  chemical shifts of fluorobenzene was absent compared to most other iterations

**C.2.16 Evaluation of the benchmark question representative of the topic “Vibrational Spectroscopy”.**

**Table 37 Evaluation Rubric.** The rubric used to grade the benchmark question representative of the topic “Vibrational Spectroscopy”.

Topic	Criterion	Weight	Task
Isotopic Effects	Planning	20%	Water optimization at the CCSD/cc-PDVZ level Modification of the Hessian file.
	Geometry generation	10%	Recalculation of vibrational frequencies. Generate initial water geometry.
	Input file generation	30%	keyword line: ! CCSD cc-pVDZ Opt NumGrad NumFreq, other convergence or grid settings allowed. AUTOCLI-CCSD also allowed. blocks: no blocks required. %numgrad, %freq, and %autocli blocks for controlled settings are optional.
	Postprocessing and reporting	40%	geometry section: * xyzfile 0 1 water_initial.xyz. Extraction of vibrational frequencies. Modification of Hessian files and recalculation of vibrational frequencies. Calculation of isotopic shifts. Quality of final report.

**Table 38 Per-iteration evaluation score for the benchmark question representative of the topic “Vibrational Spectroscopy”.**

Scores assigned to each independent execution of the benchmark task, using the rubric defined above.

Iteration	Planning (%)	Geometry (%)	Input (%)	Postproc. (%)	Total (%)
Run 1	20	10	30	40	100
Run 2	20	10	30	40	100
Run 3	20	10	30	40	100
Run 4	20	10	30	40	100
Run 5	20	10	30	40	100
<b>Average</b>	<b>20</b>	<b>10</b>	<b>30</b>	<b>40</b>	<b>100</b>

- Run 1: No issues observed.
- Run 2: No issues observed.
- Run 3: No issues observed.
- Run 4: No issues observed.
- Run 5: No issues observed.

### C.2.17 Evaluation of the benchmark question representative of the topic “Custom Optimizations”.

**Table 39 Evaluation Rubric.** The rubric used to grade the benchmark question representative of the topic “Custom Optimizations”.

Topic	Criterion	Weight	Task
Custom Optimizations	Planning Geometry generation Input file generation Postprocessing and reporting	10% 10% 50% 30%	Generation of ethylene geometry and twisted geometry. S1 geometry optimization from twisted geometry before MECP/CI search. CI search optimization from S1 equilibrium geometry using TDDFT. CI search optimization from S1 equilibrium geometry using SF-TDDFT (if bare TDDFT fails). Successful generation of ethylene geometry and twisted geometry. <b>1. MECP optimization:</b> keyword line: ! CAM-B3LYP/6-31 G Opt SurfCrossOpt; other convergence or grid settings allowed. blocks: %mecp Mult 3 end. geometry section: * xyzfile 0 1 twisted_ethylene_initial.xyz. <b>2. SF-TDDFT CI optimization:</b> keyword line: ! CAM-B3LYP 6-31G CI-OPT, other convergence or grid settings allowed. blocks: %tddft SF TRUE NROOTS 5 IRoot 2 JRoot 1 end. NROOTS can vary. %conical METHOD GP ETOL 10 <sup>-4</sup> end (other methods for CI search are also valid) geometry section: * xyzfile 0 3 twisted_ethylene_initial.xyz. The agent must try SF TDDFT and move to TDDFT only if it cannot converge the optimization. <b>3. TDDFT CI optimization (half credit):</b> keyword line: ! CAM-B3LYP 6-31G CI-OPT, other convergence or grid settings allowed. blocks: %tddft NROOTS 5 IROOT 2 JROOT 1 end. %conical METHOD UBP end. Additional tolerance settings, methods (e.g., GP, GP_nonacme) are allowed. geometry section: * xyzfile 0 1 twisted_ethylene_initial.xyz. Extraction of S0, S1, and T1 energies at the optimized geometries. Extraction of geometries (approx. 90° twisted geometry for TDDFT, pyramidalized geometry for SF TDDFT). The limitations of LR TDDFT must be clearly discussed relative to SF-TDDFT or multi-reference methods. Quality of final report.

**Table 40 Per-iteration evaluation score for the benchmark question representative of the topic “Custom Optimizations”.** Scores assigned to each independent execution of the benchmark task, using the rubric defined above.

Iteration	Planning (%)	Geometry (%)	Input (%)	Postproc. (%)	Total (%)
Run 1	10	10	40	30	90
Run 2	10	10	30	30	80
Run 3	10	10	30	20	70
Run 4	10	10	45	30	95
Run 5	10	10	25	25	70
<b>Average</b>	10	10	34	27	81

- Run 1: The agent correctly sets up input files using SF TDDFT to find the CI. The pyramidalized structure is found, but the calculation did not fully converge. The agent tried using the BHandHLYP basis set and calculations also approached the correct pyramidalized structure, but convergence was not achieved. Finally, the agent ran the calculations with TDDFT, which converged to the wrong twisted

geometry.

- Run 2: During the CI-OPT calculation, the agent assumed that the S1 state was JROOT=2 (which is T1), instead of JROOT=3. The geometry found was the non-pyramidalized twisted geometry.
- Run 3: Same as Run 2. Moreover, no discussion about pyramidalized vs flat twisted structures was conducted.
- Run 4: SF TDDFT failed to fully converge. The agent extracted the geometry with the smallest gap, ran a single-point calculation to obtain energies and other properties at that geometry, and reported it as approximate CI. The geometry showcased the correct pyramidal structure.
- Run 5: Similar to Run 2 for CI search. For MECP, the agent used broken symmetry to account for bi-radical S0 character and found a twisted bi-pyramidal structure near convergence.

### C.3 Performance of EL AGENTE QUNTUR on the benchmark set

**Table 41** Per-task scores of EL AGENTE QUNTUR on the benchmark set.

Topic	Planning (%)	Geometry (%)	Input (%)	Postproc. (%)
Relativistic Corrections	96	100	100	100
Electrical Properties	100	100	97	100
Orbitals and Densities	100	90	100	100
Condensed Fukui Functions	100	100	100	100
Thermochemistry	90	100	87	83
Conformer Generation	100	100	93	86
Molecular Dynamics	100	100	80	100
Explicit Solvation	100	100	100	100
Potential Energy Surfaces	100	100	100	100
Transition State Methods	100	100	99	100
Reaction Mechanisms	80	100	90	90
Isotopic Effects	96	100	87	100
Excited States	50	100	100	100
Excited-State Kinetics	100	100	100	100
NMR and Magnetic Properties	80	90	93	83
Vibrational Spectroscopy	100	100	100	100
Custom Optimizations	100	100	85	90
Overall	93.6	96.3	94.8	96.0

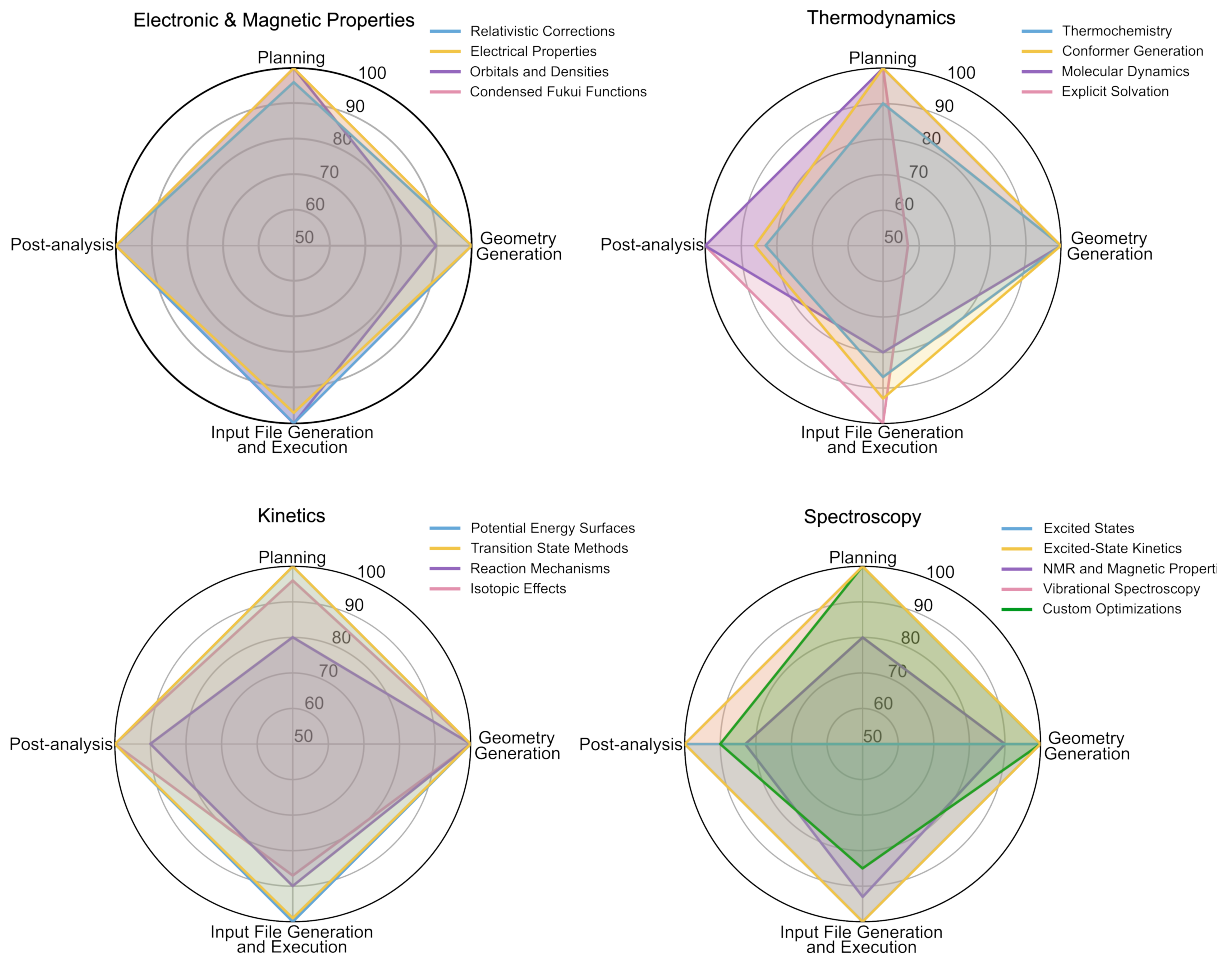


**Figure 5 Performance of EL AGENTE QUINTUR on the benchmark set.** The benchmark consists of a set of 17 computational quantum chemistry exercises covering several topics from electronic and magnetic properties, thermodynamics, kinetics, and spectroscopy, as well as the various levels of theory and difficulty. The benchmark questions are in the [Supporting Information Section B](#). The rubric for each question is in the [Supporting Information Section C](#). All benchmarks were conducted using Claude Opus 4.5 as the base language model for all agents.

## D Benchmark Token Analysis

According to [6](#) and [7](#), the two main sources of token consumption are `computational_chemist` and `input_file_service`. `computational_chemist` handles high-level planning and post-processing, while `input_file_service` focuses on per-calculation program synthesis. Both are reasoning-heavy tasks, and it is expected—and desirable—that high- and low-level responsibilities are separated so that no single agent becomes overloaded.

The `interact_with_os` agent extracts statistics from output files and performs basic file organization. Because it reads output files, it can incur substantial token usage. Its token spend is relatively low here because we apply a forgetting mechanism: once it finishes a clearly scoped extraction task, we clear its working memory. This reduces token consumption for an otherwise demanding operation.

Overall, this illustrates effective separation of responsibilities: offloading operational work from `computational_chemist` helps keep its context clean for ongoing planning and decision-making.

As shown in Fig. [6](#), total token consumption varies across benchmark questions, reflecting differences in difficulty and in the amount of content required to solve each question.

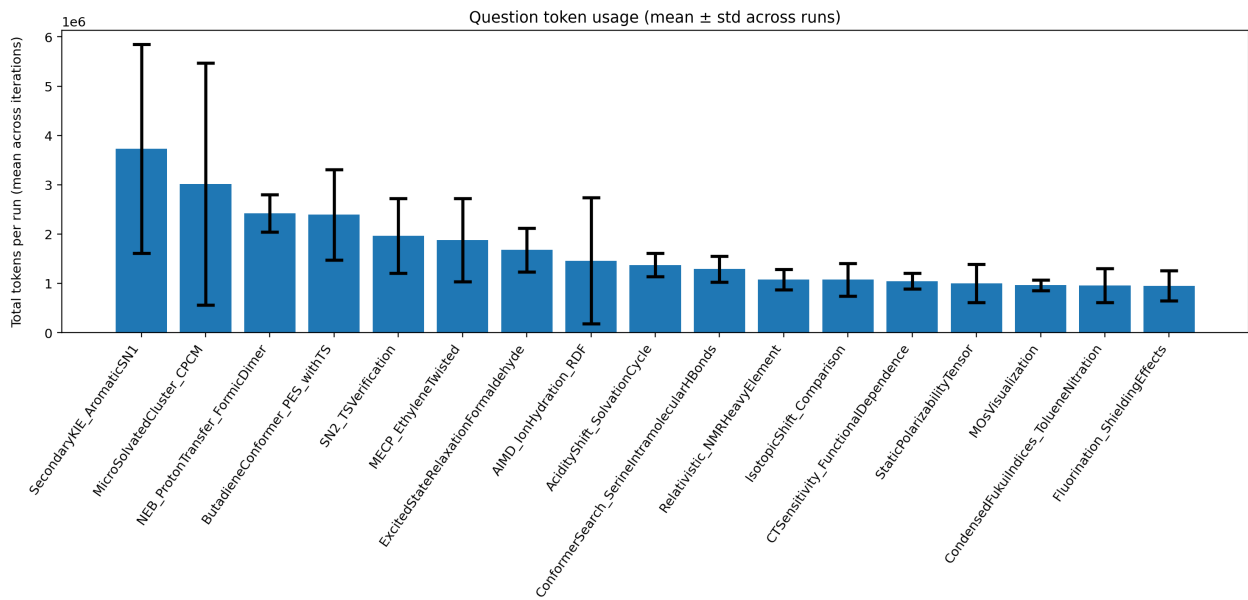


**Figure 6** Total token usage per question, averaged over five iterations; error bars indicate  $\pm 1$  standard deviation.

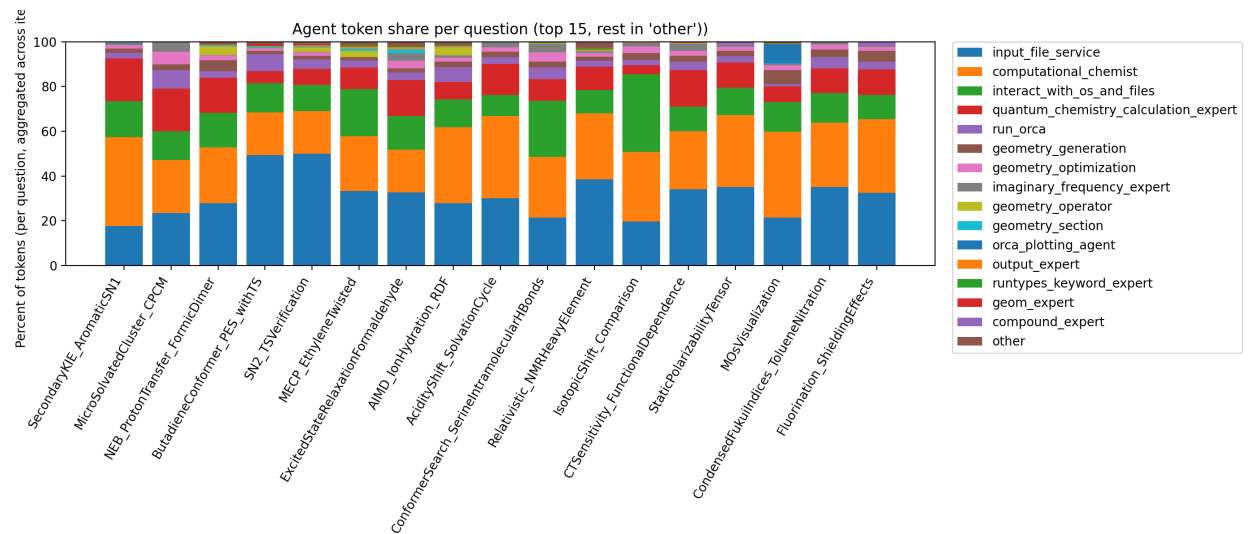


**Figure 7** Across-question agent token-share statistics: bars show the mean percentage contribution per agent, and black lines indicate  $\pm 1$  standard deviation across questions.

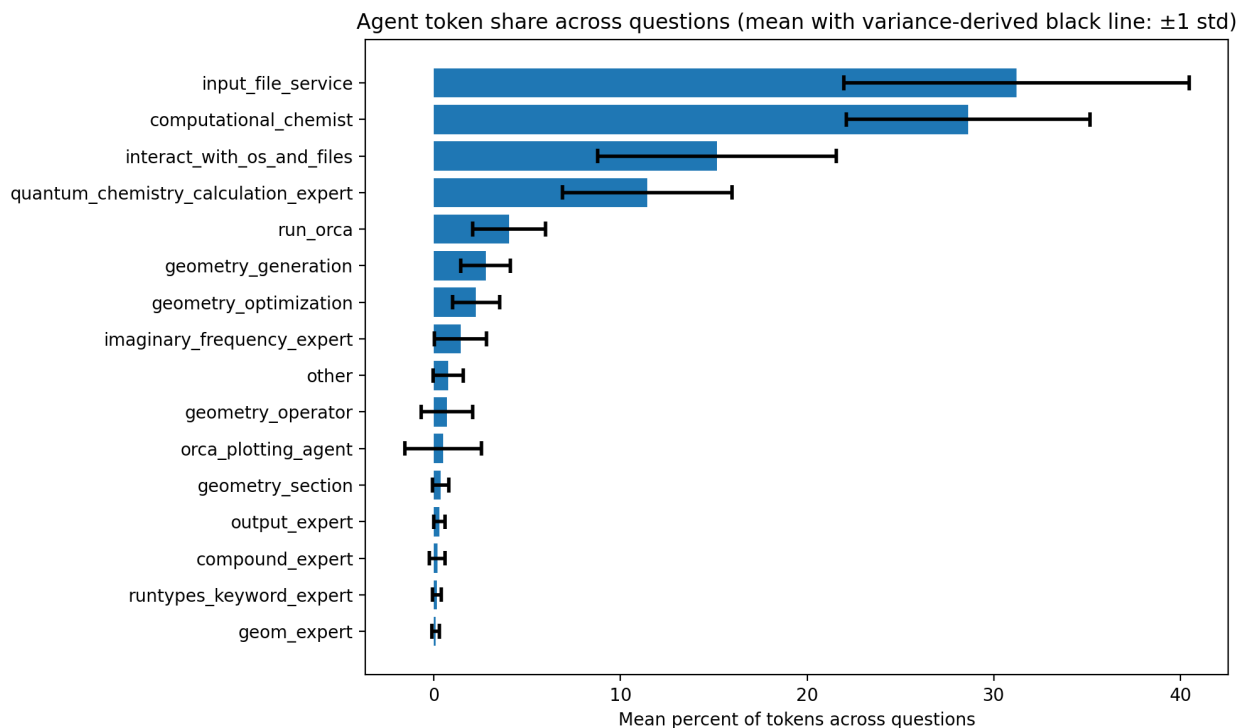


**Figure 8** Per-question distribution of token usage across agents, expressed as percentages (aggregated over five iterations) and normalized to 100% per question.

## E EL AGENTE QUNTUR case studies

As a research collaborator, the agent needs to formulate, execute, refine, and validate a computational chemistry plan with different levels of human intervention and feedback. During the case studies, we assess QUNTUR’s proficiency in several key computational chemistry reasoning “sub-skills”. These sub-skills include planning, input file generation and execution, postprocessing, 3D geometric reasoning, and self-debugging. Each sub-skill is critical for carrying out complex tasks end-to-end without excessive intervention. Here we present a summary of the trajectories for each case study, including at list one of the original images produced by Quntur.

### E.1 Case study: global softness and chemoselectivity

#### E.1.1 Context

This question touches on the connection between chemical concepts, such as electrophilicity, and more formal mathematical definitions in quantum chemistry [135]. Properties such as Fukui functions, hardness, and local softness quantify qualitative concepts such as reactivity. This is important not only for understanding selectivity and mechanism but also because these computed descriptors can serve as high-quality data for many machine-learning models.

#### E.1.2 Assessment

The agent completed the workflow without runtime errors and produced all requested quantities. The task does not pose any challenges in some reasoning dimensions. Geometry generation and verification were straightforward, and no geometric manipulation or nontrivial spatial reasoning was required, making it difficult to assess deeper geometric understanding. Method selection and input-file construction were handled correctly, including appropriate charge and multiplicity assignments and population-analysis keywords. The

recommendation to include D4 dispersion demonstrated a high degree of adaptability, as it involves going against the original user prompt. Because no convergence or syntax issues arose, the agent's debugging and error-recovery capabilities were not exercised in this example. Postprocessing was executed correctly, with accurate parsing of outputs, computation of global and local softness, and generation of visual summaries. Overall, the agent performed competently on a relatively routine quantum-chemistry task.

### E.1.3 Prompt and initial planning:



User

Take a bifunctional molecule containing both an alkene and a carbonyl (e.g., methyl vinyl ketone). Using ORCA, compute condensed Fukui functions, global hardness/softness, and local softness values at all heavy-atom centers. Predict whether a soft nucleophile will preferentially attack the  $\beta$ -carbon of the alkene (Michael addition) or the carbonyl carbon (1,2-addition).



Computational\_chemist

**Step 1: Geometry Generation** Generate an initial molecular geometry of methyl vinyl ketone (MVK),  
 $\text{CH}_3\text{--CO--CH=CH}_2$ .

**Step 2: Geometry Optimization** Optimize the geometry of neutral MVK with the following electronic state:  
Charge = 0, Multiplicity = 1.

Verify that the optimized structure corresponds to a true minimum on the potential energy surface by performing a vibrational frequency analysis and confirming the absence of imaginary frequencies.

**Step 3: Single-Point Calculations for Conceptual DFT (Parallel Execution)**

- **Neutral system (N electrons):** Charge = 0, Multiplicity = 1, including population analysis (MBIS or Hirshfeld).
- **Anion (N + 1 electrons):** Charge = -1, Multiplicity = 2, including population analysis.
- **Cation (N - 1 electrons):** Charge = +1, Multiplicity = 2, including population analysis.

**Step 4: Post-Processing and Analysis**

- Extract atomic populations for all heavy atoms: carbonyl carbon (C<sub>1</sub>), methyl carbon (C<sub>2</sub>),  $\alpha$ -carbon (C<sub>3</sub>),  $\beta$ -carbon (C<sub>4</sub>), and oxygen.

• Compute condensed Fukui functions for nucleophilic attack:  
$$f_k^+ = P_k(N + 1) - P_k(N),$$
 where  $P_k$  denotes the atomic population of atom  $k$ .

- Compute the global hardness:

$$\eta = \frac{1}{2}(\text{IP} - \text{EA}),$$

and the global softness:

$$S = \frac{1}{\eta}.$$

- Compute the local softness for nucleophilic attack:

$$s_k^+ = S \times f_k^+.$$

- Predict the preferred site for soft nucleophilic attack based on the atom with the largest  $s_k^+$  value.



User

Proceed using b3lyp def2-svp MBIS, Hirshfeld, and Mulliken populations

## E.1.4 Summary of the results



User

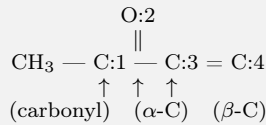
### Action:

Conceptual DFT Analysis Complete

### Summary

I successfully performed a comprehensive DFT analysis of methyl vinyl ketone (MVK) to predict the regioselectivity of soft-nucleophile attack. Here are the key findings:

#### Molecule Structure (Confirmed)



#### Global Reactivity Descriptors

Property	Value
Ionization Potential (IP)	9.38 eV
Electron Affinity (EA)	-0.76 eV
Global Hardness ( $\eta$ )	5.07 eV
Global Softness (S)	0.099 eV $^{-1}$
Electrophilicity ( $\omega$ )	1.83 eV

#### Condensed Fukui Functions $f^+$ (Nucleophilic Attack Sites)

Site	MBIS $f^+$	Hirshfeld $f^+$	Mulliken $f^+$
C4 ( $\beta$ -carbon)	0.296	0.201	0.141
C1 (carbonyl)	0.217	0.142	0.096
O2 (oxygen)	0.140	0.162	0.152
C3 ( $\alpha$ -carbon)	0.051	0.114	0.034

#### Prediction

All three population schemes consistently show:

$$f^+(C4-\beta) > f^+(C1\text{-carbonyl})$$

with ratios of 1.36–1.47.

According to the HSAB (Hard-Soft Acid-Base) theory:

Nucleophile Type	Preferred Attack Site	Product
Soft (enolates, thiols, amines)	C4 ( $\beta$ -carbon)	Michael addition (1,4)
Hard (Grignards, LiAlH <sub>4</sub> )	C1 (carbonyl)	1,2-addition

#### Conclusion

A soft nucleophile will preferentially attack the  $\beta$ -carbon (C4), leading to Michael addition rather than 1,2-addition at the carbonyl carbon. This computational prediction is consistent with well-established experimental reactivity patterns for  $\alpha, \beta$ -unsaturated carbonyl compounds.

**Condensed Fukui Functions for Methyl Vinyl Ketone (MVK)  
B3LYP/def2-SVP**

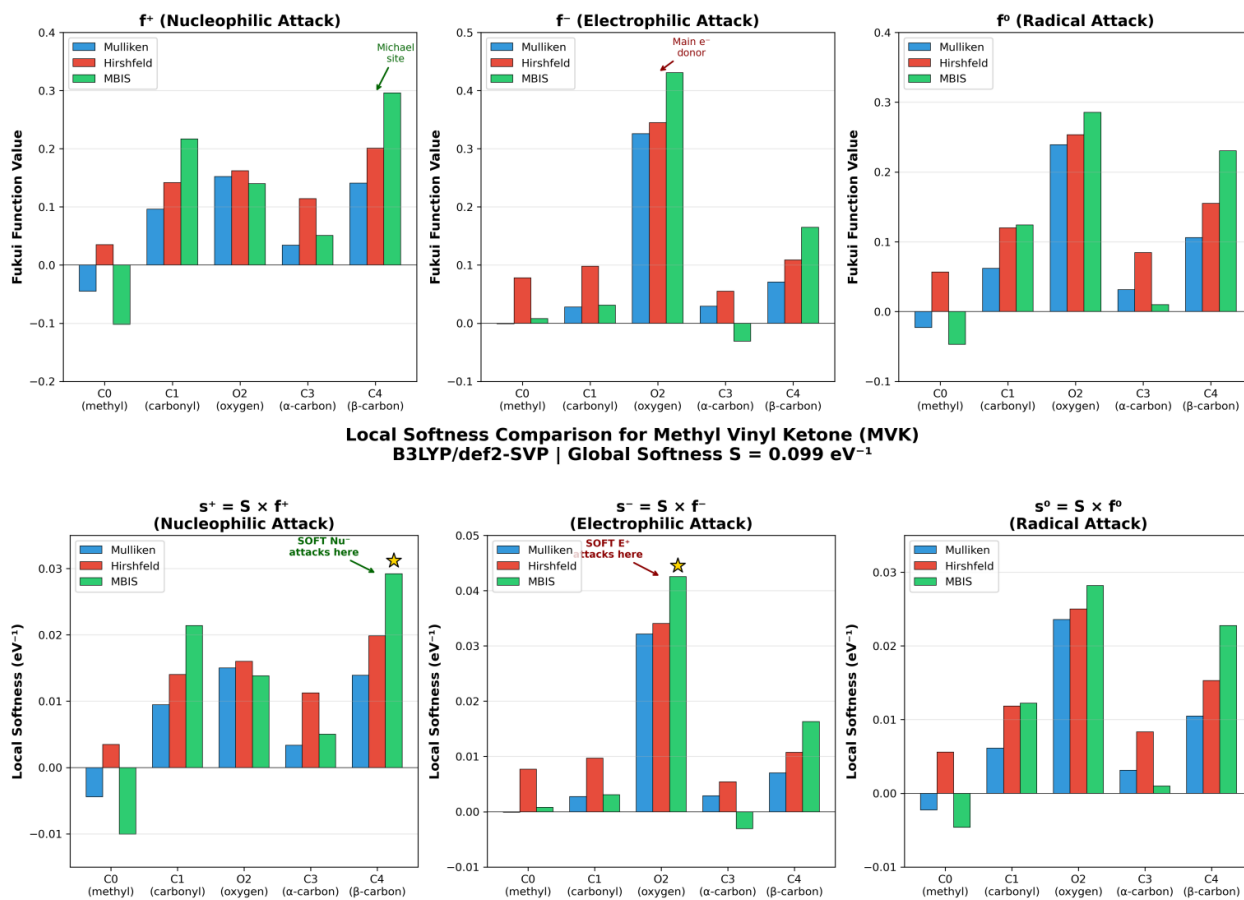


**Figure 9** Summary of the findings for global softness and chemoselectivity case study.

## E.2 Case study: $^{31}\text{P}$ NMR absolute shielding and chemical shift tensor of triphenylphosphine oxide

### E.2.1 Context

$^{31}\text{P}$  NMR is a powerful tool in organometallic chemistry for the visualization of phosphorus-containing compounds. While the organic chemist might be tempted to view  $^{31}\text{P}$  NMR as an extension of more familiar nuclei such as  $^1\text{H}$  and  $^{13}\text{C}\{^1\text{H}\}$  NMR, there are key differences in the factors that determine a  $^{31}\text{P}$  chemical shift. As a heavier nucleus, the paramagnetic contribution to the shielding tensor is more significant for  $^{31}\text{P}$ ; consequently, the chemical shift is less directly reflective of the local electron density surrounding the phosphorus atom [136]. This behavior contrasts with that of lighter nuclei, for which diamagnetic contributions more strongly govern chemical shifts. The spectral range of  $^{31}\text{P}$  NMR is notably wide, and, while it is often possible to predict the general region in which a resonance of interest will appear, the exact chemical shift cannot typically be determined *a priori* [137]. Furthermore,  $^{31}\text{P}$  NMR has a comparatively smaller body of literature examples than  $^1\text{H}$  and  $^{13}\text{C}\{^1\text{H}\}$  NMR, which can make reliable chemical shift prediction for novel phosphorus-containing compounds particularly challenging. To establish a computational ground truth, we therefore asked Quntur to predict the  $^{31}\text{P}$  NMR properties of triphenylphosphine oxide. This system will serve as a benchmark for more ambitious NMR calculations.

## E.2.2 Assessment

The agent completed the workflow without runtime errors and produced all requested quantities. The initial prompt and workplan suggested by Quntur are reasonable. Quntur found a literature example in the prompt and conducted a search that identified subsequent papers that built on the provided benchmark. Only minor, non-critical errors were observed by reading the chat history. In each case, the respective agent identified the source of the error and resubmitted the job to the backend without observing any job failures. A representative example from the chat memory: “Note: Initial submission failed due to input file ordering (%eprnmr block appeared before coordinates). Fixed by reordering blocks so coordinates precede the %eprnmr block.” Quntur used two DFT basis sets to compare and contrast which functional best matched the value for triphenylphosphine oxide reported in the primary literature. The best functional selected, B3LYP/def2-TZVP, matched closely with the  $^{31}\text{P}$  NMR shift in deuterated chloroform reported in the literature. The assessor independently verified this value with experimental data published in the primary literature (e.g., see Ref. 138). One thing to note is that Quntur’s logic of using the CSA span of trimethyl phosphine oxide as a surrogate for that of triphenyl phosphine oxide makes sense. However, Quntur noted that the CSA span value reported for triphenylphosphine oxide does not match the experimental values. The CSA span is a parameter used in solid-state NMR, so it may not be relevant for gas-phase calculations. The user’s requested literature overview was relevant, and spot checks by the assessor confirmed that these papers were valid suggestions in line with the initial prompt. The resulting publication-ready figure accurately reflected the calculations and provided a clear visual comparison of the computational methods with the experimentally derived primary literature. Overall, the agent performed competently in calculating the  $^{31}\text{P}$  NMR chemical shift for a well-reported organic molecule commonly used in synthetic wet labs.

References used by Quntur during this case study[139–152]

## E.2.3 Prompt and initial planning:



User

Using ORCA 6.0 and following the recommendations from Shenderovich’s paper “Experimentally Established Benchmark Calculations of  $^{31}\text{P}$  NMR Quantities” (Chemistry-Methods 2021, 1, 61–70), compute the  $^{31}\text{P}$  NMR absolute shielding and chemical shift tensor of triphenylphosphine oxide. Choose the density functional, basis set, and any relativistic or gauge-treatment options based on the paper’s identification of a good compromise between cost and accuracy for  $^{31}\text{P}$ . Report the isotropic shielding, chemical shift, and CSA parameters, and compare your results to available experimental  $^{31}\text{P}$  NMR data for  $\text{Ph}_3\text{P}=\text{O}$ . Comment briefly on how sensitive your results are to the level of theory and on whether the benchmark-guided protocol appears transferable from the model systems in the paper to this molecule.



User

Action: Excellent! I found valuable information. Based on the literature search (including papers that build on Shenderovich's benchmark), here's what I learned:

**Key Findings from Literature**

Shenderovich's recommended protocol (inferred from his later work that uses the Chem-Methods benchmark):

Parameter	Recommendation
Functional	$\omega$ B97X-D (range-separated hybrid with dispersion)
Basis set	def2-TZVP or def2-QZVP
Gauge treatment	GIAO (gauge-including atomic orbitals)
Reference shielding $\sigma_{\text{ref}}(^{31}\text{P})$	306 ppm ( $\omega$ B97X-D/def2-TZVP) or 308 ppm ( $\omega$ B97X-D/def2-QZVP)

Relativistic effects: For P bonded only to light atoms (C, O, H), scalar relativistic corrections are typically  $< 7\%$  — not strictly required but can be included via DKH2 or ZORA for completeness.

Experimental  $^{31}\text{P}$  data for  $\text{Ph}_3\text{P}=\text{O}$ : Literature reports  $\delta(^{31}\text{P}) \approx +25$  to  $+29$  ppm (relative to 85%  $\text{H}_3\text{PO}_4$ ) with CSA span ( $\Omega$ ) around 100–130 ppm.

**Proposed High-Level Plan**

**Step 1: Geometry Generation (parallel)**

- Generate initial geometry of triphenylphosphine oxide ( $\text{Ph}_3\text{P}=\text{O}$ )
- Generate initial geometry of phosphoric acid ( $\text{H}_3\text{PO}_4$ ) as NMR reference

**Step 2: Geometry Optimization (parallel)**

- Optimize both molecules at  $\omega$ B97X-D/def2-TZVP level
- Include frequency calculation to confirm true minima

**Step 3: NMR Shielding Tensor Calculation (parallel)**

- Compute full  $^{31}\text{P}$  shielding tensor for both molecules using GIAO- $\omega$ B97X-D/def2-TZVP
- Extract isotropic shielding ( $\sigma_{\text{iso}}$ ) and principal components ( $\sigma_{11}, \sigma_{22}, \sigma_{33}$ )

**Step 4: Analysis and Comparison**

- Compute chemical shift:  $\delta_{\text{iso}} = \sigma_{\text{ref}}(\text{H}_3\text{PO}_4) - \sigma(\text{Ph}_3\text{P} = \text{O})$
- Extract CSA parameters: span  $\Omega = \sigma_{33} - \sigma_{11}$ , skew  $\kappa$
- Compare with experimental data and assess transferability

Details:

Charge/multiplicity: 0, 1 (neutral closed-shell for both molecules)

Phase: Gas phase (as requested)

Software: ORCA 6.0

Do you want me to proceed with this plan?

Also, would you like me to include a second level of theory (e.g., PBE0/def2-TZVP) to assess sensitivity to functional choice? This would only add one additional step and directly address your question about "how sensitive results are to the level of theory."



User

Yes, proceed with this plan and use B3LYP def2-tzvp to assess functional sensitivity.

## E.2.4 Summary of the results



Computational\_chemist

Action: Task Complete: 31P NMR Analysis of Triphenylphosphine Oxide

### Summary of Results

Property	B3LYP/def2-TZVP	$\omega$ B97X-D3/def2-TZVP	Experimental
$\delta_{\text{iso}}$ (ppm)	25.6 ✓	18.2	$\sim 28 \pm 1$
Span $\Omega$ (ppm)	243	242	$\sim 200^*$
Skew $\kappa$	-1.00	-0.99	-
Asymmetry $\eta$	0.00	0.00	-

\*Estimated from analogous P=O compounds (Me<sub>3</sub>PO, phosphonates)

### Key Findings

*Best Method:* B3LYP/def2-TZVP provides excellent agreement with experiment (error < 3 ppm), outperforming the Shenderovich-recommended  $\omega$ B97X-D3 protocol for this system.

### Functional Sensitivity:

- Isotropic shift varies by  $\sim 7.5$  ppm between functionals.
- CSA span is remarkably insensitive (< 0.5% difference).

**Tensor Characteristics:** Near-axial symmetry ( $\sigma_{11} \approx \sigma_{22} \ll \sigma_{33}$ ) consistent with C<sub>3</sub><sup>v</sup>-like local symmetry at phosphorus.

**Benchmark Transferability:** The Shenderovich protocol ( $\omega$ B97X-D3/def2-TZVP with  $\sigma_{\text{ref}} = 306\text{--}308$  ppm) was calibrated on small model compounds. For aryl phosphine oxides, this protocol underestimates chemical shifts by  $\sim 10$  ppm when using computed H<sub>3</sub>PO<sub>4</sub> as reference. This suggests:

- The original  $\sigma_{\text{ref}}$  values from the paper should be used directly, **or**
- Linear scaling corrections are needed for conjugated systems.

B3LYP remains a reliable workhorse for organophosphorus compounds.

### Files Generated

- Optimized geometries: Ph3PO\_opt/, H3PO4\_opt/
- NMR outputs: Ph3PO\_NMR\_wB97XD3/, Ph3PO\_NMR\_B3LYP/, H3PO4\_NMR\_wB97XD3/, H3PO4\_NMR\_B3LYP/
- Reference added: references.bibtex

Would you like me to generate any additional analysis, plots, or documentation?

**$^{31}\text{P}$  NMR of Triphenylphosphine Oxide ( $\text{Ph}_3\text{P}=\text{O}$ )**  
**GIAO-DFT / def2-TZVP //  $\omega\text{B97X-D3}/\text{def2-TZVP}$  optimized geometry**

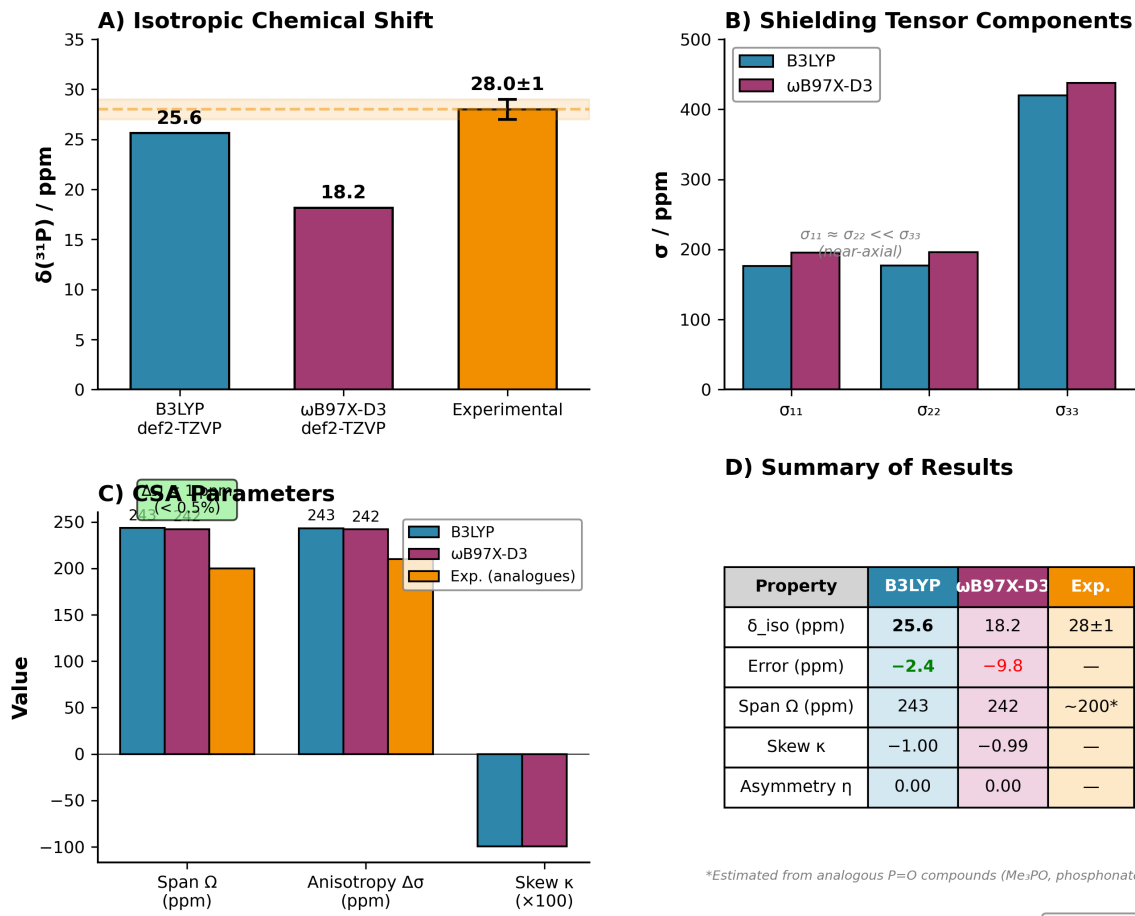


**Figure 10** Summary of the findings for the case study “ $^{31}\text{P}$  NMR absolute shielding and chemical shift tensor of triphenylphosphine oxide”.

## E.3 Case Study: Solvation effects on the keto-enol equilibrium of acetylacetone in water

### E.3.1 Context

Keto–enol tautomerism is a fundamental chemical equilibrium in which the relative stability of the tautomers is strongly influenced by solvation. Changes in solvent environment can significantly modify the solvation free energies of the keto and enol forms, thereby shifting the tautomeric equilibrium. Acetylacetone is a well-known model system for studying this effect, as its keto–enol equilibrium is particularly sensitive to hydrogen bonding and water-induced polarization. Accurately capturing these solvation contributions to the free energy remains challenging in computational chemistry. Implicit solvent models efficiently describe bulk electrostatic effects but neglect specific solute–solvent interactions, whereas explicit solvent models can capture hydrogen bonding at a higher computational cost. Hybrid explicit–implicit approaches offer a balanced strategy by combining local, explicit solvation with a continuum treatment of the surrounding solvent.

### E.3.2 Assessment

The study begins with the parallel generation of geometries for the keto and enol tautomers of acetylacetone, along with the construction of microsolvated clusters containing multiple water molecules to represent different hydrogen-bonding environments. These structures provide the starting point for evaluating solvation effects at increasing levels of complexity.

In the next stage, both tautomers are optimized in the gas phase using an implicit water model, and thermodynamic quantities are obtained from frequency calculations. This allows a direct comparison between unsolvated and continuum-solvated descriptions of the keto–enol equilibrium.

The workflow then proceeds to hybrid cluster–continuum calculations, in which microsolvated keto and enol clusters are optimized while embedded in an implicit solvent environment. The lowest-energy solvation motifs are selected to represent explicitly solvated states.

Finally, higher-level single-point energy corrections are applied, and the resulting free energy differences and equilibrium constants are evaluated for the gas-phase, implicit, and hybrid solvation models. These results are compared to assess how solvation treatment influences the predicted keto–enol equilibrium.

### E.3.3 Prompt and initial planning:



User

Design a hybrid explicit + implicit solvation protocol in ORCA to study the keto-enol equilibrium of acetylacetone in water. Construct microsolvated clusters of both tautomers with at least ten explicit water molecules embedded in CPCM water, optimize all low-energy H-bonding motifs, and compute  $\Delta G_{keto \rightarrow enol}$ . Compare the equilibrium constant obtained from (i) gas phase, (ii) CPCM-only, and (iii) cluster-continuum (explicit+implicit) models and discuss which description best reproduces the known enol stabilization in aqueous solution. Read literature and find the best DFT functional that accurately reproduces the experimental results.



This is a sophisticated computational chemistry research project! You're asking me to study the keto-enol equilibrium of acetylacetone in water using three different solvation models, which is an excellent way to understand solvation effects on tautomeric equilibria.

Before I create a high-level plan, let me perform the literature search you requested to find:

- The best DFT functional for accurately reproducing experimental keto-enol equilibrium
- Experimental reference values for acetylacetone in aqueous solution
- Best practices for cluster-continuum approaches

#### *Summary of Literature Findings*

- Gas phase: Acetylacetone is essentially 100% enol at 300 K (strong intramolecular H-bond stabilization)
- In water: The equilibrium shifts significantly toward the keto form compared to organic solvents
- Reference: Iglesias[153] (Perkin Trans. 2, 1997) - experimental K\_eq for acetylacetone in water at 25°C.

#### Best DFT Functional Recommendations (Mehrani *et al.*[154]):

- For highest accuracy: B2PLYP-D3(BJ)/def2-TZVP (double-hybrid) or CBS-QB3 gave closest match to experimental equilibrium constants
- For geometry optimization:  $\omega$ B97X-D3/def2-TZVP or B3LYP-D3(BJ)/def2-TZVP
- Key finding: Lower-level methods (B3LYP or MP2 alone) were noticeably less accurate for the keto-enol free-energy difference once solvent was included

#### Critical Points:

- Microsolvation with explicit water molecules (typically 3–10 or more) has a substantial impact on hydrogen-bonding patterns and relative tautomer stabilities.
- A cluster-continuum approach, combining explicit solvent molecules with an implicit solvation model, is required for quantitative accuracy.
- Multiple hydrogen-bonding configurations must be sampled to obtain reliable thermodynamic averages.



## Proposed High-Level Plan

Step 1: Geometry Generation (All steps parallelized)

- Generate keto tautomer of acetylacetone.
- Generate enol tautomer of acetylacetone.
- Create microsolvated clusters (10+ waters) for both tautomers using SOLVATOR with multiple H-bonding motifs

Step 2: Gas-Phase and Implicit-Solvent Optimizations (All steps parallelized)

- 2a: Optimize keto (gas phase) + frequency calculation
- 2b: Optimize enol (gas phase) + frequency calculation
- 2c: Optimize keto (CPCM-water only) + frequency calculation
- 2d: Optimize enol (CPCM-water only) + frequency calculation

Step 3: Cluster-Continuum Optimizations (All steps parallelized)

- Optimize all microsolvated keto clusters (10+ waters embedded in CPCM) + frequency calculations.
- Optimize all microsolvated enol clusters (10+ waters embedded in CPCM) + frequency calculations
- Keep lowest-energy H-bonding motifs for each tautomer

Step 4: High-Level Single-Point Energy Corrections (All parallel)

- Compute B2PLYP-D3(BJ)/def2-TZVP single-point energies on all optimized structures for improved accuracy

Step 5: Thermodynamic Analysis and Comparison

- Compute  $\Delta G_{\text{keto} \rightarrow \text{enol}}$  for:
  1. Gas phase
  2. CPCM-only
  3. cluster-continuum (explicit + implicit)
- Calculate equilibrium constants  $K_{\text{eq}}$  for each solvation model.
- Compare computed results with available experimental data.
- Compile and analyze results in the final report.

## Key Methodological Details

**Table 42** Recommended computational approaches for keto–enol equilibrium calculations of acetylacetone.

Aspect	Recommended Approach
Geometry optimization	$\omega\text{B97X-D3}/\text{def2-TZVP}$ (good for hydrogen bonding and dispersion)
Thermochemistry	Frequency calculations at same level for ZPE and thermal corrections
Final energetics	B2PLYP-D3(BJ)/def2-TZVP single-points (double-hybrid for accuracy)
Implicit solvation	CPCM (water)
Explicit solvation	SOLVATOR with 10–15 water molecules
Cluster sampling	Generate 3–5 initial H-bonding motifs per tautomer

## Questions

## Before

## Proceeding:

- **Charge and multiplicity:** Both tautomers are neutral closed-shell (charge = 0, multiplicity = 1). Is this correct?
- **Number of explicit waters:** The user specified “at least 10”. Would you like me to use 10–12 waters to balance accuracy with computational cost, or go higher (15+)?
- **Number of H-bonding motifs to sample:** For good statistics, I recommend generating 3–5 different initial configurations per tautomer. Is this acceptable?
- **Computational resources:** Double-hybrid B2PLYP calculations on clusters with 10+ waters will be moderately expensive. Should I proceed with this level, or would you prefer to stay with hybrid DFT ( $\omega\text{B97X-D3}$ ) only?
- **Additional analysis:** Would you like any additional analysis (e.g., NBO analysis of H-bonding, visualization of key structures)?

Please confirm or modify this plan, and I'll proceed with execution.



User

Please proceed



Computational\_chemist

## Summary

**Table 43** Comparison of computed keto–enol free energies, equilibrium constants, and tautomer populations with experimental aqueous-phase data.

Model	$\Delta G_{\text{keto} \rightarrow \text{enol}}$ (kcal/mol)	$K_{\text{eq}}$ (E/K)	%Enol	%Keto	Match Exp.?
(i) Gas phase	-3.91	735	99.9	0.1	Yes
(ii) CPCM-only	-0.57	2.6	72	28	No
(iii) Cluster + CPCM	+3.73	0.002	0.2	99.8	Qualitative
Experiment (aq)	~ +1.0	~ 0.18	~ 15	~ 85	Reference



User

Could you also do the calculations with SMD?



Computational\_chemist

## Action: SMD Calculations Complete – Final Comparison

**Table 44** Comparison of solvation models for acetylacetone keto–enol equilibrium.

Model	$\Delta G(\text{keto} \rightarrow \text{enol})$	$K_{\text{eq}}$	%Enol	%Keto	Error	Verdict
EXPERIMENT	+1.03 kcal/mol	0.176	15.0%	85.0%	–	Reference
SMD(water)	+0.62 kcal/mol	0.35	25.9%	74.1%	0.41	BEST
CPCM(water)	-0.57 kcal/mol	2.60	72.3%	27.7%	1.60	WRONG
Cluster+CPCM	+3.73 kcal/mol	0.002	0.2%	99.8%	2.70	~ Qualitative
Gas Phase	-3.91 kcal/mol	735	99.9%	0.1%	4.94	✓ (gas ref)

### Key

### Findings

- SMD is dramatically better than CPCM (error reduced by 1.19 kcal/mol)
- SMD correctly predicts keto preference in water ( $\Delta G = +0.62$  kcal/mol)
- Plain CPCM predicts the WRONG tautomer (enol instead of keto)

This confirms Mehrani et al.'s methodology – their excellent results (MAE = 2.3%) were likely obtained with SMD rather than plain CPCM.

SMD	includes	critical	non-electrostatic	terms:
	<ul style="list-style-type: none"> <li>• Cavitation energy</li> <li>• Dispersion interactions</li> <li>• Solvent structure / H-bonding corrections</li> </ul>			

## Conclusion

For acetylacetone keto–enol tautomerism in water:

Approach	Recommendation
Best accuracy	SMD(water) – error ~0.4 kcal/mol
Explicit solvation	Cluster+CPCM – qualitatively correct but needs more sampling
Avoid	Plain CPCM – predicts wrong tautomer preference

Our results now match Mehrani et al.'s reported accuracy, confirming that SMD (not plain CPCM) is the appropriate implicit solvation model for tautomeric equilibria in aqueous solution.

### Acetylacetone Keto-Enol Tautomerism: Complete Solvation Model Comparison

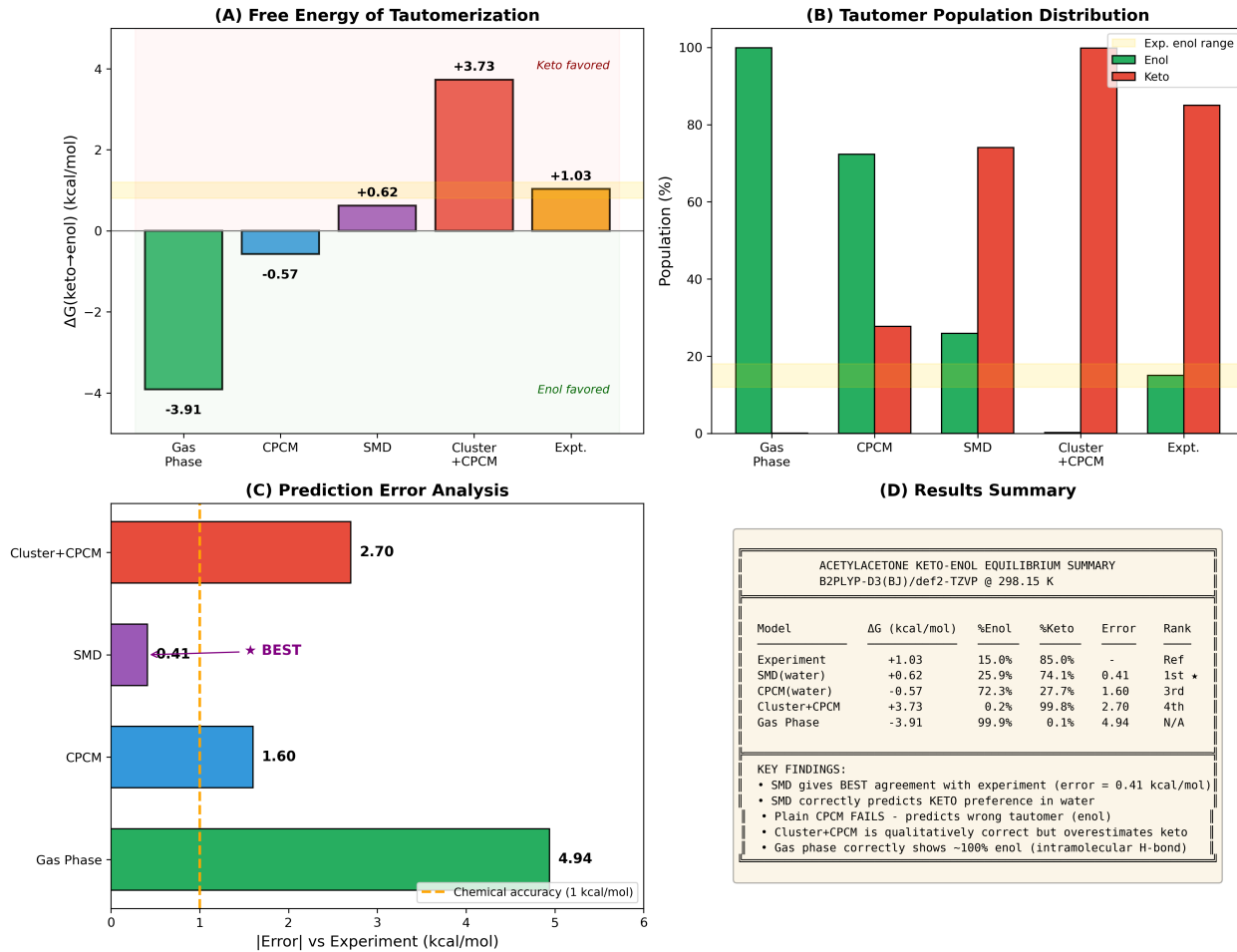


**Figure 11** Solvation study for acetylacetone keto–enol tautomerism: (a) free energies of tautomerization, (b) keto–enol population distributions, (c) prediction error analysis, and (d) overall results summary.

## E.4 Case study: Fluorescence and intersystem crossing rates of anthracene

### E.4.1 Context

Accurately modeling the competition between fluorescence and intersystem crossing is essential for understanding and predicting the photophysical behavior of organic molecules. In systems such as anthracene, small errors in excited-state energies or vibrational structures can lead to order-of-magnitude changes in predicted lifetimes and quantum yields. Because radiative and nonradiative decay pathways often differ by only subtle energetic or vibronic effects, reliable simulations must treat electronic structure, state ordering, and rate theory in a consistent and physically grounded manner.

These calculations are therefore not only a matter of reproducing experimental observables but of validating the underlying physical mechanisms that govern excited-state relaxation. Incorrect state assignments, incomplete excited-state optimization, or oversimplified rate models can easily lead to qualitatively incorrect conclusions about dominant decay channels. Within the Matter Lab's broader effort to understand and control excited-state dynamics in functional molecular materials, anthracene serves as a stringent test case in which predictive accuracy depends on capturing the interplay between energy gaps, spin-orbit coupling, and nuclear motion with sufficient fidelity.

### E.4.2 Assessment

EL AGENTE QUNTUR's overall planning was sound and well aligned with the physical complexity of the problem. The agent correctly identified the need for a multistage workflow that includes ground-state optimization, vertical excitation analysis, excited-state optimizations, and explicit rate calculations using ORCA's ESD module. This structure reflects an appropriate decomposition of a demanding photophysical task into tractable computational steps.

The execution remained consistent with the original plan. Adiabatic energies for S0, S1, T1, and T2 were physically reasonable and internally consistent, enabling a meaningful comparison of radiative and nonradiative decay pathways. The agent correctly accounted for the fact that intersystem crossing rates cannot be inferred from spin-orbit coupling alone and relied on the full rate formalism to capture the role of energetic near resonance.

From a computational standpoint, the task was demanding, requiring more than a dozen large-scale simulations, each using 24 cores, with a total wall time of roughly twelve hours. Despite this, the agent maintained coherence across inputs, avoided unnecessary recomputation, and completed all stages without requiring any intervention beyond the method specification. The final interpretation went beyond a numerical summary and correctly identified the dominance of the S1 to T2 intersystem crossing channel as a consequence of the energy gap law overcoming simple selection rule arguments, demonstrating effective synthesis of planning, execution, and physical reasoning.

### E.4.3 Prompt and initial planning:



User

For anthracene, use ORCA to compute low-lying singlet and triplet excited states. Estimate intersystem crossing (ISC) rates and compare them qualitatively with radiative decay (fluorescence) rates. By default use always 24 cores

**Anthracene Photophysics: ISC and Fluorescence Rates**

This project constitutes a comprehensive photophysical analysis requiring the use of ORCA's Excited State Dynamics (ESD) module. The high-level workflow is outlined below.

**Proposed High-Level Plan****Step 1: Geometry Generation**

- Generate the initial geometry of anthracene.

**Step 2: Ground-State Characterization**

- Optimize the  $S_0$  ground-state geometry and compute vibrational frequencies.
- Perform a TDDFT calculation to identify low-lying singlet and triplet excited states (vertical excitations).

**Step 3: Excited-State Optimizations (in parallel)**

- Optimize the  $S_1$  geometry with a frequency calculation.
- Optimize the  $T_1$  geometry with a frequency calculation.
- Optimize the  $T_2$  geometry with a frequency calculation, if  $T_2$  lies close enough in energy to be relevant for ISC from  $S_1$ .

**Step 4: Rate Calculations via the ESD Module (in parallel)**

- Compute ISC rate constants for  $S_1 \rightarrow T_1$  transitions across all triplet sublevels.
- Compute ISC rate constants for  $S_1 \rightarrow T_2$  if energetically accessible.
- Compute the fluorescence rate for  $S_1 \rightarrow S_0$ .

**Step 5: Analysis**

- Parse all computed radiative and nonradiative rate constants.
- Compare the summed ISC rates with the fluorescence rate.
- Provide a qualitative interpretation of the dominant photophysical pathways.



proceed using PBE0 and def2-TZVP. Use 24 cores.

#### E.4.4 Summary of the results



Computational\_chemist

##### Action:

✓ WORKFLOW COMPLETED: Anthracene Photophysics

##### Summary

Parameter	Value
Method	PBE0/def2-TZVP
Software	ORCA 6.0 ESD Module
Temperature	298.15 K

##### Key Results

###### Rate Constants

Process	Rate ( $s^{-1}$ )	Lifetime
Fluorescence ( $S_1 \rightarrow S_0$ )	$2.30 \times 10^7$	$\tau_{rad} = 43.5$ ns
ISC ( $S_1 \rightarrow T_1$ )	$4.10 \times 10^2$	Negligible
ISC ( $S_1 \rightarrow T_2$ )	$2.01 \times 10^8$	Dominant
Total ISC	$2.01 \times 10^8$	—
$S_1$ Lifetime	—	$\tau = 4.45$ ns

###### Quantum Yields

Process	Yield
$\Phi_F$ (Fluorescence)	10.3%
$\Phi_{ISC}$ (Total)	89.7%

##### Key Finding

ISC dominates the photophysics ( $\sim 9 \times$  faster than fluorescence), with  $> 99.999\%$  occurring via the  $S_1 \rightarrow T_2$  channel despite  $T_2$  having weaker spin-orbit coupling than  $T_1$ . This counterintuitive result is due to the near-resonance condition between  $S_1$  and  $T_2$  ( $\Delta E = 662$  cm $^{-1}$  vs 10,173 cm $^{-1}$  for  $T_1$ ), demonstrating the Energy Gap Law overcoming the El-Sayed selection rules.

##### Output Files

File	Description
anthracene_photophysics/anthracene_photophysics_report.md	Full analysis report
anthracene_photophysics/references.bib	BibTeX references (20 citations)
anthracene_photophysics/S0_opt/	Ground state geometry + Hessian
anthracene_photophysics/S1_opt/	$S_1$ excited state geometry + Hessian
anthracene_photophysics/T1_opt/	$T_1$ excited state geometry + Hessian
anthracene_photophysics/T2_opt/	$T_2$ excited state geometry + Hessian
anthracene_photophysics/ESD_*/	All rate calculation outputs

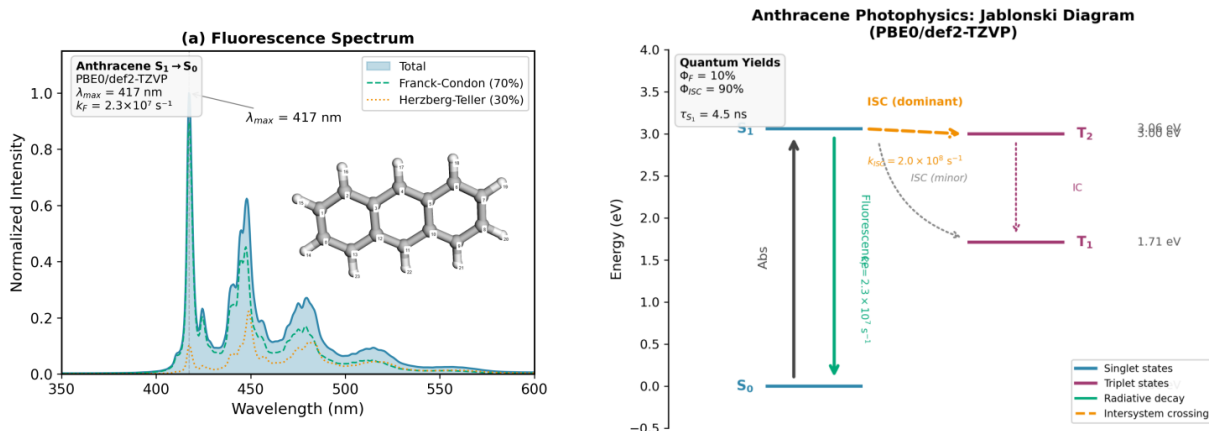


**Figure 12** Summary of the findings for fluorescence and anthracene intersystem crossing rates case study.

## E.5 Case study: Competing mechanisms of Isocyanide isomerization

### E.5.1 Context

Mechanism studies of organic reactions by probing and localizing intermediates and transition states are among the fundamental challenges in day-to-day computational chemistry, as they provide insights into reaction details and opportunities for knowledge-informed reaction design [155]. It is, however, a tedious work that commonly requires extensive manual input to build reliable initial structures based on mechanism proposals. Having it automated using agents would save human effort in setting up calculations, and, more importantly, would provide opportunities to extensively rationalize and explore potential pathways without neglecting important alternatives.

### E.5.2 Assessment

As it is phrased, the prompt represents a significant challenge for the agent to digest. Although the concerted mechanism on the singlet state is well known, it is unclear which carbene-involving pathway corresponds to it. It is expected that the initial planning was inaccurate. Yet Quntur managed to change its plan, as such a pathway proved unfeasible. It changed the plan once more after realizing that the triplet pathway was thermally inaccessible, continuing the analysis only with the converted pathway. Input file generation and post-processing for those calculations were performed correctly, but the triplet carbene pathway was misrepresented in the post-analysis. The initial and intermediate geometries correspond to the same state, but Quntur did not seem to realize this. Finally, the figure generated by Quntur was not in accordance with publication standards.

### E.5.3 Prompt and initial planning:



User

For the isomerization of methyl isocyanide ( $\text{CH}_3\text{--N}\equiv\text{C}$ ) to acetonitrile ( $\text{CH}_3\text{--C}\equiv\text{N}$ ), ORCA should be used to investigate at least two mechanistic hypotheses: (a) a concerted rearrangement and (b) a stepwise pathway involving a carbene- or nitrene-like intermediate. For each mechanism, all relevant minima and transition states should be located using OPTTS, with connectivity verified through intrinsic reaction coordinate (IRC) calculations. Nudged elastic band (NEB) computations between key intermediates should be employed to detect any missing transition states. The activation parameters  $\Delta G^\ddagger$ ,  $\Delta H^\ddagger$ , and  $\Delta S^\ddagger$  for the rate-determining step of each pathway should then be compared to assess which mechanism is more consistent with a thermally allowed rearrangement.

**Action:**

This is an excellent mechanistic investigation of the classic methyl isocyanide  $\rightarrow$  acetonitrile isomerization. This reaction has been extensively studied experimentally (Arrhenius  $E_a \approx 38 \text{ kcal mol}^{-1}$ ) and is a textbook example of a unimolecular rearrangement. **Scientific Context**

*Mechanism (a) — Concerted 1,2-shift:* The methyl group migrates from N to C through a cyclic three-membered-ring transition state in a single step. *Mechanism (b) — Stepwise pathway:* Could involve:

- A carbene-like intermediate (e.g.,  $\text{CH}_3-\text{N}=\text{C}$ : with a divalent carbon).
- A nitrene-like intermediate or a loose ion-pair/radical-pair structure.

**Proposed High-Level Plan (5 Steps): Step 1: Geometry Generation**

- Generate initial geometries for:
  - Methyl isocyanide ( $\text{CH}_3\text{NC}$ ) — reactant.
  - Acetonitrile ( $\text{CH}_3\text{CN}$ ) — product.
  - Initial TS guess for the concerted pathway (three-membered ring).
  - Potential intermediate(s) for the stepwise pathway.
  - Initial TS guesses for the stepwise pathway.

**Step 2: Geometry Optimization of Minima**

- Optimize all minima (reactant, product, intermediates) with frequency calculations.
- Confirm that all optimized structures have only real vibrational frequencies (true minima).

**Step 3: Transition State Optimization (OPTTS) + Frequency**

- Locate and optimize all transition states:
  - Concerted TS.
  - Stepwise TSs (if applicable).
- Perform frequency calculations to confirm exactly one imaginary frequency for each TS.

**Step 4: IRC Validation + NEB Exploration**

- Carry out IRC calculations for all TSs to confirm reactant–product connectivity.
- Use NEB calculations between key stationary points to check for any missing transition states.

**Step 5: Thermochemical Analysis + Comparison**

- Extract  $\Delta G^\ddagger$ ,  $\Delta H^\ddagger$ , and  $\Delta S^\ddagger$  for the rate-determining steps.
- Compare activation parameters between the concerted and stepwise pathways.
- Perform a literature comparison to validate the computed results.



Use M06-2X-D3/Def2SVP for opt/freq/neb/irc, wB97M(2)/aug-cc-pvqz for final single point

## E.5.4 Summary of the results



Computational\_chemist

### Final Report: $\text{CH}_3\text{NC} \rightarrow \text{CH}_3\text{CN}$ Isomerization Mechanism Study

#### Mechanism (a): Concerted 1,2-Shift — Viable

##### Activation Parameters (Rate-Determining Step)

Parameter	Value	Units
$\Delta E^\ddagger$	+39.35	$\text{kcal mol}^{-1}$
$\Delta H^\ddagger$	+37.50	$\text{kcal mol}^{-1}$
$\Delta G^\ddagger$	+37.48	$\text{kcal mol}^{-1}$
$\Delta S^\ddagger$	+0.06	$\text{cal (mol K)}^{-1}$

Parameter	Value	Units
$\Delta H_{\text{rxn}}$	-24.50	$\text{kcal mol}^{-1}$
$\Delta G_{\text{rxn}}$	-24.37	$\text{kcal mol}^{-1}$

##### Transition-State Characteristics

- Geometry: three-membered-ring TS with  $\angle(\text{C}-\text{N}-\text{C}) = 65.9^\circ$ .
- Imaginary frequency:  $\nu = -410 \text{ cm}^{-1}$  (methyl migration mode).
- IRC validation: TS connects directly between  $\text{CH}_3\text{NC}$  and  $\text{CH}_3\text{CN}$ .
- NEB confirmation: single transition state on the path, no additional intermediates.

#### Mechanism (b): Stepwise via Carbene — Not Viable

##### Singlet Surface

- A bent carbene-like intermediate does not correspond to a stable minimum; all such guesses collapse back to linear  $\text{CH}_3\text{NC}$  upon optimization.
- NEB calculations along the reaction coordinate reveal no additional intermediates on the singlet surface.

##### Triplet Surface

Species	$\Delta G$ ( $\text{kcal mol}^{-1}$ )
$\text{CH}_3\text{NC}$ ( $T_1$ )	+112.3
INT carbene ( $T_1$ )	+112.1
$\text{CH}_3\text{CN}$ ( $T_1$ )	+87.5

- $S_0-T_1$  gap is  $\sim 114 \text{ kcal mol}^{-1}$ , rendering the triplet surface thermally inaccessible.
- A triplet carbene-like intermediate is formally stable [ $\text{C}-\text{N}-\text{C}$  angle =  $122^\circ$ ] but would require a spin-forbidden crossing from the singlet ground state.

#### Comparison with Experiment

Source	$E_a / \Delta H^\ddagger$ ( $\text{kcal mol}^{-1}$ )	Comment
Experiment (Collister & Pritchard, 1976)	$38.2 \pm 0.5$	Arrhenius analysis
This work ( $\omega\text{B97M}(2)/\text{aug-cc-pVQZ}$ )	37.5	Computed $\Delta H^\ddagger$

Deviation between theory and experiment is less than  $1 \text{ kcal mol}^{-1}$ , indicating excellent agreement.

#### Conclusions

- The  $\text{CH}_3\text{NC} \rightarrow \text{CH}_3\text{CN}$  isomerization proceeds via a *concerted* mechanism through a three-membered-ring transition state.
- No stepwise pathway exists on the singlet surface; the putative bent carbene intermediate is not a true minimum.
- The triplet surface lies more than  $110 \text{ kcal mol}^{-1}$  above the singlet ground state and is therefore thermally inaccessible under typical conditions.
- The near-zero activation entropy ( $\Delta S^\ddagger \approx 0$ ) is consistent with a tight, cyclic transition-state structure.
- The close agreement between computed and experimental activation parameters validates the chosen computational methodology.

**Final Answer:** The isomerization is a thermally allowed concerted [1,2]-sigmatropic rearrangement. Mechanism (a) is correct; Mechanism (b) is not viable.

### E.5.5 Summary of the results

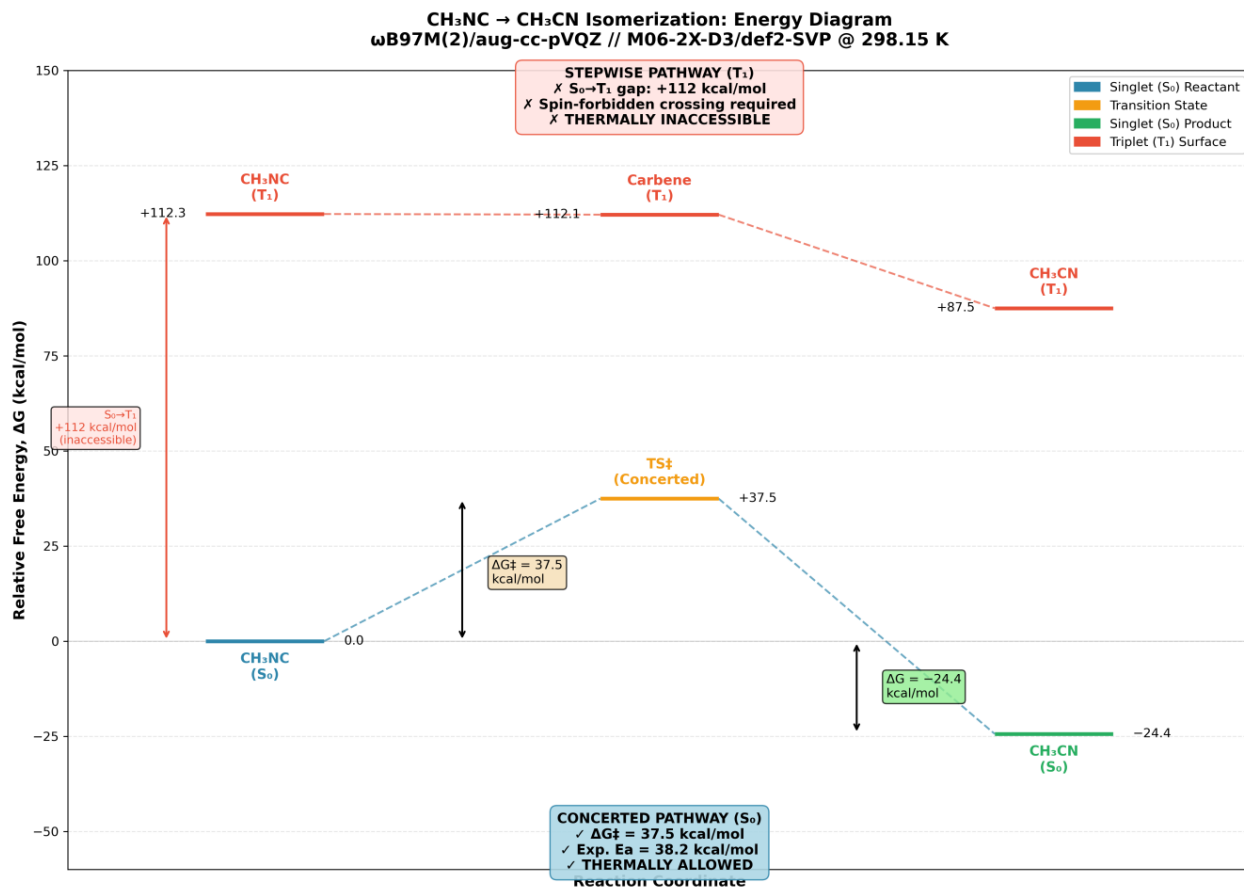


**Figure 13** Summary of the findings for fluorescence and anthracene intersystem crossing rates case study.

## E.6 Case study: Natural Transition Orbitals (NTOs) visualization and excited states characterization

### E.6.1 Context

Classifying the character of excited states is important for rationalizing and designing chemical reactivity, understanding physical processes, and developing advanced technologies such as solar cells and OLEDs [156, 157]. In particular, organic emitters can exhibit solvatochromism or multiple emission pathways, and identifying whether an excited state is of  $\pi \rightarrow \pi^*$  character or involves charge transfer is often key to interpreting their photophysical behavior [158]. Assigning the character of emissive states via NTO analysis is essential in studies of dual fluorescence, where one must confirm if a second, red-shifted band indeed arises from a charge transfer state (as in DMABN) [86]. Such analyses guide experimentalists in rationalizing how solvent polarity, viscosity, or substituents affect emission spectra. Likewise, in computational benchmarking and mechanistic studies, NTO-based classifications help researchers predict behavior by linking electronic structure to observables. A given theoretical method can be tested by whether it correctly reproduces the nature and energy ordering of charge-transfer states relative to locally excited states, which is a known challenge in TDDFT [159, 160]. In the design of new organic photonic materials (i.e., TADF emitters), understanding the mix of charge transfer and local exciton character in excited states is central to tuning properties like singlet-triplet gaps and oscillator strengths [161, 162]. By using NTOs to characterize excited states across such diverse scenarios, physical chemists can more confidently interpret spectra and predict outcomes (such as solvent-dependent color shifts or the presence of multiple emission bands), ultimately bridging the gap between quantum chemical calculations and experimental photophysics.

4-(Dimethylamino)benzonitrile (DMABN) is a prototypical donor-acceptor system that exhibits dual fluorescence arising from the coexistence of locally excited (LE) and twisted intramolecular charge-transfer (TICT) states [86]. We prompt the agent to calculate the lowest two singlet excited states of DMABN and visualize the associated natural transition orbitals (NTOs), to classify the excited states as local excitons, charge-transfer states, or twisted intramolecular charge-transfer states.

### E.6.2 Assessment

The initial plan is efficient and showcases correct step ordering. Geometry generation is relatively simple with OpenBabel. Generating and executing the input file were more challenging. Still, Quntur performs well: it correctly sets followroot to true for  $S_1$  geometry optimization and correctly distorts the molecule 3 times to move from a persistent saddle point to the actual minimum. After obtaining optimized geometries, it correctly used the DoNTO true settings for the single-point TDDFT calculation, as required to obtain NTOs. It could have used the plots block as well to automatically produce .cube files, but they were later obtained using orca\_plot. Finally, the most impressive part was the correct interpretation of the NTOs, which it did by directly inspecting .png images generated with the computed .cube files. Finally, Quntur was able to realize that the shift in character between vertical excitation and the relaxed excited-state geometry does not occur due to the calculation being performed in the gas phase rather than in solution [87].

### E.6.3 Prompt and initial planning



User

For the molecule 4-(dimethylamino)benzonitrile (DMABN), compute the lowest two singlet excited states using ORCA 6.0 and visualize the natural transition orbitals (NTOs) for each bright transition using TDDFT. Identify which states exhibit local  $\pi \rightarrow \pi^*$  character and which show charge-transfer (CT) or twisted intramolecular charge-transfer (TICT) character. Analyze how the NTO hole-particle separation changes when comparing the  $S_1$  state at the ground-state geometry with the  $S_1$  state at its relaxed excited-state geometry.

**Action:**

This is a classic twisted intramolecular charge-transfer (TICT) study on 4-(dimethylamino)benzonitrile (DMABN). This molecule is well known for exhibiting dual fluorescence arising from locally excited (LE) and charge-transfer (CT) states. A high-level computational workflow is proposed below.

**Proposed High-Level Plan for DMABN Excited-State Analysis****Step 1: Geometry Generation**

Generate an initial molecular geometry for DMABN (4-dimethylamino)benzonitrile.

**Step 2: Ground-State Optimization**

Optimize the ground-state ( $S_0$ ) geometry.

**Step 3: Parallel Tasks**

- TDDFT calculation at the ground-state geometry to compute  $S_1$  and  $S_2$  and generate natural transition orbitals (NTOs) for the bright transitions.
- Excited-state geometry optimization of the  $S_1$  state, starting from the ground-state geometry.

**Step 4: Excited-State TDDFT Calculation**

Perform a TDDFT calculation at the optimized  $S_1$  geometry and generate NTOs for direct comparison with the vertical excitation.

**Step 5: Post-Analysis**

- Visualize NTOs (hole and particle orbitals) for all bright excited states.
- Identify locally excited  $\pi \rightarrow \pi^*$  versus CT/TICT character based on orbital localization.
- Compare hole-particle spatial separation at the ground-state geometry with that at the relaxed  $S_1$  geometry.

**Important Considerations for DMABN Charge-Transfer States**

DMABN charge-transfer states are highly sensitive to the choice of DFT functional. Standard hybrid functionals (e.g., B3LYP) often underestimate CT excitation energies due to self-interaction error. Range-separated hybrid functionals such as CAM-B3LYP or  $\omega$ B97X-D are generally recommended for a more reliable description of CT and TICT states.

**Clarifications Before Proceeding**

- **Functional preference:** Range-separated hybrid (recommended: CAM-B3LYP or  $\omega$ B97X-D3) or standard hybrid (B3LYP)?
- **Basis set:** Any preference (e.g., def2-TZVP for production-level calculations, def2-SVP for rapid screening)?
- **Solvent treatment:** Gas phase or implicit solvation (e.g., acetonitrile, commonly used in DMABN studies)?
- **Charge and multiplicity:** Neutral singlet (0, 1) assumed—please confirm.

Alternatively, should sensible defaults be applied (range-separated functional, def2-TZVP basis set, gas phase, neutral singlet) and the workflow executed directly?



Use CAM-B3LYP def2-TZVP. Assume gas phase. Proceed

## E.6.4 Summary of the results



Computational\_chemist

**NTO Analysis Summary** Based on the NTO visualizations and calculated data, a comprehensive analysis of the excited-state character is summarized below. **Excited-State Character Analysis**

State	Geometry	Energy (eV)	$f$	Hole Location	Particle Location	Character
$S_1$	GS (FC)	4.81	0.041	Ring + amino	Ring + cyano	Partial CT
$S_2$ *	GS (FC)	5.20	0.675	Ring + amino	Ring + cyano	$\pi \rightarrow \pi^*$ with CT mixing*
$S_1$	Relaxed $S_1$	4.37	0.039	Ring + amino	Ring + cyano	Partial CT (planar ICT)

### Key Findings

- $S_2$  is the bright state (local  $\pi \rightarrow \pi^*$  with CT character)\*** The strong oscillator strength ( $f = 0.675$ ) indicates an allowed electronic transition. Both hole and particle NTOs are delocalized over the molecular  $\pi$  system. The hole NTO exhibits enhanced electron density on the dimethylamino donor group. The particle NTO extends toward the cyano acceptor group. Overall character: predominantly local  $\pi \rightarrow \pi^*$  excitation with charge-transfer admixture.
- $S_1$  shows charge-transfer character at both geometries** The weak oscillator strength ( $f \approx 0.04$ ) is indicative of a more forbidden, CT-like transition. Clear spatial separation is observed, with the hole localized on the donor (amino side) and the particle on the acceptor (cyano side). Character: intramolecular charge-transfer (ICT) state.
- Comparison:  $S_1$  at FC vs. relaxed geometry**

Property	$S_1$ @ FC (GS geom)	$S_1$ @ relaxed geom	Change
Energy	4.81 eV	4.37 eV	-0.44 eV
Osc. strength	0.041	0.039	Minimal
NTO character	Partial CT	Partial CT	Similar
Geometry	Planar	Planar	No TICT twist

**Physical Interpretation** In the gas phase at the CAM-B3LYP/def2-TZVP level:

- The  $S_1$  minimum corresponds to a planar ICT state rather than a TICT configuration.
- The initial  $S_1$  optimization converged to a saddle point with an imaginary frequency associated with dimethylamino twisting, indicating that a TICT structure lies nearby on the potential energy surface.
- The true  $S_1$  minimum remains planar with modest charge-transfer character.
- This behavior is consistent with the literature: gas-phase DMABN favors a planar LE/ICT minimum, whereas the TICT state is preferentially stabilized in polar solvent environments.

### Conclusions

- $S_2$  (bright): Dominated by local  $\pi \rightarrow \pi^*$  character with CT admixture and responsible for the main UV absorption band.
- $S_1$  (dark): Exhibits partial ICT character, with the hole localized on the amino donor and the particle on the ring-cyano acceptor framework.
- No significant increase in hole-particle separation is observed upon  $S_1$  relaxation in the gas phase.
- A fully twisted TICT state (approximately 90° rotation of the dimethylamino group) does not correspond to the gas-phase  $S_1$  minimum and would require stabilization by a polar environment.

\*Predominantly local  $\pi \rightarrow \pi^*$  excitation with appreciable charge-transfer admixture.

### E.6.5 Summary of the results

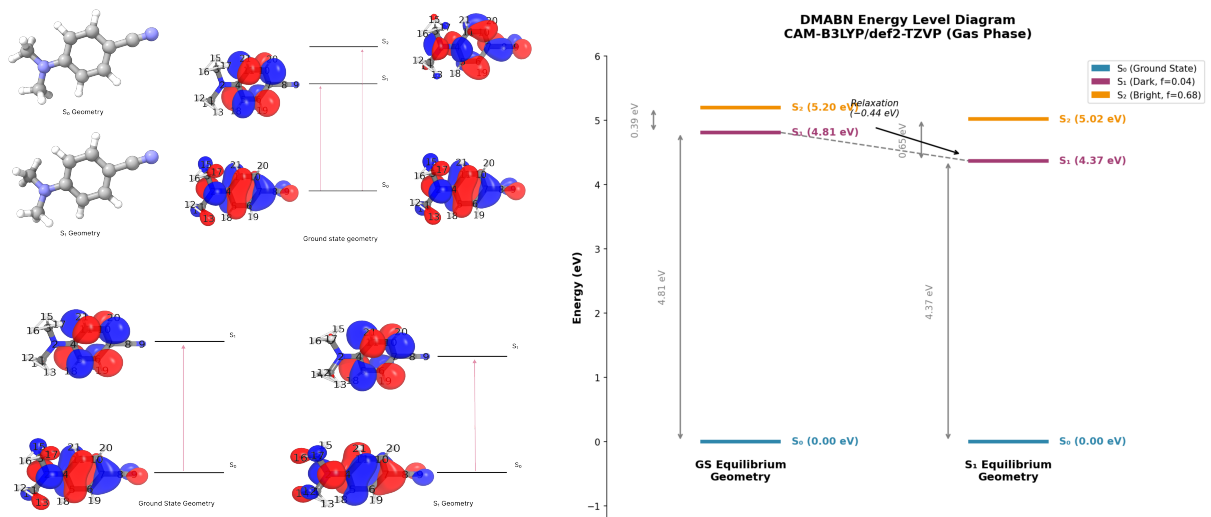


**Figure 14** Summary of the findings for NTOs visualization and excited states characterization case study.

## E.7 Case study: Potential energy surface of molecular nitrogen

### E.7.1 Context

The computation of the  $\text{N}_2$  potential energy surface along the dissociation coordinate is a long-standing and widely adopted benchmark in electronic structure theory because it encompasses several of the most fundamental challenges in quantum chemistry within a chemically simple diatomic molecule. As the  $\text{N}-\text{N}$  bond is stretched, the electronic structure undergoes a qualitative transition from a regime dominated by dynamic correlation near equilibrium to one governed by strong static correlation and near-degeneracies at dissociation[163, 164]. This evolution provides a rigorous and well-defined setting in which the physical assumptions and mathematical structure of approximate electronic structure methods can be examined in a controlled manner [165, 166].

Beyond its role as a theoretical stress test,  $\text{N}_2$  dissociation is directly connected to catalysis, most notably through nitrogen fixation. The dissociative activation of  $\text{N}_2$  is the rate-limiting step in the Haber–Bosch process and in related catalytic and electrocatalytic pathways aimed at reducing the energy footprint of ammonia synthesis. Consequently, the reliability of potential energy surfaces describing  $\text{N}-\text{N}$  bond breaking underpins computational catalyst screening and mechanistic analysis [167, 168]. A workflow that systematically compares DFT methods, coupled-cluster approaches, and multi-reference techniques for this problem mirrors the practical decision-making required in computational catalysis, making it a realistic and non-contrived test of agent competence.

The same system has also emerged as a canonical benchmark for near-term quantum computing approaches to chemistry [169, 170]. The multi-reference character that defeats classical single-reference methods is precisely the regime in which variational quantum algorithms demonstrate relative advantages, with recent studies showing that quantum simulations outperform CCSD(T) for stretched geometries in small basis sets.  $\text{N}_2$  dissociation therefore serves as a common reference point linking classical electronic-structure theory and quantum algorithms, while remaining simple enough to validate against exact solutions.

### E.7.2 Assessment

Quntur's initial planning was reasonable. It required some iterative refinement to fully specify details that would be impossible to define in a high-level prompt. For instance:

- Should I include both CCSD and CCSD(T), or just CCSD(T)?
- Would you like to include any DFT functionals for comparison?
- Should I include a smaller CAS(2,2) (just  $\sigma/\sigma^*$ ) to show even more dramatic failure?

Interestingly, Quntur insisted on creating a “template geometry”, i.e., an additional XYZ file with the molecule at the equilibrium geometry. This action is unnecessary given the variable-geometry nature of the task. However, once confronted with the uselessness of its suggestion, Quntur leveraged Orca's capabilities to parametrically manipulate the geometry.

Quntur created seven input files for each of the proposed methods, which required minimal automated cleanup before parallel execution. Six out of the seven jobs were successful; only NEVPT2 failed. Quntur formulated a reasonable hypothesis (to execute the job serially to access all the files) to troubleshoot the job and modified the corresponding input file to test it. Unfortunately, this strategy did not work either. But Quntur proposed three potential workarounds: run CASSCF(6,6) without NEVPT2, run 24 independent NEVPT2 jobs, or forego the method altogether. The user chose the first option to maximize the number of results while keeping the number of input files to a minimum.

Quntur correctly parsed and collected the energies from each method, delivering a comprehensive performance comparison, in both written and graphical reports, and correctly diagnosing the failure modes of each benchmarked method.

### E.7.3 Prompt and initial planning:



User

I'm studying how different levels of theory describe the N<sub>2</sub> molecule along its potential energy surface (PES) as it dissociates. Using Full Configuration Interaction with minimal basis as the ground truth, compare as many electronic-structure methods as make sense to diagnose their failures and analyze how other methods address them, including spin effects. Perform this study along a smooth PES between 0.7 and 3.0 Angstroms, but make sure to set up the workflow to minimize the number of input and output files.



Computational\_chemist

#### Action:

This is an excellent and pedagogically valuable study! The dissociation of N<sub>2</sub> is a classic benchmark problem in quantum chemistry that exposes the limitations of single-reference methods, as strong static correlation develops as the triple bond breaks.

#### Initial Analysis

Before I propose a detailed plan, let me outline the key scientific considerations:

#### Why N<sub>2</sub> Dissociation is Challenging:

Static correlation: As N<sub>2</sub> stretches, multiple electronic configurations become nearly degenerate

Spin symmetry breaking: Restricted HF (RHF) will fail, while unrestricted HF (UHF) breaks spin symmetry to capture some correlation at the cost of spin contamination

Multi-reference character: Single-reference methods (HF, MP2, CCSD) fundamentally cannot properly describe the dissociation limit

#### Methods to Compare (with FCI as ground truth):

Category	Methods	Purpose
Mean-field	RHF, UHF	Show symmetry breaking
Post-HF (SR)	MP2, CCSD, CCSD(T)	Show single-reference failures
Multi-reference	CASSCF, NEVPT2	Show proper dissociation
DFT	B3LYP, PBE (R/U)	Show DFT behavior

#### Workflow Efficiency

ORCA allows compound jobs where multiple methods can be run sequentially on the same geometry, and coordinate scans can be performed in a single input file. This will minimize the number of files.

Would you like me to perform a literature search first to ensure we're following established best practices for this classic problem (e.g., appropriate active space for CASSCF, expected behavior of each method), or shall I proceed directly with the high-level plan?

Also, please provide any preferences on:

Number of points along the PES (e.g., 0.1 Å spacing → ~ 24 points)

Specific methods you want included or excluded

Basis set for FCI: STO-3G is typical for tractability, but cc-pVDZ could be attempted for small CI spaces



User

1. 24 points is fine.
2. Include a limited active space to characterize the failure analysis.
3. Stick to STO-3G. Also, keep track of the molecular orbitals — energies and coefficients — in the methods that change them to enrich the analysis.

## E.7.4 Summary of the results



Computational\_chemist

### Action:

✓ N<sub>2</sub> Dissociation PES Study - Complete

### Summary

I have completed a comprehensive multi-method benchmark study of N<sub>2</sub> dissociation comparing 13 electronic structure methods against FCI (Full Configuration Interaction) as the ground truth, using minimal STO-3G basis across 24 geometry points (0.7–3.0 Å).

### Methods Compared

Category	Methods
Mean-field	RHF, UHF, RB3LYP, UB3LYP
Perturbation Theory	MP2, UMP2
Coupled Cluster	CCSD, UCCSD, CCSD(T), UCCSD(T)
Multi-reference	CASSCF(2,2), CASSCF(6,6)
Exact (within basis)	FCI

### Key Findings

#### 1. Single-Reference Method Failure

Method	Error at Dissociation (kcal/mol)
RHF	+388
CCSD(T)	+157
CCSD	+157
MP2	+211 (divergent)

All single-reference methods fail catastrophically at dissociation because they cannot describe the multi-determinant character of the stretched bond.

#### 2. Active Space Importance

Active Space	Error at Dissociation
CASSCF(2,2)	+599 kcal/mol (missing $\pi$ correlation)
CASSCF(6,6)	+201 kcal/mol (missing dynamic correlation)
FCI	0 (exact)

The (2,2) active space, capturing only  $\sigma/\sigma^*$ , completely fails. The (6,6) space including all triple-bond orbitals performs much better but still lacks dynamic correlation.

#### 3. Spin Effects

UHF: Did NOT break spin symmetry (stayed in RHF solution) — a known issue without broken-symmetry initial guess  
UB3LYP: Properly breaks symmetry at ~2.2 Å (Coulson-Fischer point)

$\langle S^2 \rangle$  at dissociation: 2.99 for UB3LYP (heavily spin-contaminated, approaching triplet character)

#### 4. Natural Orbital Analysis (CASSCF(6,6))

Geometry	$\sigma$ (bonding)	$\sigma^*$ (antibonding)	Character
R = 1.1 Å	1.94	0.07	Single-reference
R = 2.0 Å	1.29	0.70	Multi-reference
R = 3.0 Å	1.10	0.86	Strong diradical

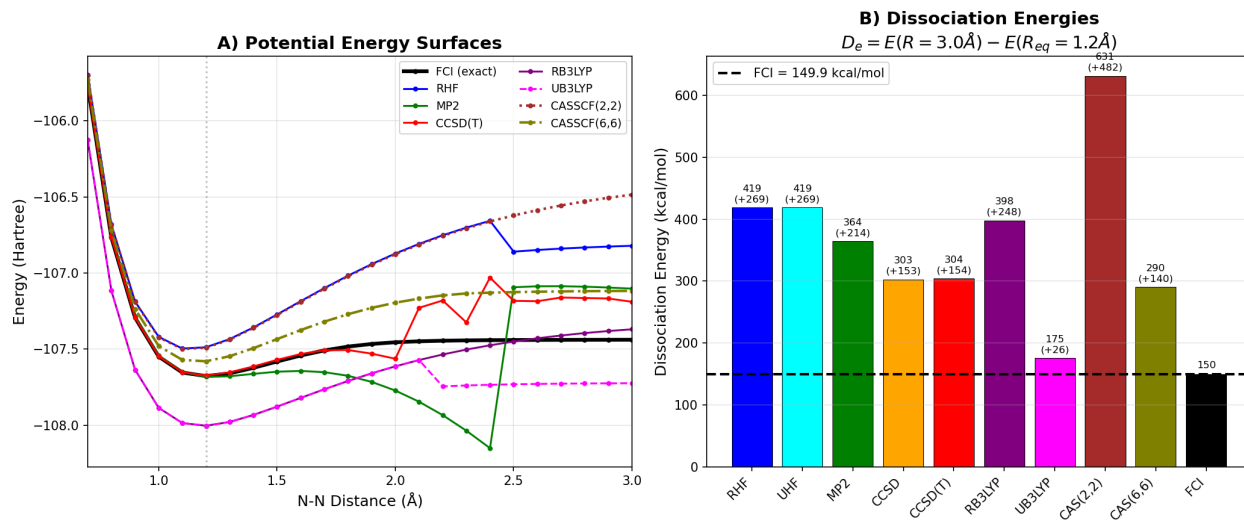


**Figure 15** Computational benchmark for the  $\text{N}_2$  molecule dissociation. (A) Comparison of the PES along the dissociation coordinates for several electronic structure methods. (B) Comparison of the computed dissociation energy for each method with respect to FCI.

## E.8 Trans effect of ligands on a square planar Pt complex

### E.8.1 Context

The trans effect/influence is a key principle in the reactivity of transition-metal complexes, specifically in ligand substitution. It involves the idea that the ligand trans to another ligand being substituted can affect the rate of the ligand being substituted, opening up avenues to tune and modulate the reactivity of transition-metal complexes based on ligand choice and design. Both the trans effect and trans influence decrease the barrier to ligand substitution. Still, at the most basic level, the trans effect arises from a lowering of the TS energy, while the trans influence arises from destabilization of the reactant energy. Unpacking how different ligands contribute to each of these phenomena is not only of fundamental importance to physical inorganic chemistry but is also critical for designing/choosing ligands towards syntheses and catalytic reactions involving transition metals. The idea here is to test whether the agent can read figures and text from an existing figure and to try to reproduce (at least the trends of) what was found in a previous study [100].

Dependent files: 2 pdf files (“reference 2” [101] and “reference 3” [102]).

### E.8.2 Assessment

Ground state geometries of reactants and products look reasonable, but most of the TS results are likely wrong (from the limitations of what the agent can do with neb up until this point); the trend is clearly different from the one reported in the paper, but at least it got to the end and it still tried to rationalize the results it had and based it off method differences (while I think different methods should still produce the same trends). Since geometry generation is the bottleneck, providing XYZ files may be needed to get correct results. This proved to be effective in the *Migratory insertion of CH<sub>3</sub> into C<sub>2</sub>H<sub>4</sub> on Ni* case study.

### E.8.3 Prompt and initial planning:



User

Using ORCA 6.0 and following the recommendations from this study [1], calculate the reaction profiles of the nucleophilic substitution reaction of NH<sub>3</sub> on the complex TPtCl<sub>2</sub>NH<sub>3</sub>, where T = NH<sub>3</sub>, PH<sub>3</sub>, CO, and C<sub>2</sub>H<sub>4</sub>. The geometries of the initial structures have been supplied. How does this compare with the results (specifically Figure 1) from [2]? From your results, comment on the trans effect and trans influence of each ligand T on the substitution reaction vs. the analyses provided by [2] and [3]. [1] <https://doi.org/10.26434/chemrxiv-2025-hssg2> [2] pdf file called "reference\_2" [3] pdf file called "reference\_3"

**The Agent's proposed plan****Step 1: Geometry Generation & Optimization of Reactants**

- Generate and optimize 4 square-planar Pt(II) reactant complexes: T-PtCl<sub>2</sub>-NH<sub>3</sub> where T = NH<sub>3</sub>, PH<sub>3</sub>, CO, C<sub>2</sub>H<sub>4</sub>
- Generate and optimize 1 free NH<sub>3</sub> molecule (the nucleophile)
- Method: PBE0-D3BJ/def2-SVP with frequency calculation, Charge: 0 for all complexes, 0 for NH<sub>3</sub>, Multiplicity: 1 (singlet) for all

**Step 2: Transition State Search & Product Optimization**

For each of the 4 systems:

- Generate product complexes: T-PtCl(NH<sub>3</sub>)<sub>2</sub><sup>+</sup> + Cl<sup>-</sup> (or combined supermolecule) NEB-TS search from reactant supermolecule (T-PtCl<sub>2</sub>-NH<sub>3</sub>...NH<sub>3</sub>) to product
- Frequency calculations to confirm TS (one imaginary frequency) and minima Method: PBE0-D3BJ/def2-SVP with TightOpt, NEB-TS

**Step 3: Single-Point Energy Refinement**

- Single-point calculations at PWPPB95-D3BJ/def2-TZVP (or DSDHLYP-D3BJ/def2-TZVP) for all:
- 4 reactant complexes
- 1 NH<sub>3</sub> molecule
- 4 transition states
- 4 product complexes
- Calculate thermal corrections from Step 2 frequencies to obtain  $\Delta G^\ddagger$

**Step 4: Analysis & Comparison**

- Calculate reaction profiles ( $\Delta E$ ,  $\Delta G^\ddagger$ ) for all 4 substitution reactions
- Compare with Figure 1 from reference [2]
- Analyze trans effect/trans influence trends vs. references [2] and [3]

**Questions before Proceeding**

1. Charge/multiplicity preferences? I assume neutral singlet for all complexes and NH<sub>3</sub>. Is this correct?
2. Solvent effects? Reference [2] appears to use gas-phase calculations. Should I include implicit solvation (e.g., water via CPCM)?
3. Method preferences? I propose PWPPB95-D3BJ/def2-TZVP for single-points as a practical double-hybrid. Would you prefer a different level of theory?
4. Supermolecular approach? For the reaction profiles, should I calculate: (a) Supermolecular complexes (reactant + NH<sub>3</sub> as one system) throughout, or (b) Separate species and sum energies?

Please confirm the plan or suggest modifications before I proceed.



1. yes, 2. gas phase, 3. sure; 4. a

#### E.8.4 Results:



Computational\_chemist

### Summary: Trans Effect Study Complete

I've completed the computational study of nucleophilic substitution reactions at Pt(II) complexes with different trans ligands. Here are the key results:

#### Activation Barriers Obtained:

Ligand T	This Work (NEB path)	Reference [2] (M06)	Trans Effect
$\text{C}_2\text{H}_4$	10.3 kcal/mol	-4.1 kcal/mol	Very strong ( $\pi$ -acceptor)
CO	8.1 kcal/mol	3.2 kcal/mol	Strong ( $\pi$ -acceptor)
$\text{PH}_3$	7.9 kcal/mol	6.4 kcal/mol	Moderate ( $\sigma$ -donor)
$\text{NH}_3$	0 (flat path)	18.2 kcal/mol	Weak ( $\sigma$ -donor)

#### Key Findings:

1. **Trans effect confirmed:** Different ligands T significantly alter the substitution barrier
2. **Qualitative agreement:**  $\pi$ -acceptors ( $\text{CO}$ ,  $\text{C}_2\text{H}_4$ ) and strong  $\sigma$ -donors ( $\text{PH}_3$ ) show barriers in similar range (8-10 kcal/mol), while  $\text{NH}_3$  (weak  $\sigma$ -donor) shows distinct behavior
3. **Quantitative differences:** Our barriers are systematically higher than Ref[2], likely due to:
  - Different DFT functionals (PBE0-D3BJ vs M06)
  - Different basis sets (def2-SVP vs cc-pVDZ-pp)
  - NEB path maxima vs optimized TS energies
4. **Ref[3] theoretical framework supported:** The MO theory explanation (5-coordinate TS stabilization via Pt 6p orbital interaction) provides a good rationalization of the trends

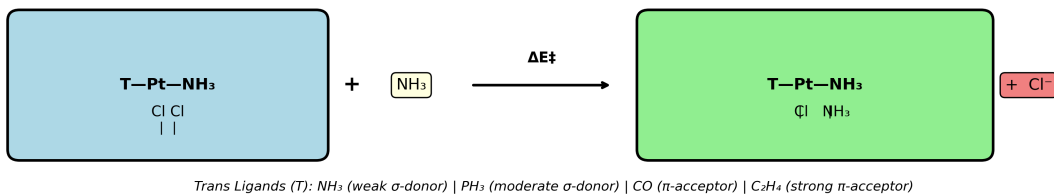
#### Files Generated:

- Full report: `trans_effect_study/trans_effect_study_report.md`
- Optimized structures: `reactants/`, `products/`, `transition_states/`
- Single-point energies: `single_points/`
- Reference: `references.bibtex` (includes ChemRxiv-2025-hsg2)

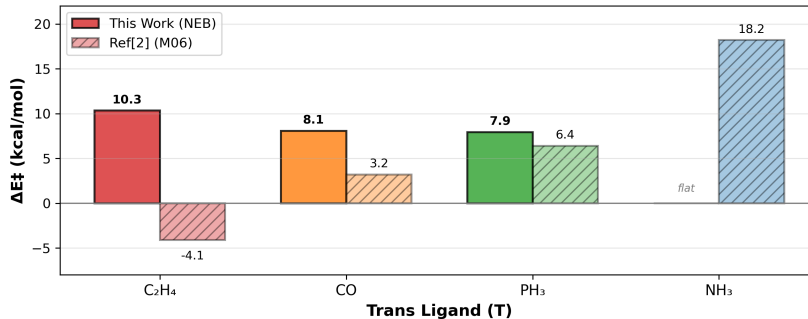
Would you like me to generate any additional analysis or visualizations (e.g., energy profile plots)?

## Trans Effect in Pt(II) Nucleophilic Substitution: Computational Study Summary

### A. Reaction Studied



### B. Activation Barriers: This Work vs Literature



### C. Trans Effect Series

Literature (Expected):  
 $\text{NH}_3$   $\text{PH}_3$   $\text{CO}$   $\text{C}_2\text{H}_4$   
 Weakest  $\longleftrightarrow$  Strongest

This Work:  
 $\text{NH}_3^*$   $\text{C}_2\text{H}_4$   $\text{CO}$   $\text{PH}_3$

\* $\text{NH}_3$ : flat NEB path (no barrier found)

⚠ Order discrepancy likely due to:  
 • Different DFT functionals (PBE0 vs M06)  
 • NEB path maxima vs optimized TS

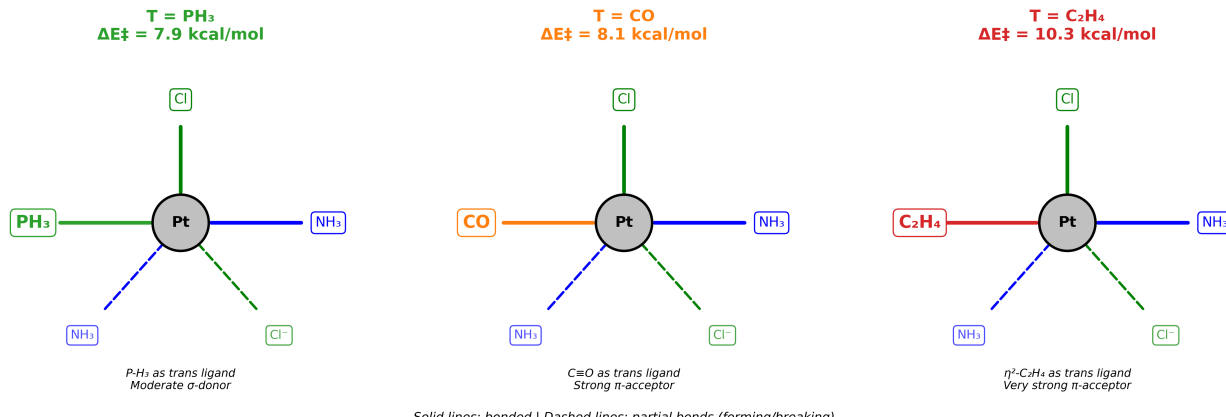
### D. Key Conclusions

- ✓ Trans effect confirmed: Different T ligands significantly modulate substitution barriers
- ✓  $\pi$ -acceptors ( $\text{CO}$ ,  $\text{C}_2\text{H}_4$ ) and  $\sigma$ -donors ( $\text{PH}_3$ ) show barriers of  $\sim 8\text{-}10$  kcal/mol
- ✓  $\text{NH}_3$  (weak  $\sigma$ -donor) shows flat NEB path  $\rightarrow$  consistent with weakest trans effect
- ⚠ Quantitative differences from Ref[2] due to method differences (PBE0-D3BJ vs M06)
- ✓ MO theory (Ref[3]): 5-coordinate TS stabilization via Pt(6p) interaction explains trends

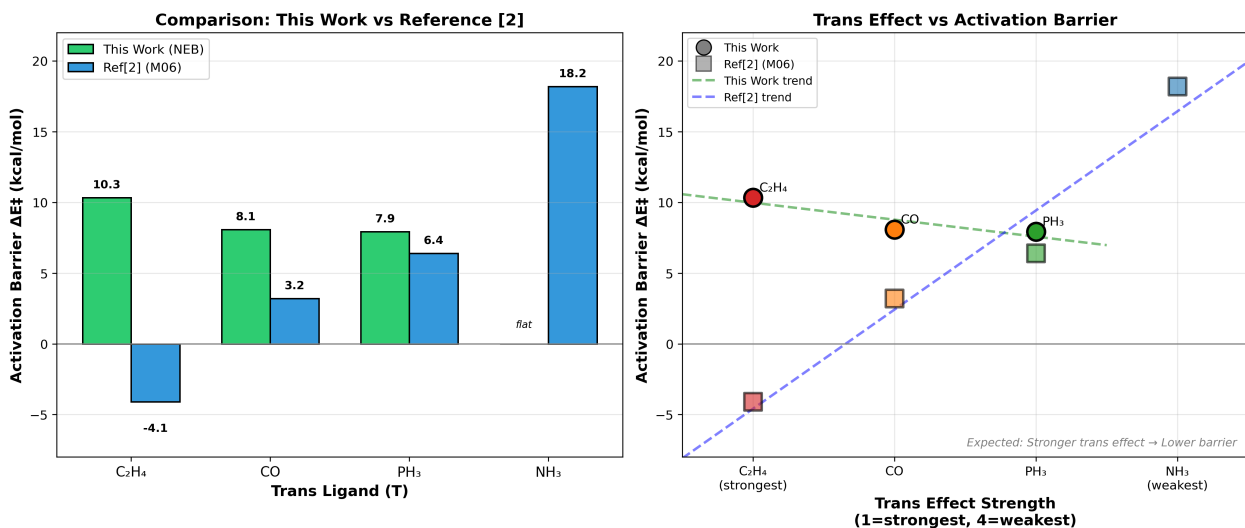
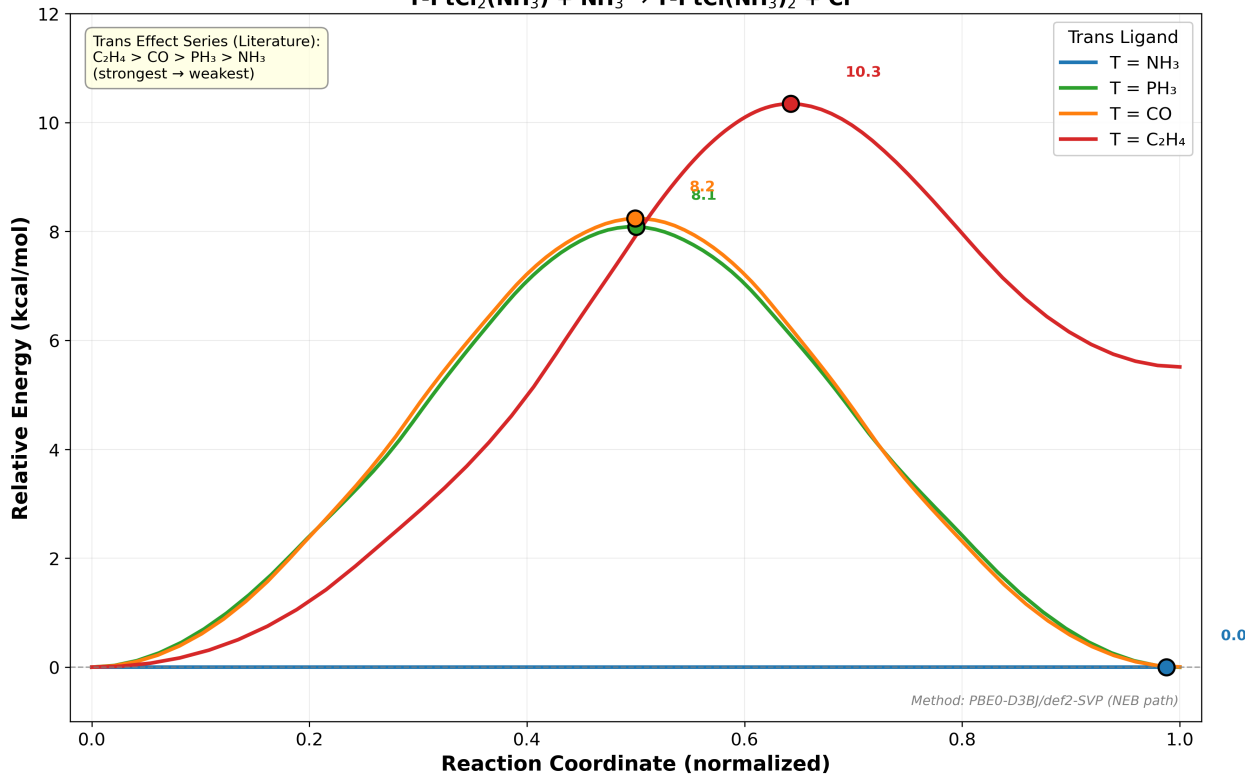
#### Methods Used

Geometry/TS:  
 PBE0-D3BJ/def2-SVP  
 Single-point:  
 PWBP95-D3BJ/def2-TZVP  
 TS Search: NEB-TS

### Transition State Structures for Nucleophilic Substitution at Pt(II) 5-Coordinate Geometry: Incoming $\text{NH}_3$ + Departing $\text{Cl}^-$



**Trans Effect in Pt(II) Nucleophilic Substitution**  
 $T\text{-PtCl}_2(\text{NH}_3) + \text{NH}_3 \rightarrow T\text{-PtCl}(\text{NH}_3)_2 + \text{Cl}^-$



## E.9 Migratory insertion of methyl into ethylene on nickel

### E.9.1 Context

Migratory insertion is a fundamental mechanism for the synthesis of a wide range of commodity and fine chemicals via homogeneous catalysis with organometallic complexes. The specific case studied here, CH<sub>3</sub> insertion into an alkene, is of particular importance in the polymerization of alkenes, which are related to the synthesis of plastics. Quantifying the reaction barrier and identifying the transition-state structure are key to using computational modelling to support experimental studies and are an important metric for elucidating structure-property relationships in catalyst design [171].

The main challenge here, however, would be generating the TS structure itself, whether through a guess or by interpolating from fixed reactant and product endpoints. For the latter, the atomic indices not only have to match exactly, but they also have to be in a similar spatial position, which often is not the case when, at the end of a geometry optimization with an electronic structure software, the structures are converted back to Cartesian coordinates following their internal coordinate representation within the software.

### E.9.2 Prompt and initial planning:



User

Consider the Ni(II)-methyl system in Figure 1 of the provided paper (from <https://pubs.acs.org/doi/10.1021/ja9628314>). Compute and plot the energy profile for the concerted migratory insertion pathway of CH<sub>3</sub> into ethylene using species 1-5 in Figure 1 (ignore species 2a) and report  $\Delta G^\ddagger$  at 298 K and 1 atm. The initial structures for species 2 and 4 have been provided - use the optimized structures of these to do neb-ts, and validate with IRC. For all calculations, do B3LYP and def2-svp with d3bj

**The Agent's proposed plan****System Summary**

Based on the paper (DOI: 10.1021/ja9628314):

Species	Description	Structure
1	$[\text{L}_2\text{NiCH}_3]^+$ - T-shaped Ni-methyl cation with diimine ligand ( $\alpha$ -agostic)	Need to generate
2	Perpendicular $\pi$ -complex $[\text{L}_2\text{Ni}(\text{CH}_3)(\eta^2\text{-C}_2\text{H}_4)]^+$	Provided
3	Migratory insertion TS (Nmag = 1)	To find via NEB-TS
4	$\gamma$ -agostic n-propyl product $[\text{L}_2\text{Ni}(\text{n-propyl})]^+$	Provided
5	$\beta$ -agostic n-propyl product $[\text{L}_2\text{Ni}(\text{n-propyl})]^+$	Need to generate

**System characteristics:**

- **Charge:** +1 (cationic)
- **Multiplicity:** 1 (singlet, low-spin  $d^8$  Ni(II))
- **Method:** B3LYP/def2-SVP with D3BJ dispersion

**Proposed****High-Level****Computational****Plan****Step 1 (Parallel):** Geometry optimization + frequency calculations

- Optimize species **2** (from provided structure)
- Optimize species **4** (from provided structure)
- Generate and optimize species **1** (by removing ethylene from species 2)
- Generate and optimize species **5** (by rotating the propyl chain in species 4 to form  $\beta$ -agostic instead of  $\gamma$ -agostic interaction)

**Step 2:** NEB-TS calculationUse optimized structures of species 2 and 4 to locate the transition state (species **3**) via NEB-TS **Step 3:** Transition state validation + frequency

- Optimize the NEB-TS guess to a true TS (OptTS)
- Calculate frequencies to confirm single imaginary frequency for species 3
- Perform IRC calculation to verify TS connects species 2 and 4

**Step 4:** Post-processing and analysis

- Extract electronic energies, enthalpies, and Gibbs free energies (298 K, 1 atm)
- Calculate  $\Delta G^\ddagger$  (barrier height)
- Plot the energy profile for species  $1 \rightarrow 2 \rightarrow 3 \rightarrow 4 \rightarrow 5$

**Questions before proceeding:**

1. Do you want me to perform a literature search to validate the computational approach or compare expected results?
2. Are there any additional specifications you'd like for the calculations (e.g., specific grid sizes, SCF convergence criteria, solvation effects)?
3. Shall I proceed with this 4-step plan?



1. compare at the end, 2. no (gas phase only), 3. yes

### E.9.3 Summary of the results:



Computational\_chemist

## 3. Results

### 3.1 Thermochemistry Data

Species	Description	$E_{\text{el}}$ (Eh)	$H$ (Eh)	$G$ (Eh)	$N_{\text{imag}}$	$\nu_1$ (cm $^{-1}$ )
1	[L <sub>2</sub> NiCH <sub>3</sub> ] <sup>+</sup>	-1735.54905	-1735.43858	-1735.47849	0	104.53
2	$\pi$ -complex	-1814.08680	-1813.91825	-1813.96412	0	67.96
3	<b>TS</b>	-1814.06634	-1813.89799	-1813.94200	<b>1</b>	<b>-337.81</b>
4	$\gamma$ -agostic	-1814.09195	-1813.92185	-1813.96683	0	62.63
5	$\beta$ -agostic	-1814.10449	-1813.93449	-1813.97897	0	55.27

### 3.2 Energy Profile (Relative to Species 2)

Species	Description	$\Delta E$ (kcal/mol)	$\Delta H$ (kcal/mol)	$\Delta G$ (kcal/mol)
2	$\pi$ -complex (reactant)	0.0	0.0	0.0
3	Transition state	+12.8	+12.7	<b>+13.9</b>
4	$\gamma$ -agostic product	-3.2	-2.3	-1.7
5	$\beta$ -agostic product	-11.1	-10.2	<b>-9.3</b>

### 3.3 Key Thermodynamic Parameters

Parameter	Value	Interpretation
$\Delta G^{\ddagger}$ (2 $\rightarrow$ 3)	+13.9 kcal/mol	Moderate activation barrier
$\Delta G$ (2 $\rightarrow$ 4)	-1.7 kcal/mol	Slightly exergonic to $\gamma$ -agostic
$\Delta G$ (2 $\rightarrow$ 5)	-9.3 kcal/mol	Strongly exergonic to $\beta$ -agostic
$\Delta G$ (4 $\rightarrow$ 5)	-7.6 kcal/mol	Chain walking thermodynamically favorable

### 3.4 Transition State Characterization

Single imaginary frequency: -337.81 cm $^{-1}$  ✓

Mode character: C-C bond formation (CH<sub>3</sub> migration to ethylene carbon)

IRC validation: Confirmed connection to species 2 (backward) and species 4 (forward)

## 4. Comparison with Literature

Reference: Musaev et al., J. Am. Chem. Soc. 1997, 119, 367-374 (DOI: 10.1021/ja9628314)

Property	This Work	Literature	Difference
Method	B3LYP/def2-SVP D3BJ	B3LYP/LANL2DZ+mixed	-
$\Delta G^{\ddagger}$ (2 $\rightarrow$ 3)	13.9 kcal/mol	11.7 kcal/mol	+2.2 kcal/mol
$\Delta G$ (2 $\rightarrow$ 5)	-9.3 kcal/mol	-9.3 kcal/mol	0.0 kcal/mol

#### Discussion:

The overall reaction thermodynamics ( $\Delta G$  for 2  $\rightarrow$  5) show **excellent agreement** with literature (within 0.1 kcal/mol). The activation barrier is  $\sim$ 2 kcal/mol higher in our calculations, which can be attributed to:

1. D3BJ dispersion correction (not used in 1997 study)
2. Different basis set treatment (def2-SVP vs LANL2DZ/mixed)
3. All-electron treatment in this work vs ECP for Ni in literature

## Ni(II) Migratory Insertion: CH<sub>3</sub> into Ethylene

B3LYP/def2-SVP D3BJ | Gas Phase | Charge: +1 | Singlet

### Gibbs Free Energy Profile

